Structure and thermodynamics of inclusion complexes between cyclodextrins and bile salts in aqueous solution

Enthalpy-entropy compensation, convergence temperatures and other features of hydrophobic dehydration

Schönbeck, Jens Christian Sidney

Publication date:
2012

Document Version
Early version, also known as pre-print

Citation for published version (APA):
Schönbeck, J. C. S. (2012). *Structure and thermodynamics of inclusion complexes between cyclodextrins and bile salts in aqueous solution: Enthalpy-entropy compensation, convergence temperatures and other features of hydrophobic dehydration*. Roskilde Universitet.

Structure and thermodynamics of inclusion complexes between cyclodextrins and bile salts in aqueous solution

Enthalpy-entropy compensation, convergence temperatures and other features of hydrophobic dehydration

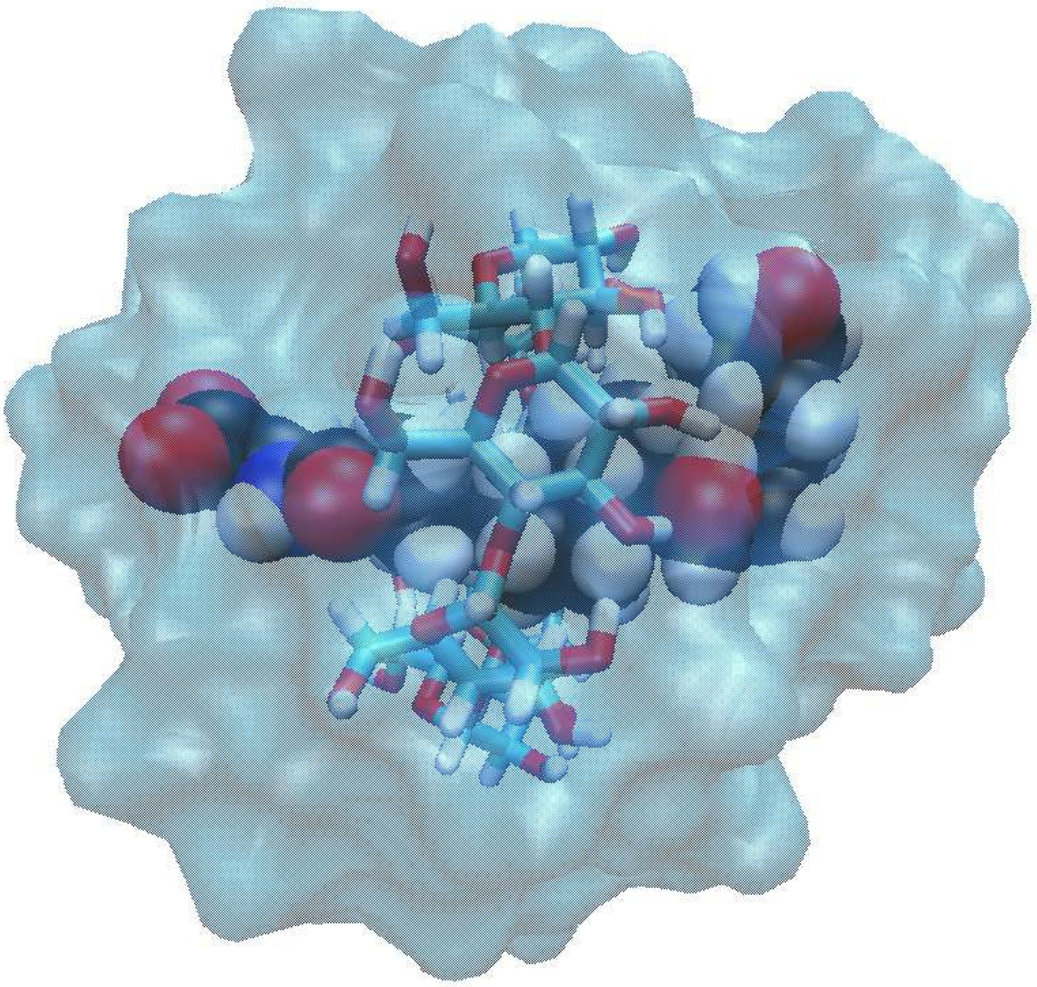

Ph.D. dissertation

by

Christian Schönbeck

November 2012

Roskilde University
Department of Nature, Systems and Models

Abstract

The inclusion complexes between cyclodextrins and bile salts are structurally and thermodynamically characterized. Special attention is given to the influence of methyl, hydroxypropyl and sulfobutyl substituents attached to the rims of the modified cyclodextrins. The wide range of employed cyclodextrins are characterized in terms of the number and position of the substituents using mass spectrometry and NMR. Detailed insight into the structures of the inclusion complexes formed with 6 different bile salts is obtained from different NMR techniques and molecular dynamics simulations. Complexation constants are determined by capillary electrophoresis, calorimetry (ITC) and NMR. The thermodynamic characterization includes complexation enthalpies and entropies for most of the complexes and heat capacity changes for a selected group of complexes.

The complexation constants are primarily determined by the radius of the cyclodextrin and the presence of a hydroxyl group on C12 of the bile salt. The type, number and position of substituents on the cyclodextrin also affect the complex stabilities but to a lesser extent, even though the presence of substituents results in increased hydrophobic contacts with the bile salt. The increased dehydration of hydrophobic surface, which is the result of all types of substituents, leads to a large increase in the enthalpies and entropies of complexation and to more negative heat capacity changes. It is concluded that the altered complexation thermodynamics of the modified cyclodextrins to a large extent is caused by hydration differences. The dehydration of hydrophobic surface gives rise to enthalpy-entropy compensation and convergence temperatures around 110 °C at which the temperature-extrapolated enthalpies and entropies of complexation for a series of complexes intersect.

Resumé (Abstract in Danish)

Der gives en termodynamisk og strukturel karakterisering af inklusionskomplekser mellem cyklodextriner og galdesalte. Der kigges specielt på effekten af at have substituenter, i dette tilfælde methyl, hydroxypropyl og sulfobutyl, siddende på kanten af cyklodextrinen. Det store udvalg af undersøgte cycklodextriner karakteriseres med hensyn til antallet og placeringen af substituenter ved brug af massespektrometri og NMR. Brugen af to forskellige NMR teknikker samt molecular dynamics simuleringer giver et præcist billede af kompleksernes struktur. Bindingskonstanter for komplekserne bestemmes ved kapillar elektroforese, kalorimetri (ITC) og NMR. Tilvæksten i entalpi og entropi bestemmes for dannelsen af de fleste af komplekserne mens også ændringen i varmekapacitet bestemmes for udvalgte komplekser.
Radius af cyclodextrinen samt tilstedeværelsen af en hydroxy gruppe på C12 i galdesaltet er de væsentligste strukturelle faktorer der påvirker bindingskonstanten. Substituenternes type, antal og placering har også nogen indflydelse på bindingskonstanten omend knap så markant. Dette til trods for at substituenterne giver en øget hydrofob kontaktflade med galdesaltene. Alle typer af substituenter giver anledning til en forøget dehydrering af hydrofob overflade, hvilket fører til en kraftig forøgelse af entalpien og entropien samt et negativt bidrag til varmekapaciteten. Det konkluderes at de store ændringer i termodynamik som substituenterne giver anledning til primært skyldes hydreringsforskelle. Dehydreringen af de hydrofobe overflader giver anledning til entalpi-entropi kompensation og hypotetiske konvergenstemperaturer i omegnen af 110 °C hvor entalpi- og entropitilvæksten er den samme for alle komplekser i en given serie.

Table of contents

List of abbreviations

2D: 2-dimensional

ASA: solvent Accessible Surface Area

ACE: Affinity Capillary Electrophoresis

BS: Bile salt

CD: Cyclodextrin

CIS: Complexation Induced Shift

CMC: Critical Micelle Concentration

DS: Degree of Substitution

GC: Glycocholate

GCDC: Glycochenodeoxycholate

GDC: Glycodeoxycholate

HMBC: Heteronuclear Multiple Bond Correlation

HP: 2-hydroxypropyl

H-S compensation: Enthalpy-entropy compensation

HSQC: Heteronuclear Single Quantum Coherence

ITC: Isothermal Titration Calorimetry

mβCD: Methyl-β-cyclodextrin

NOE: Nuclear Overhauser Enhancement

ns: nanosecond(s)

ROESY: Rotating frame NOE spectroscopy

SB: Sulfobutyl

TC: Taurocholate

TCDC: Taurochenodeoxyxholate

TDC: Taurodeoxycholate

Chapter 1: Introduction

Cyclodextrins (CDs) are important pharmaceutical solubilizers due to their ability to form water-soluble inclusion complexes with a large variety of poorly soluble drugs. Bile salts (BSs) are present in the intestine and affect the release and uptake of CD-complexed drugs by competitive inclusion. To correctly model the release and uptake of CD-complexed drugs it is therefore necessary to understand the interaction between CDs and BSs, and this is the starting point for the work described in this dissertation.

CDs are often modified by attachment of various substituents, and much of the present work focuses on how the thermodynamics of complexation is affected by the presence of substituents in classes of pharmaceutically relevant CDs. Although some work has been conducted on the issue, a more comprehensive and systematic approach is required. Especially, the influence of the type, number and position of the substituents has not been fully explored so far.

In addition to obtaining binding constants to be used in the competitive modelling, the present work contributes to the understanding of non-covalent molecular interactions in aqueous solution and the associated thermodynamics. Since water is a highly abundant molecule in all living organisms, it plays a vital role for many biological functions. Thus, non-covalent interactions in aqueous solution is a highly studied subject and the present contribution is just a small drop in the sea. Nevertheless, interesting conclusions about the thermodynamics of hydration of hydrophobic molecular surfaces are proposed and discussed in Chapter 5.
On the more technical side, certain tools are developed that are useful, not only for the study of CD inclusion phenomena, but also for the general analysis of calorimetric titrations and NMR titrations. Thus, this dissertation may serve as a handbook on how these experimental techniques may be exploited to provide detailed information about the structure (Chapter 3) and thermodynamics (Chapter 4) of CD inclusion complexes, and possibly other types of intermolecular interactions.

I have not included a long review of the covered topic in a separate chapter, but I have tried to include already established knowledge at the relevant places in the

dissertation. This is usually in connection with my own results, where I relate my own work to previously published work and put things into perspective. To distinguish my own contributions from the work of others, all statements that are a result of the work of others, are clearly referenced, unless if it is common knowledge. Everything else in this dissertation should be considered the contribution of the author.

All instrumental and experimental details, including the computational details for the MD simulations, are given in the published papers in the appendix.

Section 1.1: Scope of the dissertation

To understand the structural factors governing the thermodynamics of the interaction between BSs and various natural and modified CDs, with emphasis on the influence of the substituents of the modified CDs.

Section 1.2: Acknowledgements

Thanks to my two supervisors, René Holm at Lundbeck and Peter Westh at Roskilde University. René, for coming up with great ideas for the overall project, his ever-present drive and optimism, and an always quick response to whatever question I have had. Among the contributions from Peter I would like to emphasize his great overview of the literature and valuable inputs to the interpretation of thermodynamics.

Günther Peters at the Technical University of Denmark is gratefully acknowledged for teaching me about molecular dynamics simulations and helping me setting up some of the simulations.

Jens Christian Madsen is acknowledged for helping me interpret the NMR spectra.

Many of the illustrations in the dissertation were made using the software VMD[1] (Visual Molecular Dynamics) and the molecular dynamics simulations were made using the NAMD software[2], both are free of charge. NAMD was developed by the Theoretical and Computational Biophysics Group in the Beckman Institute for Advanced Science and Technology at the University of Illinois at Urbana-Champaign.

Chapter 2: Background and motivation

This chapter gives an introduction to the fascinating world of CDs and the formation of inclusion complexes. The use of CDs as drug solubilizers is briefly reviewed and it is discussed how the presence of BSs in the intestine may affect the release and uptake of the drug. The formation of CD inclusion complexes is also interesting from a fundamental point of view since more general lessons about intermolecular interactions in aqueous solution might be learned.

Section 2.1: Cyclodextrins as host molecules

CDs are cyclic oligosaccharides consisting of glucose units linked by α-glycosidic bonds and shaped as truncated cones (Figure 1). The most common CDs are α, β, and γCD consisting of 6, 7 and 8 glucose units, respectively, but CDs comprising a larger number of glucose units have been prepared and characterized.[3] As seen on Figure 1 the hydrophilic hydroxyl groups of the glucose units are arranged at the two rims of the CD, while no polar groups are present in the interior. The combination of a hydrophobic interior and a hydrophilic exterior give CDs their ability to form water-soluble inclusion complexes with a large number of guest molecules, in which the hydrophobic part of the guest molecules is included in the cavity of the CD.[4]

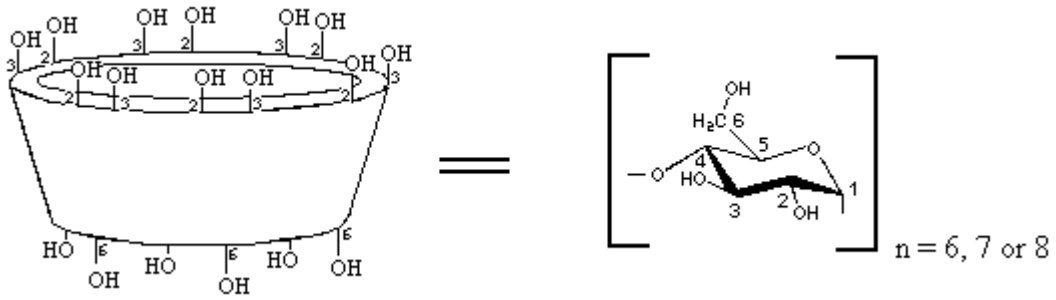

Figure 1: CDs are cyclic oligosaccharides consisting of 6, 7 or 8 glucose units.

It is generally accepted that hydrophobic interactions constitutes a major driving force for the formation of CD inclusion complexes but also van der Waals and electrostatic interactions are important.[5] The latter may significantly contribute to the complex stability of modified charged CDs binding oppositely charged guests.[6] The diameter of the CD ring increases with the number of glucose units as shown in Table 1 while the height is unaffected. The relative sizes of the CD and guest molecules strongly influence the complex stability as the hydrophobic part of the guest molecule must be

small enough to fit into the cavity and large enough to secure a tight fit in order to maximize van der Waals interactions. Consequently, straight chain aliphatic guests prefer αCD over βCD while cyclic and aromatic guests form more stable complexes with βCD.[4] Adamantane derivatives and BSs (Figure 3) seem to have the perfect shape and size to fit into the cavity of βCD.[4,7]

Table 1: Dimensions and solubilities of unmodified CDs. Adapted from Szejtli, 1998.[8]

	αCD	**βCD**	**γCD**
No. of glucose units	6	7	8
Diameter of cavity, Å	4.7 - 5.3	6.0 – 6.5	7.5 – 8.3
Height, Å	7.1	7.1	7.1
Volume of cavity, $Å^3$	ca. 174	ca. 262	ca. 427
Aqueous solubility, g/100 ml	14.5	1.85	23.2

Section 2.2: The use of cyclodextrins as drug solubilizers

The ability of CDs to form water-soluble inclusion complexes make them suitable for use as pharmaceutical solubilizers. That is, they may increase the aqueous solubility of poorly soluble drugs through the formation of inclusion complexes. The need for suitable pharmaceutical solubilizers is illustrated by the fact that 40% of all drugs on the market are poorly soluble in water and 90% of the drugs in development are characterized as such.[9] In 2010 around 35 drug products on the market contained CDs.[9]

To qualify as a drug solubilizer the CD must fulfil certain physico-chemical requirements: It must form a sufficiently strong complex with the drug molecule and both the solubility of the CD itself as well as the solubility of the complex must be satisfactory. The use of unmodified, or natural, βCD is limited by its modest aqueous solubility (see Table 1). Replacing some of the hydroxyl hydrogens at the rim of the CD with various short-chain substituents in many cases result in a dramatically increased solubility,[10] even when the substituents are nonpolar methyl groups. A vast number of modified CDs containing different substituents have been synthesized, but for pharmaceutical purposes the most commonly used CDs are methylated, 2-hydroxypropylated and the negatively charged sulfobutylated CDs (Figure 4).

The use of cyclodextrins may complicate the absorption kinetics. Only the non-complexed form of the drug can penetrate the intestinal wall, and the bioavailability of the drug may thus be severely reduced if the drug is strongly bound in the complex, as demonstrated by *in vivo* experiments.[11] There are thus several considerations to take into account when deciding on the type and amount of CD to be used in the drug formulation.

Section 2.3: Bile salts affect drug release

The rate of uptake of the drug depends on the concentration of free drug in the intestine, which to a first approximation can be predicted from the stability constant of the drug:CD complex and the concentrations of the complexing species. However, the presence of other molecular species with an affinity for CDs will complicate the situation as these will compete with the drug for the CDs, as illustrated in Figure 2. This may actually be an advantage as the competing species to some extent will liberate the drug, depending on the relative affinities and concentrations of drugs and competitors.

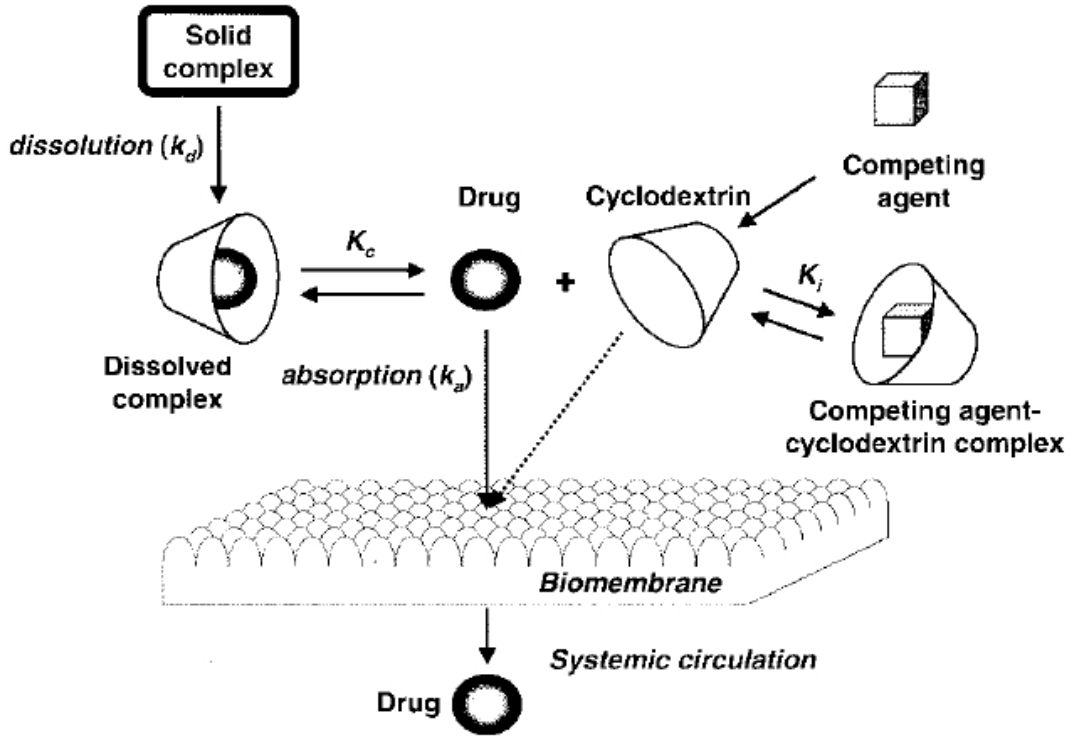

Figure 2: Only the free drug is available for uptake through the intestinal wall. The presence of competing agents shifts the equilibrium towards the free drug. Copy of Figure 5 in Uekama *et al.*, 1998.[12]

BSs are present in significant amounts in the small intestine[13,14] and are known to form stable inclusion complexes with both natural and various modified CDs,[7,15-18] except αCDs which are too small to provide a sufficient inclusion.[19] It is therefore a reasonable assumption that BSs will promote release of the drug, and this is supported by the observation that ligation of the bile duct (severing the bile duct to stop supply of BSs to the intestine) in rats reduces the bioavailability of ibuprofen co-administered with βCD.[20]

Bile salts constitute a large family of molecular structures sharing a steroid-like body (see Figure 3). The abundance of the various bile salts differ among animal species, but in rat, dog or man, which are of pharmaceutical interest, the seven bile salts in Figure 3 are present.[21] The only structural differences between these bile salts are the position of hydroxyl groups on the steroid body, and the tail which is conjugated with either taurine or glycine.

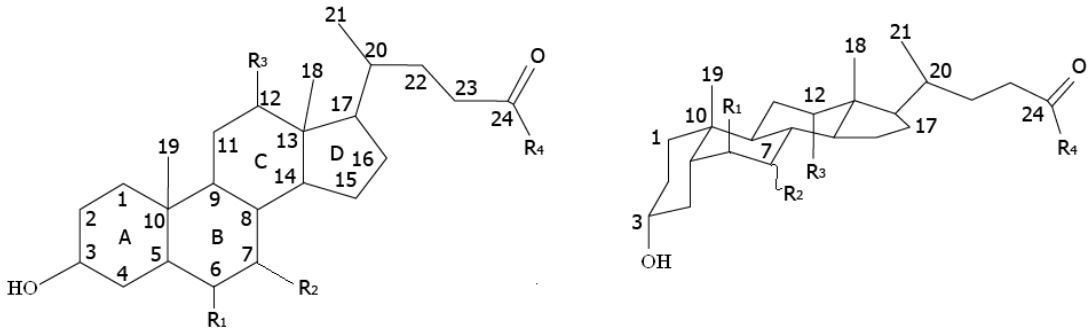

Bile salt anion	Abbreviation	R_1 (C6)	R_2 (C7)	R_3 (C12)	R_4 (C24)
Taurocholate	GC	H	OH	OH	$NHCH_2CH_2SO_3^-$
Glycocholate	TC	H	OH	OH	$NHCH_2COO^-$
Taurodeoxycholate	TDC	H	H	OH	$NHCH_2CH_2SO_3^-$
Glycodeoxycholate	GDC	H	H	OH	$NHCH_2COO^-$
Taurochenodeoxycholate	TCDC	H	OH	H	$NHCH_2CH_2SO_3^-$
Glycochenodeoxycholate	GCDC	H	OH	H	$NHCH_2COO^-$
Tauroβmuricholate	TβMC	OH	OH	H	$NHCH_2CH_2SO_3^-$

Figure 3: Sketch of the seven bile salts present in rat, dog or man. The hydroxyl on C7 is either equatorial as in TβMC or axial as in the other BSs.

Due to the orientation of the hydroxyl groups, one side of the steroid body is hydrophobic while the other is hydrophilic and BSs therefore form micelles in aqueous solution at concentrations above the critical micelle concentration (CMC). In pure water the CMC is 12, 6 and 6 mM for GC, GDC and GCDC, respectively, and 10, 6 and 7 mM for the corresponding tauroconjugated ones, but decreases

considerably in the presence of 0.15 M Na^+.[22] This complicates the calculation of free drug further, as it might be necessary to include the equilibrium between micellized and free BS in the competitive model.

Section 2.4: Understanding molecular assembly processes in aqueous solution.

Only a relatively small part of the CD research is driven by pharmaceutical interest and CDs have potential applications in many other areas. A thorough understanding of how the substituents influence the ability of CDs to form complexes with various guest molecules might make it possible to tailor CDs for specific purposes. The systematic variation in the type, number and position of the substituents of the CDs employed in the present study will contribute to this understanding.

Only the binding constants are of direct interest for pharmaceutical and most other applications, but isothermal titration calorimetry (ITC) provides more thermodynamic information in the form of enthalpies and entropies of complexation and also the change in heat capacity if the experiments are conducted at different temperatures. These thermodynamic functions provide a more complete picture of the molecular association process and may thereby assist the understanding of the forces driving molecular assembly in aqueous solution.

Chapter 3: Structural characterization of cyclodextrins, bile salts and their complexes

A successful investigation of the relations between the structure and thermodynamics of the CD-BS interactions requires a detailed structural characterization of the interacting molecules. All of the investigated samples of CDs and BSs were purchased from commercial vendors and were used without further purification. The BS samples were of minimum 97% purity and each sample consisted of only one type of structurally well-defined molecule. The samples of modified CDs, however, were mixtures of CDs with different degrees and patterns of substitution. These samples required a thorough characterization in order to draw any valid conclusions on the relations between structure and complexation thermodynamics.

In addition to the characterization of the free molecules, the present chapter also focuses on the structures of the complexes, which are determined by NMR.

Section 3.1: Characterization of cyclodextrins

3.1.1 Types of investigated CDs

The natural CDs may be modified by replacing the hydroxyl hydrogens on O2, O3 and O6 (Figure 1) with various substituents. The most common substituents are methyl-, 2-hydroxypropyl- and the negatively charged sulfobutyl-groups, as shown in Figure 4. Although it is possible to synthesize mixed CD derivatives in which different substituents are attached to the same CD molecule,[23-25] the vast majority of commercially used CDs contain only one type of substituent.

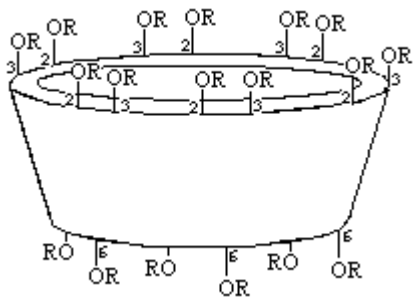

	Structure of substituent	Name of CD
R = H	**a**	
and/or:	CH_3	mβCD
	a b c	
	$CH_2CH(OH)CH_3$	HPβCD
	a b c d	
	$CH_2CH_2CH_2CH_2SO_4^-$	SBβCD

Figure 4: Structures and names of modified βCDs and labelling of the nuclei on the substituents. See Figure 1 for labelling of CD nuclei. Most modified CDs are partially substituted and the substituents are distributed among the 3 substitution sites, O2, O3 and O6.

In most modified CDs only a fraction of the hydroxyl hydrogens are substituted. The degree of substitution (DS) denotes the number of substituents per glucose unit such that a mβCD of DS 1 contains 1 methyl group per glucose unit which is equal to 7 methyl groups per βCD. In the present work I have investigated the interaction of BSs with natural α-, β- and γCDs as well as some of their modified analogues. Most emphasis has been put on the βCDs for which hydroxypropylated, methylated and sulfobutylated CDs were investigated. Additionally, a large number of differently substituted HPβCDs and mβCDs were investigated to determine how the complexation thermodynamics is influenced by the DS as well as the site of substitution. All investigated CDs appear from Table 3. In the following, each CD sample is systematically named according to the number of glucose units (α, β or γ), the type of substituent (m, HP or SB) and the DS. For example, mβ067 is a sample of methylated βCD of DS 0.67.

3.1.2 Most CD samples are mixtures

The synthesis of modified CDs produces CD samples that are mixtures of a large number of differently substituted CDs. On each glucose unit there are three substitution sites (O2, O3 and O6) and a βCD thus contain 21 sites. Distributing e.g. 7 substituents randomly among these 21 sites yields a large number of different isomers. To complicate the situation further, MALDI-TOF mass spectrometry of the HPβCD and mβCD samples revealed that each of the samples contained a mixture of CDs of various DS (Paper I and II). In most samples the distribution of CDs of different DS resembled a gaussian distribution (Figure 5), although a few exceptions were found (Figure 6). The only samples that are not mixtures are the natural (i.e. un-modified) CDs and the fully methylated βCD.

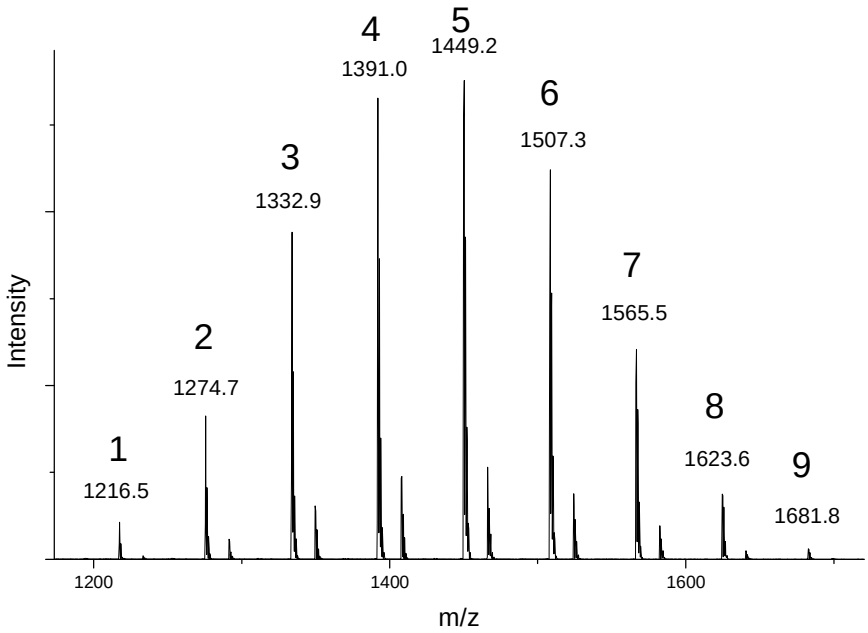

Figure 5: Mass spectrum of a moderately substituted HPβCD (HPβ063, see Table 3). The masses and the number of HP substituents are written above each peak. The largest peaks correspond to Na^+ adducts while the smaller peaks are the K^+ adducts.

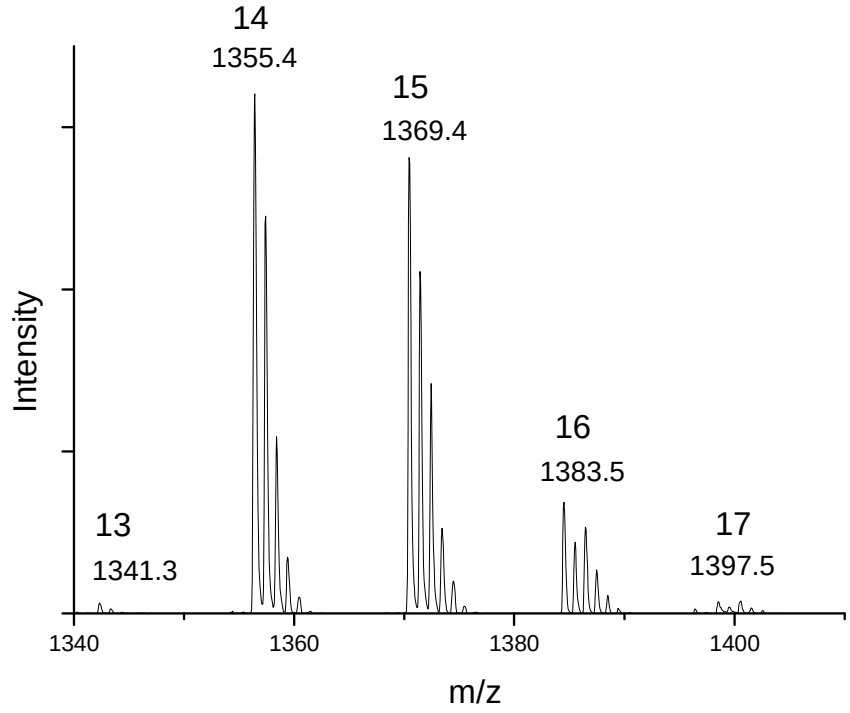

Figure 6: Mass spectrum of a highly methylated βCD (mβ209, see Table 3). The masses and the number of methyl substituents are written above each peak. The largest peaks correspond to Na^+ adducts while the peaks of the K^+ adducts coincide with the third isotope peak of the higher substituted CD.

From an academic point of view it would be preferable to run all experiments with pure samples containing only a single kind of CD, but from a practical point of view it is interesting to investigate the properties of the mixed samples as these are the ones being used for practical purposes (e.g. drug delivery). Although it is possible to synthesize pure samples of mβCDs where one or more of the three sites are per-substituted,[26] it is also relevant to study the mixed samples that contain CDs that are only partially substituted at each of the three sites. These are unfortunately not available as pure samples.

The term "DS" will in the following denote the *average* DS of the CD samples, irrespective of whether it is a pure or mixed CD sample. Likewise, the number of substituents at each of the three sites will also be an average value.

3.1.3 Degree of substitution

The DS of the CD samples were determined by NMR and/or mass spectrometry. Under the assumption that the spectrometer is equally sensitive towards all CDs in the sample, the DS is calculated as:

$$DS = \frac{\sum_i I_i \cdot DS_i}{\sum_i I_i} \qquad [3.1]$$

"I_i" and "DS_i" denotes the intensity and the degree of substitution of the i'th peak, respectively. The calculated DS of all CD samples are found in Table 3.

The DS may also be determined from the NMR spectra. As shown on Figure 7 the spectra of modified CDs are more complex than those of the natural CDs. The peaks are considerably broadened due to the large number of different glucose derivatives in the sample, and new peaks appear. Modified CDs contain glucose units with both substituted and unsubstituted sites, leading to a doubling of some peaks. If e.g. a HP-substituent is located at O2 the peaks of H2 and C2 are shifted 0.15 ppm upfield and 8.5 ppm downfield, respectively (Paper I). These new peaks are denoted $H2_{sub}$ and $C2_{sub}$ (see Figure 7 and Figure 8). Also the peaks of nuclei next to a substituted site experience shifts, although somewhat smaller. Upon HP-substitution of O2 the peaks of H3 and C3 are shifted 0.1 ppm downfield and 0.8 ppm upfield, respectively, and these new peaks are denoted H3' and C3' (Paper I). Similar changes in the chemical shifts are observed upon substitution of the other two sites (O3 and O6), irrespective

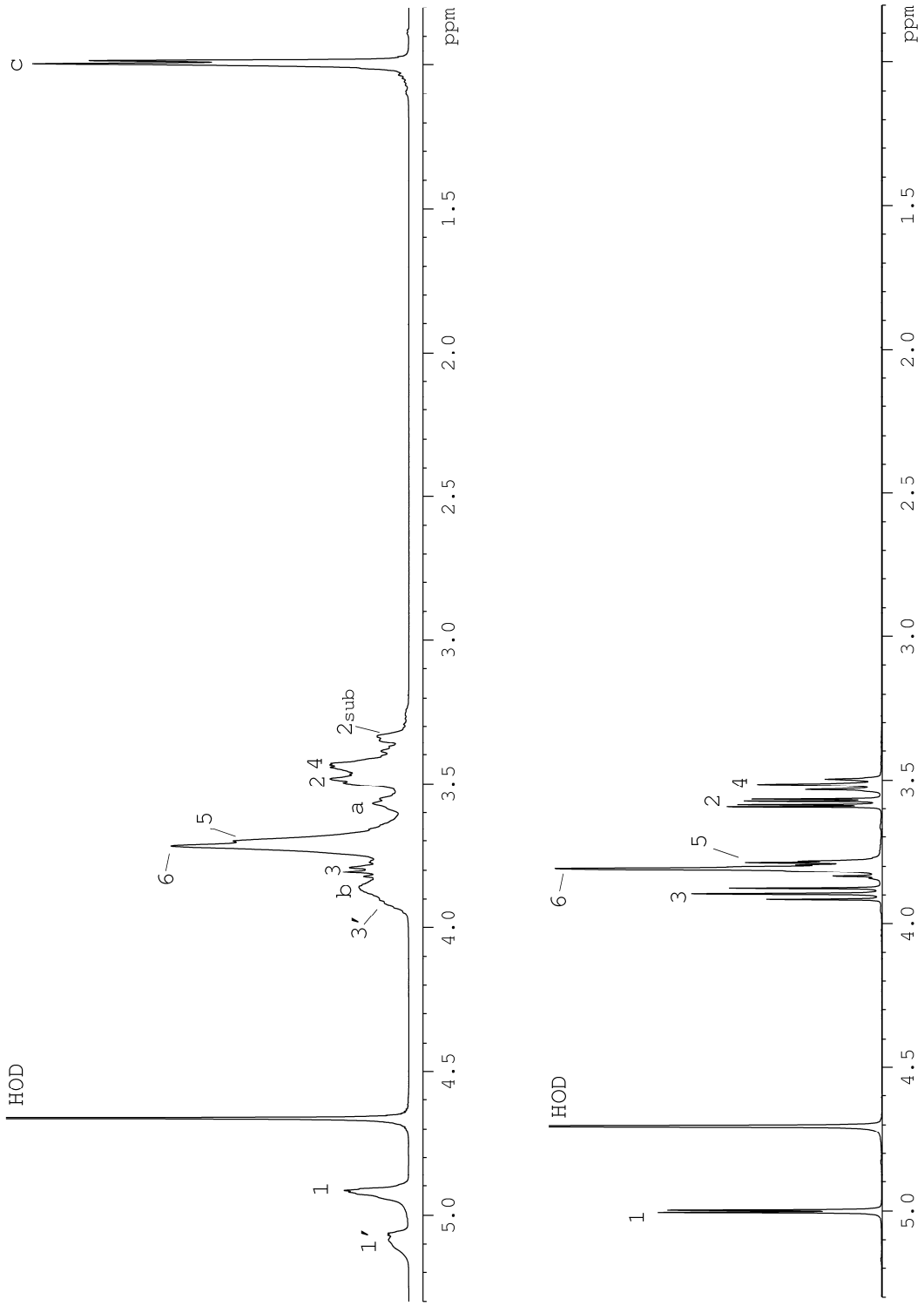

Figure 7: ^{1}H NMR spectrum of βCD (right) and HPβ063 (left). Nuclei at a substituted site are denoted by a subscript (N_{sub}) while neighbouring nuclei are denoted by a ‘ (N’). Confer Figure 1 and Figure 4 for labelling of the nuclei.

of whether the substituent is a methyl, HP or SB group (Paper I, II and VI). These changes can more or less be predicted from table values of increments in chemical shifts upon replacing a hydroxyl group with an ether (see tables A6.1 and A8.3 in Pavia *et al.*[27]) and have previously been observed in similarly substituted CDs.[23]

The areas of these new peaks may be exploited to determine the DS (Paper I and II). This can often be done in several ways using different peaks, depending on how well the peaks are separated. This is illustrated in the following where the DS of the HPβCDs are determined from the ^{1}H-NMR spectra in three different ways:

Method 1: The combined areas of H1 and H1' integrates 1H (1 proton per glucose unit), and the methyl group of the HP-chain (Hc) integrates 3H*DS. This leads to the following equation:

$$DS = \frac{A_{Hc}}{3\left(A_{H1} + A_{H1'}\right)} \qquad [3.2]$$

Method 2: The large peak in the middle of the ^{1}H spectrum in Figure 7 integrates the 6 CD protons (H2, H3, H4, H5 and the two H6 protons) plus the two Ha´s and the single Hb on the HP-chain. If the area of this peak is denoted A_{large}, we have that:
A_{large} = 6H + 3H*DS
Compared to the area of the Hc peak which integrates 3H*DS, the DS can be calculated:

$$DS = \frac{2A_{Hc}}{A_{large} - A_{Hc}} \qquad [3.3]$$

Method 3: Alternatively, A_{large} can be compared to the combined areas of H1 and H1':

$$DS = \frac{A_{large} - 6\left(A_{H1} + A_{H1'}\right)}{3\left(A_{H1} + A_{H1'}\right)} \qquad [3.4]$$

The results are summarized in Table 2. All 3 methods place the HPβCDs in the same order, but method 3 yields slightly larger values of DS than the two other methods. I assess method 2 to be the most reliable since it does not rely on the H1 peaks which are small and close to the water peak. These values will be used in the following.

Table 2: DS of the investigated HPβCDs determined from the ^{1}H NMR spectra by using the areas of different peaks.

	Method 1	Method 2	Method 3
HPβ054	0.559	0.542	0.624
HPβ063	0.626	0.627	0.626
HPβ082	0.837	0.818	0.883
HPβ102	1.052	1.022	1.109
HPβ106	1.094	1.060	1.157

3.1.4 Identifying the pattern of substitution

Not only the total degree of substitution but also the pattern of substitution is of relevance to the complexation properties of CDs. Two of the substitution sites (O2 and O3) are located at the wider rim of the CD while the substitution site at O6 is located at the narrow rim (Figure 4). As the BSs enter the CD from the wider opening,[7] it is not hard to imagine that a substituent at O6 will affect the complexation differently than a substituent at O2 or O3. To assist the identification of substitution sites, several NMR techniques were employed. An associated proton test (APT) is a ^{13}C spectrum in which the peaks of methyl and methine carbons are positive while the peaks of methylene and quarternary carbons are negative. A 2-dimensional (2D) Heteronuclear Single Quantum Coherence[28] (HSQC) spectrum shows the normal 1D ^{1}H spectrum along one axis and a ^{13}C spectrum along the other. Protons and ^{13}C nuclei linked by a single bond give rise to correlation peaks and the ^{13}C peaks can thus be assigned if the attached protons are identified, and *vice versa*. 2D Heteronuclear Multiple Bond Correlation[29] (HMBC) is a similar technique in which ^{1}H and ^{13}C nuclei separated by two, three or four bonds results in correlation peaks. A 2D H2BC[30] spectrum only shows couplings through two bonds. The application of these techniques expands the usual 1D spectra into 2 dimensions and thus reduce problems with assigning overlapping peaks. Further, the connectivities between the nuclei are established, which is a great help in the assignment of the peaks.
An example of overlaid HSQC and HMBC spectra of a mβCD are shown in Figure 8.

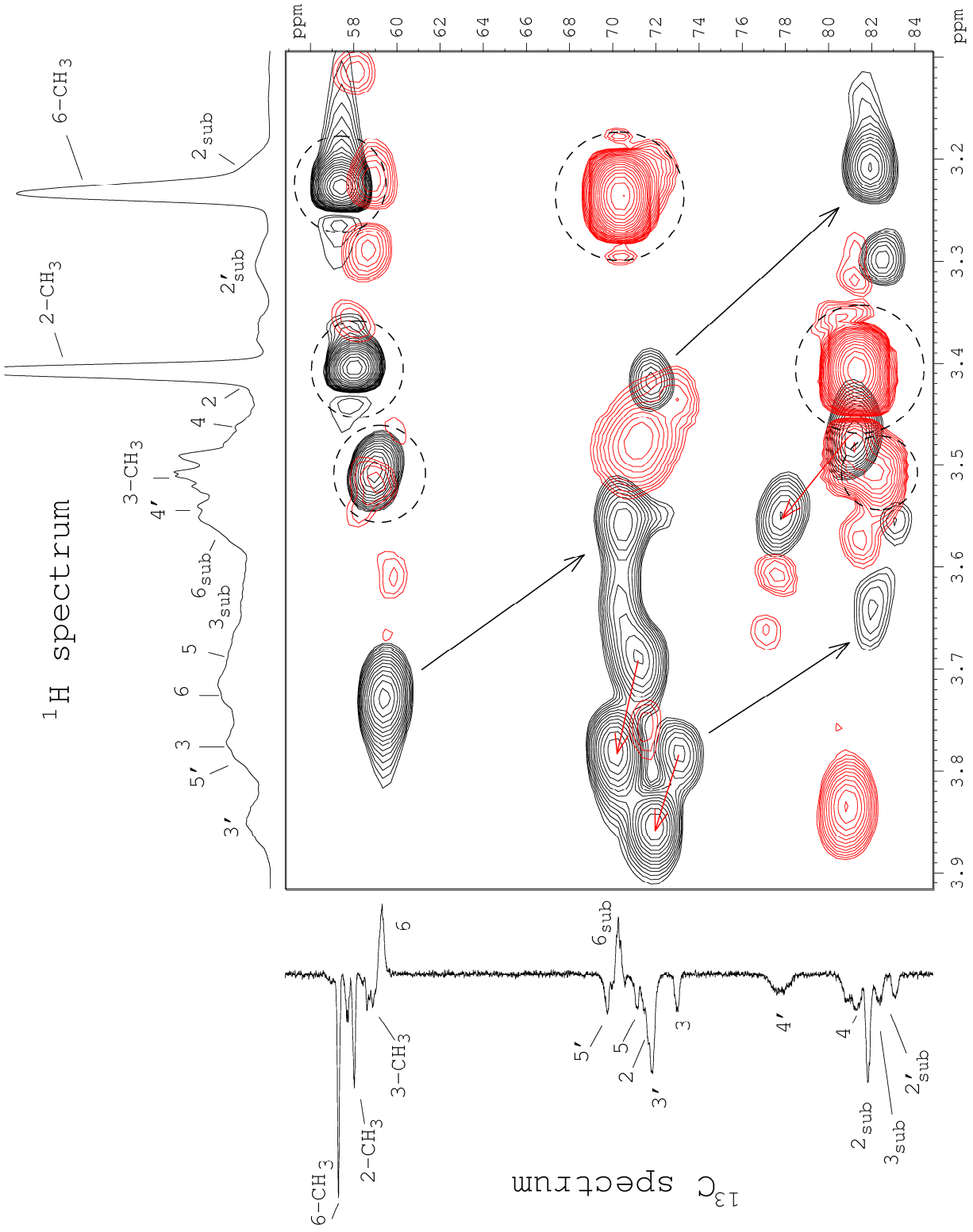

Figure 8: Partial overlaid HSQC (black) and HMBC (red) spectra of a methylated βCD (mβ167, see Table 3). The three black arrows show the changes in chemical shifts induced by direct methylation, while the three red arrows show the effects on nuclei next to a methylated site. The encircled red peaks show the 3-bond HMBC correlations between the carbons at the substituted sites and the protons of the methyl substituents. The encircled black peaks show the HSQC correlations of the methyl substituents.

Strong HSQC correlations are observed between the protons and the carbons of the methyl substituents. The nuclei of the substituted sites are easily identified by the strong 3-bond HMBC correlations between the ^{13}C nuclei of the substituted sites ($C2_{sub}$, $C3_{sub}$ or $C6_{sub}$) and the protons on the methyl substituents. In the present example these correlations prove that all three sites are substituted. The nuclei of the unsubstituted sites are also identified, thereby showing that each of the sites is only partially substituted. As mentioned above, substitution shifts the peaks of the substituted site but also the peaks of neighbouring nuclei. These characteristic shifts are indicated by black and red arrows in Figure 8.
The example in Figure 8 is recorded on a 10 mM solution of a highly methylated βCD, but the same features are seen in the spectra of HPβCDs and SBβCDs.

The HSQC, HMBC and H2BC spectra enable a reliable assignment of the relatively complicated spectra of modified CDs and provide *qualitative* information about the pattern of substitution. *Quantitative* information about the substitution pattern can be obtained from the peak areas in the 1D ^{1}H and ^{13}C spectra. As mentioned above, partial substitution at O3 splits H1 into two relatively separated peaks corresponding to a substituted and an unsubstituted glucose unit and the DS at O2 (DS(O2)) is readily obtained from the relative areas of these two peaks. Just like the DS denotes the average number of substituents per glucose unit, so does DS(O2) denote the average number of substituents on O2 per glucose unit. Theoretically, DS ranges from 0-3 and DS(O2), as well as DS(O3) and DS(O6), ranges from 0-1.
For all characterized cyclodextrins DS(O2) were readily determined from the relative peak areas of H1 and H1', but DS(O3) and DS(O6) could not always be determined that easily due to the absence of suitable well-separated peaks in the ^{1}H spectra. Thus it was necessary to use the ^{13}C peaks which are better separated but suffer from low signal-to-noise ratio. Further, one should be cautious using ^{13}C peak areas for quantification, as the intensities depend on the Nuclear Overhauser Enhancement (NOE) and the relaxation times. Since the NOE and the relaxation times depend on the number of hydrogens attached to the carbon and its molecular environment, the peak area does not only reflect the abundance of that particular carbon. However, the areas of chemically similar carbons may be compared, such that the areas of *e.g.* C6 and $C6_{sub}$ can be compared to obtain DS(O6). Similarly, the areas of methyl substituents at the three different sites may be compared. The latter are reasonably

well separated to be used for the determination of the relative distribution of substituents in the methylated CDs (see the 1D ^{13}C spectrum in Figure 8). This relative distribution is converted to DS(OX) (X = 2,3 or 6) using the total DS as determined by NMR or MS.[i] The low signal-to-noise ratio of the ^{13}C spectrum and the partial overlap of some peaks introduce some error into the DS(OX), but the numbers are validated by calculating DS(OX) from several other peak areas. For example, DS(O2) may be estimated from the peak areas of H1 vs H1', C1 vs C1' or the methyl carbon attached to O2.
The total DS and DS(OX) for all characterized CDs are presented in Table 3 along with the DS reported by the supplier. In general, there is agreement between reported and experimentally determined values.

The HPβCDs pose a special problem, since it is not possible to determine the site of substitution for all substituents. The total DS and DS(O2) are both rather precisely determined from the ^{1}H spectra and approximately 50% of the substituents are attached to O2, but none of the typical characteristics for substitution at O3 and O6 are observed. So where are the remaining 50% of the HP-substituents located? Although it has been reported that HP-groups to a small extent may oligomerize such that a HP-chain is attached to the hydroxyl oxygen of another HP-chain,[31] it is not likely that this is the case for all of the "missing" HP-chains. It is more likely that the characteristic peaks and correlations associated with substitution at O3 and O6 are too broad and weak to be detected. A previous thorough analysis of the substitution pattern of HPβCDs revealed that 55-60% of the substituents were located at O2, 30% at O3 and 15% at O6,[10,31] while a more recent study revealed that slightly more than 50% were located at O2 and the rest were equally distributed among O3 and O6, when synthesized under weak alkali conditions.[32] Similar distribution patterns are expected for my samples.

[i] For the methylated samples, the total DS determined by MS is considered more reliable than the DS determined by NMR, and the former is used. In contrast to the NMR spectra of the HPβCDs where the Hc peak is completely separated and is used for precise determination of DS, the methyl Ha in the methylated samples overlaps with many other peaks and can not be used.

Table 3: Degree and pattern of substitution of all characterized CD samples. For the HPβCDs it was not possible to determine DS(O3) and DS(O6).

CD	DS (Supplier)	DS (MS)	DS (^{1}H NMR)	DS(O2)	DS(O3)	DS(O6)
αCD	0	-	0	0	0	0
HPα	~ 0.6	-	-	-	-	-
βCD		-	0	0	0	0
mβ067	0.6	0.67	0.44	0.38	0.19	0.10
mβ069	0.57	0.69	0.63	0.52	0.12	0.05
mβ117	1.2	1.17	1.03	0.59	0.33	0.25
mβ163	-	1.63	1.28	0.62	0.34	0.67
mβ167	1.8	1.67	1.50	0.63	0.37	0.67
mβ209	2	2.09	1.90	1.00[a]	0.09[a]	1.00[a]
mβ212	2.16	2.12	1.95	1.00[a]	0.12[a]	1.00[a]
mβ300	3	3.00	2.99	1.00	1.00	1.00
HPβ054	~ 0.4	0.59	0.54	0.32	-	-
HPβ063	0.58	0.67	0.63	0.36	-	-
HPβ082	0.8	0.95	0.82	0.48	-	-
HPβ102	0.99	1.05	1.02	0.55	-	-
HPβ106	1.03	1.09	1.06	0.57	-	-
SBβ091	-	-	0.91	~ 0.4	~ 0.5	~ 0.1
γCD	0	-	0	0	0	0

a: The mass spectrum shows a large peak corresponding to 14 methylsubstituents and a few smaller peaks with a larger number of substituents. Since the NMR spectra shows no signs of unsubstituted O2 and O6, it is assumed that the large peak corresponds to heptakis(2,6-di-*O*-methyl)-βCD and that the additional methyl substituents on the higher substituted CDs in the sample must be attached to O3.

Section 3.2: Characterization of bile salts

Unlike most of the CD samples, all of the BS samples are pure samples consisting of only one kind of structurally well-defined molecule. Thus, there is no need for a structural characterization. What is required, however, is an assignment of all nuclei seen in the ^{1}H and ^{13}C NMR spectra. This assignment will form the basis for the structural characterization of the complexes (Section 3.3) but will also be used in the determination of binding constants by NMR titration (Section 4.1).

The type of conjugation on the BSs (taurine or glycine, see Figure 3) only has a slight influence on the binding affinities (Paper I and II). Recent work also shows that the topology of the complexes with natural βCD[7] as well as with mβCD and HPβCD[15] is

unaffected by the type of conjugation. This is not always the case, however. Attachment of a single glycine or aminobutanol group to the primary rim of βCD, from which the BS conjugation protrudes, results in significantly enhanced discrimination between glycine and taurine conjugated BSs.[17] Also bridged bis-βCDs, linked through the primary rims, show significant selectivity.[33] For the CDs investigated in the current work, it seems safe to assume that the type of conjugation is insignificant, and therefore only complexes with the three glycoconjugated BSs were structurally characterized.

Due to the large number of chemically similar nuclei in the BSs, a large degree of peak overlap is observed in the ^{1}H NMR spectra, as seen in the top projection in Figure 11. The peaks are much better separated in the ^{13}C spectrum where only a few peaks overlap, and the combined use of HSQC, HMBC and H2BC spectra allows for an assignment of all ^{13}C and ^{1}H nuclei, which is in agreement with previous assignments.[15,34,35]

Section 3.3: Structural characterization of complexes

The structures of the complexes have been elucidated by two different NMR approaches. The first is the widely used 2D ROESY NMR (rotating-frame NOE spectroscopy). The 2D ROESY spectrum is recorded on a solution containing the molecular complex and shows the usual 1D ^{1}H spectrum along each axis. In contrast to the above mentioned 2D techniques, which show correlations through bonds, a ROESY spectrum shows correlations through space. That is, nuclei which are close to each other (but not necessarily linked through bonds) give rise to correlation peaks, with intensities proportional to $\langle r^{-6} \rangle$, where r is the internuclear distance and <..> denotes the average value.[36] The strong distance-dependence means that only nuclei which are close to each other, typically less than 4 Å, give rise to correlation peaks.[37] In the present work a semi-quantitative approach, in which ROESY interactions were classified as very strong, strong, medium, weak or very weak, was used to derive the structure of the complexes.

The second experimental approach exploits the fact that the chemical shifts of nuclei depend on their immediate environment. Moving a BS from the aqueous phase into the cavity of a CD will change the chemical shifts of the nuclei included in the non-

polar CD cavity. These changes in the chemical shifts are termed Complexation Induced Shifts (CIS):[37]

$$CIS = \delta_{complexed} - \delta_{free} \qquad [3.5]$$

From the observation of which nuclei that experience the largest CIS one may deduce which part of the guest molecule that is included in the CD cavity. This technique has previously been successfully applied to resolve the topology of BS:CD complexes.[15,38-42] In principle, CIS of both ^{1}H and ^{13}C nuclei can be used, but due to the large overlap of ^{1}H peaks, the present work only deals with CIS of ^{13}C nuclei. It should be noted that the apparent value of $\delta_{complexed}$ was determined from solutions containing 10 mM BS and 10 mM CD. If the binding constant is low, *e.g.* 2000 M^{-1}, only 80% of the molecules are bound in the complex and the observed CIS will only be 80% of the value defined in equation 3.5. In the following, this will be accounted for by using the binding constants in Table 4 to calculate the real extrapolated CIS. In the case of the GDC:βCD complex, the CIS were obtained as fitting parameters from the NMR titration (Section 4.1).

3.3.1 Complexation induced shifts of bile salt nuclei

CIS of ^{13}C nuclei in BSs complexed with natural βCD and γCD are illustrated with colors in Figure 9. The measured CIS values are found in Paper II and V.

Several interesting observations are worth mentioning:

i) The binding modes of βCD towards all three BSs are strikingly similar. GDC possess a secondary binding site for βCD on the A-ring but the primary binding site on the D-ring and parts of the sidechain (see Figure 3), is almost identical to the binding sites on GC and GCDC. However, there are slight differences in the CIS patterns. When comparing the CIS of nuclei on the BS sidechain (C20-C24), somewhat larger values are observed for GC and GDC compared to GCDC. This indicates that the βCD resides on the sidechain of GC and GDC for a larger fraction of the time than in GCDC where the βCD has a larger affinity for the D-ring. This slight difference in binding mode is due to the absence of a hydroxyl group on C12 in GCDC.

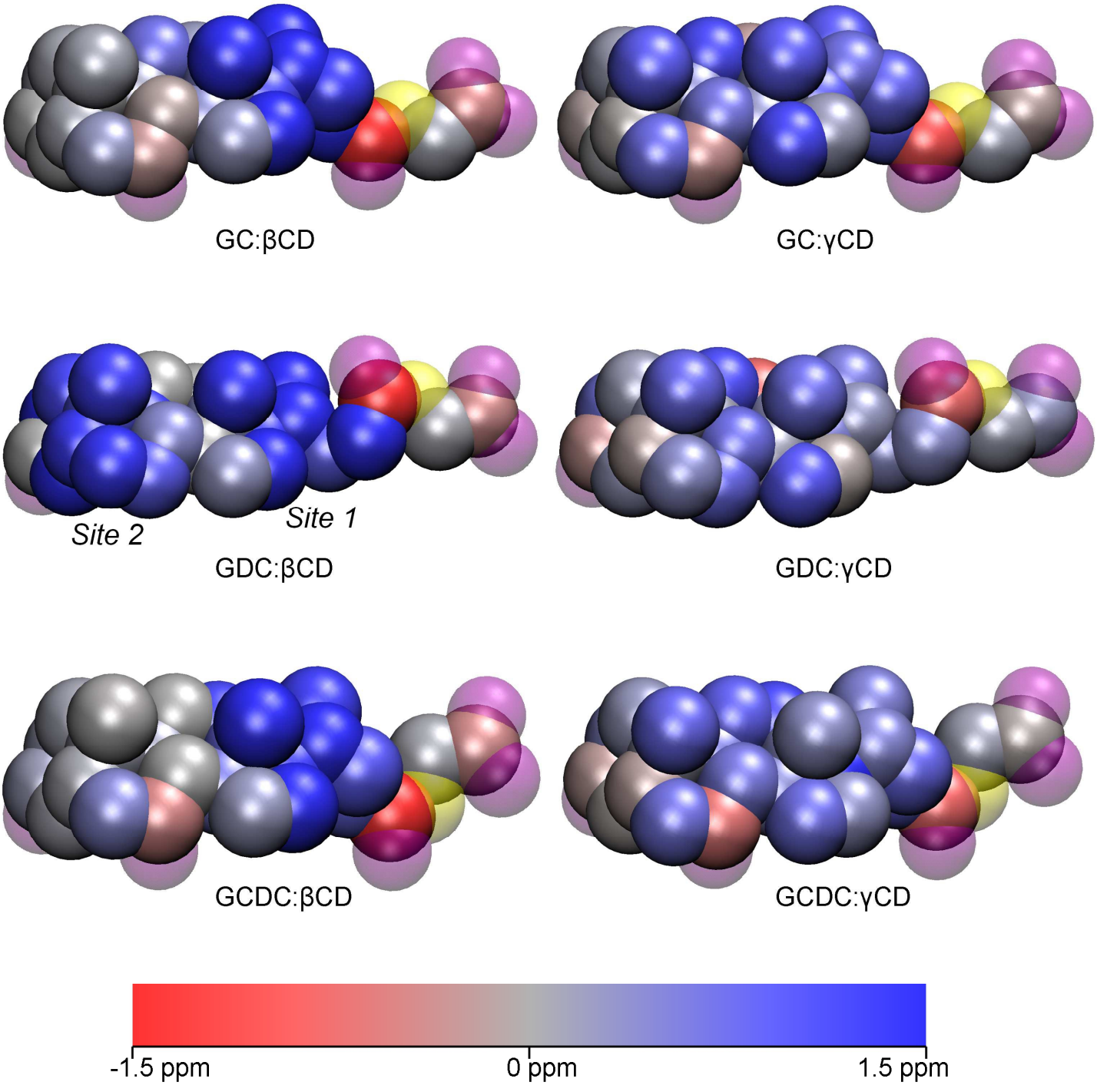

Figure 9: Illustration of CIS of ^{13}C nuclei in BSs complexed with natural βCD and γCD. Carbon atoms are shown as opaque van der Waals spheres while oxygen atoms are shown as pink transparent spheres and nitrogen as yellow transparent spheres. The CIS of the carbon atoms are shown using the color scale in the bottom of the figure. Some carbons exceed the limits of the scale. For a few carbons no CIS could be determined and they were given the CIS value 0. The order of the primary and secondary binding sites in the GDC:βCD complex was determined by NMR titration (Section 4.1).

ii) In general, the binding of γCD to the BSs induces smaller CIS than the binding of βCD, but more nuclei are affected. Especially the nuclei on the B- and C-rings are affected by γCD whereas the nuclei at the D-ring and the sidechain are affected to a smaller extent than for complexation with βCD. This leads to the interpretation that γCD, due to its larger diameter, can encroach further onto the steroid body of the BS. In contrast, βCD experiences steric hindrances as it tries to move from the D-ring onto the C-ring. The smaller CIS experienced for complexation with γCD are probably due to the shuttling back and forth of the γCD on the BS, thus resulting in a smaller time-averaged CIS.

iii) The CIS pattern does not reveal any significant differences in the binding modes of γCD towards the three BSs.

iv) The illustrations in Figure 9 clearly show that the CIS of non-polar carbons (defined as carbons bound to only hydrogen or carbon) always experience positive CIS while polar carbons (bound to either nitrogen or oxygen) experience negative CIS. The carbonyl carbon, C24, typically experience CIS of around -2.5 ppm for complexation with βCD. We observed the same trends for complexes with methylated βCDs. Obviously, the transfer of the BS from the polar aqueous environment into the non-polar cavity of the CD has different effects on the electron density around polar and non-polar carbons. These observations may be rationalized in the following way: In aqueous solution, the electron lone pair on the carbonyl oxygen is involved in hydrogen bonding, thus pulling the electron cloud away from the carbonyl carbon. As the hydrogen bonds are severed upon inclusion in the CD, the electrons flow back and shield the carbon, resulting in negative CIS. It is a little harder to rationalize the positive CIS experienced by the non-polar carbons since nonpolar groups are not expected to interact with the water molecules. Nevertheless, if the hydrogens on non-polar carbons are assumed to form weak hydrogen bonds with the water oxygens, the electrons around the hydrogen nucleus is repelled by the lone pair on oxygen and pushed back towards the carbon, resulting in a higher electron density. Upon complex formation this electron density flows away and the carbons are deshielded, leading to positive CIS.

The assumption that the CIS of the BS nuclei are primarily caused by the transfer from a polar to a non-polar environment, and not by other factors such as changes in bond lengths and bond angles, is supported by the much smaller CIS observed for the inclusion of another BS into HPβCD in the less polar solvent methanol.[38]

The CIS of BS nuclei induced by complexation with three different samples of mβCDs (mβ167, mβ209 and mβ300, see Table 3) were also recorded (Paper II). In general, the CIS are larger than for complexation with natural βCD, possibly due to the more hydrophobic cavity of the mβCDs, but the patterns suggest binding modes that are very similar to the natural βCD, including the formation of 2:1 CD:BS complexes with GDC. mβ300 is an exception and may not bind significantly to GDC and GC. The chemical shifts of GC nuclei in the solution containing 10 mM of GC and mβ300 are only slightly different from those of the free BS, suggesting the formation of a very weak complex. Conversely, the chemical shifts of almost all GDC nuclei in the solution containing the GDC:mβ300 mixture are quite different from the free GDC (Paper II). These apparent CIS could be caused by formation of GDC micelles instead of complex formation. If the binding of GDC to mβ300 is weak, as indicated by experiments (Paper II), only a small fraction of the GDC molecules are bound to the CD and the concentration of non-complexed BSs will exceed the critical micelle concentration. NMR experiments indicate that micelles of GDC start forming at concentrations above 1.5 mM (Paper IV).

The main structural effect of methylating the βCD, as judged from the CIS, seems to be an extension of the hydrophobic cavity upon methylation at O3. In Figure 10 the CIS for complexation of GCDC with mβ209 (methyl groups at O2 and O6) and mβ300 (methyl groups at O2, O3 and O6) are illustrated. This CIS pattern for complexation with mβ209 is very similar to the corresponding complex with natural βCD, but more nuclei are affected by complexation with mβ300, especially C11 and C15, which are hardly affected by complexation with βCD or mβ209. The CIS pattern for complexation with mβ167, which is partially methylated at all three sites, lies somewhere in between those for complexation with mβ209 and mβ300.

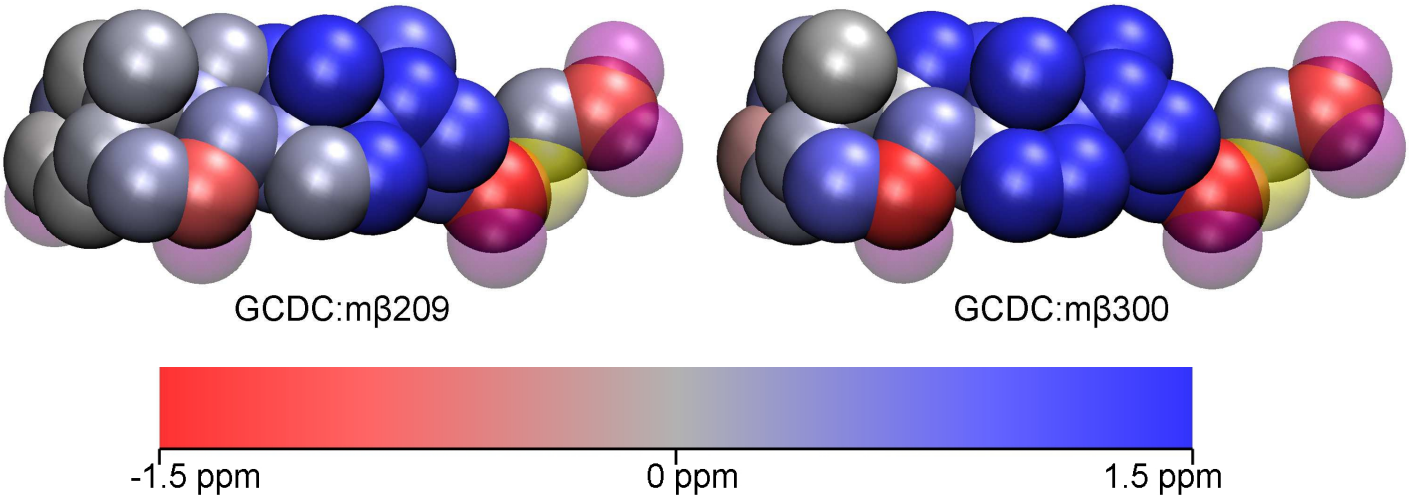

Figure 10: Illustration of CIS of ^{13}C nuclei in GCDC complexed with mβ209 and mβ300. Carbon atoms are shown as opaque van der Waals spheres while oxygen atoms are shown as pink transparent spheres and nitrogen as yellow transparent spheres. The CIS of the carbon atoms are shown using the color scale in the bottom of the figure. Some carbons exceed the limits of the scale.

3.3.2 Structure elucidation by ROESY NMR

The deduction of structures of CD inclusion complexes by ROESY NMR is primarily based on the interaction of three CD protons, H3, H5 and H6, with protons of the guest molecule.[19,43-45] In the following the CD protons will be denoted by an "H" to distinguish them from BS protons which will be denoted by a "P", *e.g.* P18. These three CD protons are located at the inner surface of the CD and thus interact with the BS protons that are included, or almost included, in the CD cavity. In contrast, H1, H2 and H4, are located at the exterior of the CD and never show any interactions with the BSs. H3 is located close to the secondary rim, H5 is close to the primary rim and H6 is attached to the primary rim.

The ROESY spectra support the structures deduced from the CIS and adds another crucial piece of information: the orientation of the CD. The CIS reveal where the CD binds to the BS but do not show whether the BS sidechain protrudes from the primary or the secondary rim. For the investigated βCD:BS complexes, H3 generally shows the strongest interactions with P18 while H5 interacts strongest with P21. Interactions between H6 and the BS protons are usually relatively weak and often limited to P23. This pattern suggests a structure in which the BS is inserted into the βCD from the secondary rim and the BS conjugation chain protrudes from the primary rim (Figure 12 and Figure 14). Many more interactions supporting such complex structures are

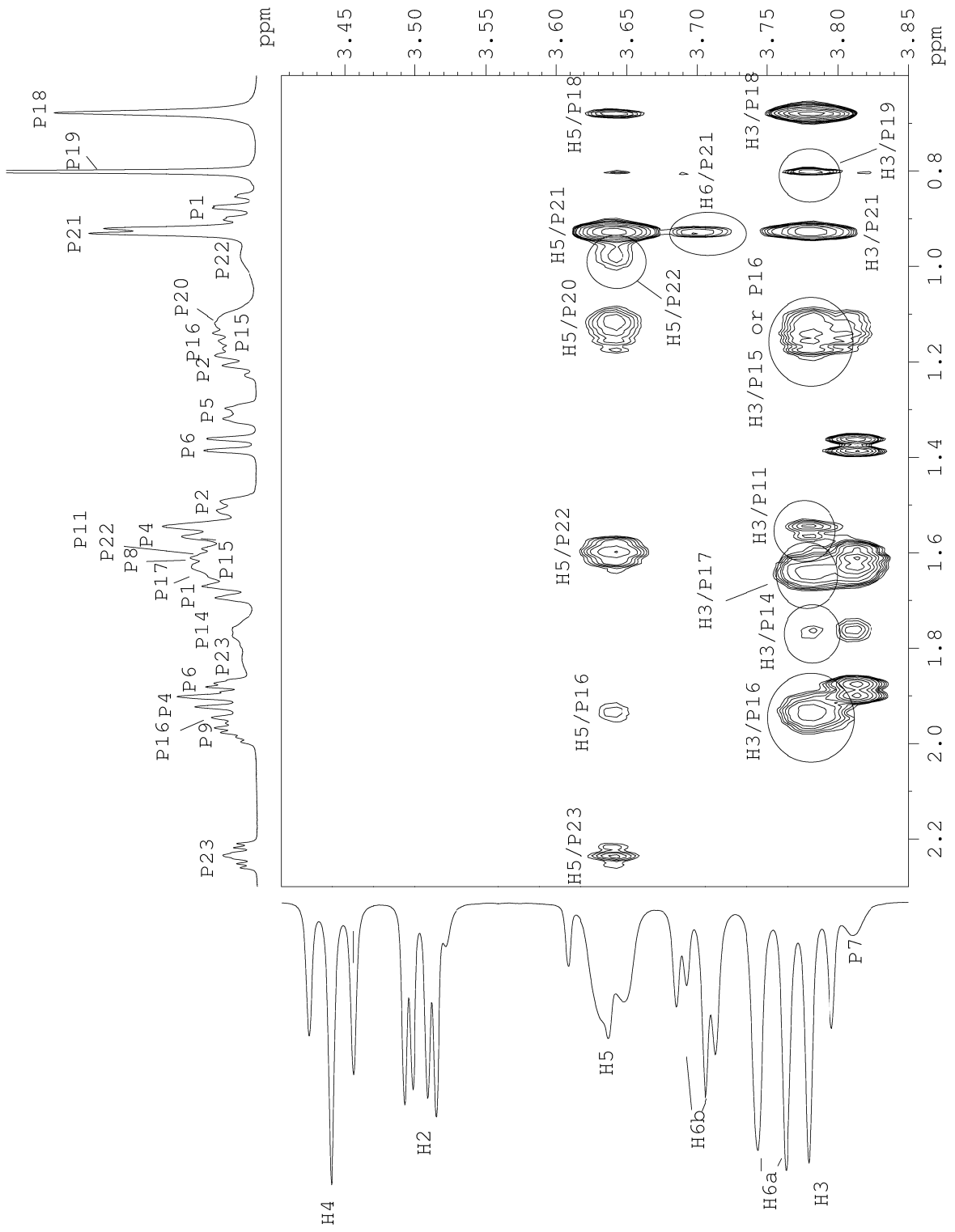

Figure 11: Partial ROESY spectrum of the GC:βCD complex. CD protons are denoted with "H" and BS protons with "P". The intermolecular ROESY cross-peaks between the CD and the BS are assigned. Also seen on the partial spectrum are the intramolecular interactions between P7 and various other BS protons.

observed on the ROESY spectra (see for example Figure 11) and these overall structures seem to be valid for complexes formed with all types of βCDs, both unsubstituted, methylated and hydroxypropylated. The only exceptions are the complexes formed by mβ300 with GC and GDC. Although some ROESY interactions are observed between the O3 methyl protons on mβ300 and several (unidentified) GC protons, no interactions are observed between H3, H5 and the GC protons, thus suggesting that GC and mβ300 do not form an inclusion complex. ROESY interactions between mβ300 and GDC are weak and dubious and do not give a clear picture of the structure of the complex.

The deeper inclusion of the BSs into γCD is confirmed by the ROESY spectra (Paper V). The correlations between γCD and GCDC unambiguously suggest an orientation of the BS in which the conjugation tail protrudes from the primary rim, as for the βCDs. The orientations of GC and GDC inside γCD are a little more unclear, and the co-existence of two types of complexes in which the conjugation protrudes from the primary and secondary rim, respectively, can not be ruled out. Likewise, the formation of 2:1 CD:BS complexes with GDC, as observed for βCD and the mβCDs, can not be excluded.

ROESY interactions of substitutents

The ROESY spectra of complexes with methylated βCDs show strong interactions between the O3 methyl protons and various protons on the steroid body of the BS (Paper II). Strong interactions with this particular methyl group have also been observed for other guest molecules.[46-48] In contrast, the interactions between the O2 methyl protons and the BS (only P19) are weak or non-existent. This indicates that O3-CH_3 points inwards towards the BS while O2-CH_3 points outwards and away from the included guest molecule, and these orientations of the methyl groups are supported by X-ray diffraction of crystalline complexes.[49] O6-CH_3 generally interacts with P21 and P23, in line with the proposed complex geometries. These orientations of the three different methyl groups are illustrated in Figure 12.
Strong “internal” ROESY interactions are observed between the protons on the HP-chains, but only Hb engages in (weak) intermolecular interactions with P19 on the BS. Otherwise no interactions with BSs are observed. Apparently, only weak contacts between the HP-chains and the BSs are present.

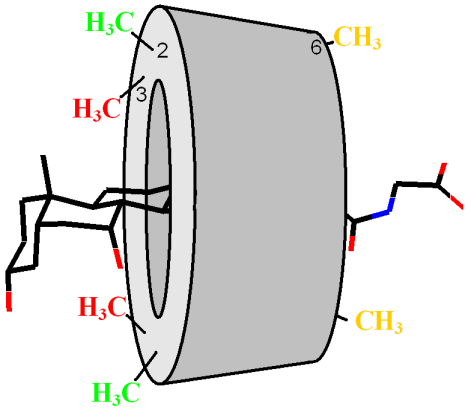

Figure 12: Illustration of a complex formed between GCDC and a methylated βCD. Methyls at O2 (green) point away from the BS while methyls at O3 (red) point towards the BS and interact with the steroid body of the BS. Methyls at the primary rim, at O6 (yellow), interact with the conjugation tail of the BS.

3.3.3 Complexation induced shifts of CD nuclei

Most CD nuclei experience CIS that are a little smaller or comparable to the CIS of BS nuclei, but C1 and C4 (and C1' and C4') of the methylated βCDs are some remarkable exceptions. The CIS of these nuclei are relatively small for the complexation of the natural βCD with all glycoconjugated BSs (~0.8 ppm for C1 and ~0.4 ppm for C4), but in mβ300 C1 and C4 increase to a staggering 4.0 and 5.8 ppm, respectively, upon inclusion of GCDC. CIS for CD nuclei were determined for the complexes of βCD, mβ167, mβ209 and mβ300 with the three glycoconjugated BSs. As seen from the plots in Figure 13, the CIS of C1 and C4 increases monotonously, almost linearly, with DS(O3), but not with the total DS. This is not the case when plotted against the total DS.

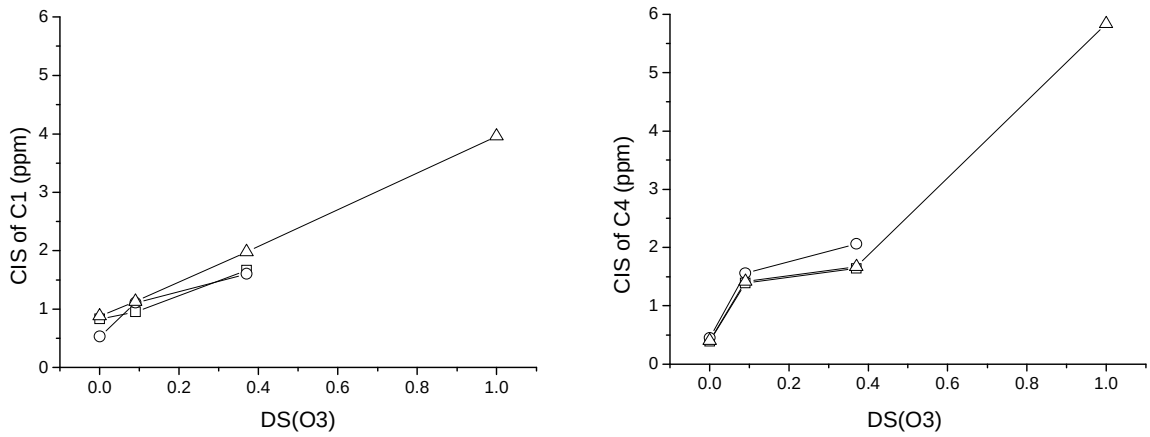

Figure 13: Plots of the CIS of the CD nuclei C1 (left figure) and C4 (right figure) in βCD, mβ209, mβ167 and mβ300 upon complexation with GC (□) , GDC (○) and GCDC (△). The data for the complexes of mβ300 with GC and GDC are not shown as these complexes are very weak.

Very large CIS of C1 and C4 (although not quite as large as those reported here) seem to be characteristic for the complexation of mβ300 with various guest molecules and has been attributed to the large conformational changes undergone by the CD upon complexation.[45,47] The glucose units are linked by α 1→4 glycosidic bonds, and large CIS of C1 and C4 are probably caused by complexation induced alterations of the tilt angles of the glucose units. The structure of the natural βCD is stabilized by the formation of a hydrogen bond network between the hydroxyls at the secondary rim,[3] but as the hydroxyls are methylated the hydrogen bond network is lost. Consequently, the structure of mβ300 is much more flexible than the natural βCD and may undergo significant structural changes upon complexation, reflected in the extraordinarily large CIS of C1 and C4. These conformational changes of mβ300 have been described as an "induced fit".[45,46] The present data sows doubt about this interpretation. If the CIS of C1 and C4 depends on the extent to which the hydrogen bond network is disrupted, one would expect larger CIS to be observed in mβ209 (in which all 2-OHs are methylated) than in mβ167. This is not the case and the CIS seem to more directly dependent on the extent of methylation at O3. Therefore a new interpretation is suggested: The steric repulsions between methyl groups at O3 and the guest molecule force a slight rotation of the glucose units around the glycosidic bonds, causing large CIS of C1 and C4. Thus, the structural change of mβ300 upon complexation is not directly driven by the increased flexibility, but rather by steric repulsions, although an increased flexibility may be a prerequisite.

3.3.4 Computer simulations of complexes

Molecular modelling of CD:BS complexes have previously been conducted by Sune Askjær who used molecular docking to determine the most probable structures of the complexes formed by the BSs TC, TDC, TCDC, GC, GDC and GDC with natural αCD (Paper III), βCD[7] and γCD (Paper V). Those results are in agreement with the structures proposed above for complexes with βCD and γCD and further shows that αCD resides on the conjugation tail, in agreement with experimental evidence.[19]
With the purpose of elucidating the behaviour of HP-chains in complexes of HPβCDs, I have conducted MD simulations of natural βCD and two HPβCDs, representing a moderately substituted and a highly substituted HPβCD, as well as their complexes with GC, GDC and GCDC (Paper VII). The simulations result in complexes that are

very similar to the experimentally derived geometries suggested above, and these simulated complexes are stable for at least 20 ns. It should be stressed, however, that the initial structures used in the simulations consisted of a BS positioned with the conjugation tail inserted into the CD from the secondary site. That is, the initial structures are close to the expected structures of the complexes. If the simulation started out with two separated molecules, it would take too long for the molecules to find each other and form the inclusion complex. It is therefore necessary to conduct the simulations from a starting position that is close to the expected structure. Within the first few ns the CD moves from the conjugation tail and onto the D-ring of the BS and this structure is more or less retained throughout the simulation. The MD simulations thus confirm that the experimental structures are possible, but do not rule out other conformations. A snapshot of the MD simulation of the GCDC:βCD complex is shown in Figure 14 and clearly show that the CIS pattern in Figure 9 is induced by the insertion into the CD cavity.

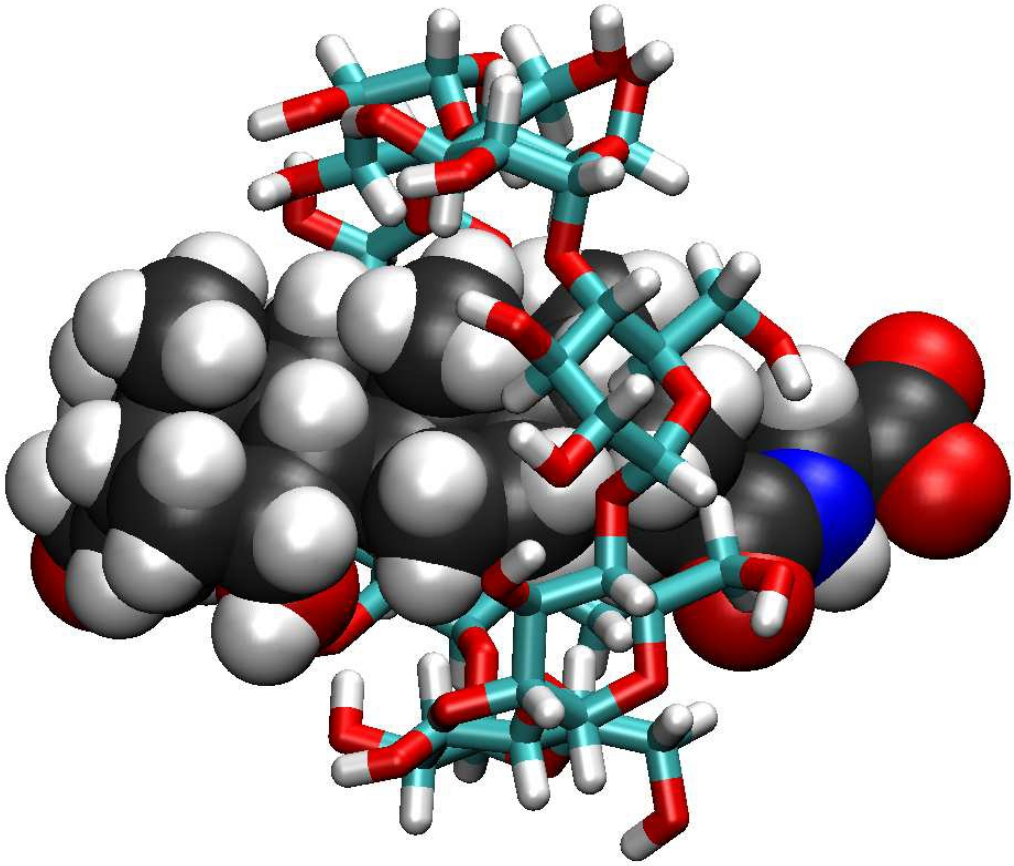

Figure 14: Snapshot from the MD simulation of the βCD:GCDC complex. During the 10 ns MD simulation, only a small fluctuation in the complex structure is observed, so the snapshot is a good representation of the time-averaged complex structure. Compare the position of the CD to the CIS pattern in Figure 9.

Burial of polar and nonpolar surfaces

The complexation thermodynamics is to a large extent interpreted in terms of dehydration of non-polar surface area (Chapter 5). In order to check the validity of this interpretation, the MD simulations were analyzed to yield the changes in solvent Accessible Surface Area (ASA) upon complexation (Paper VII). The surfaces were determined by rolling a "water molecule", a spherical probe of radius 1.4 Å, across the surfaces of the molecular species. The changes in ASA were calculated as:

$$\Delta ASA = ASA_{complex} - (ASA_{CD} + ASA_{BS}) \qquad [3.6]$$

The ASA values were divided into polar surface (heteroatoms and associated hydrogens) and nonpolar surface (carbons and associated hydrogens) to provide ΔASA_{pol} and ΔASA_{non}, respectively. The analysis revealed that for complexes with natural βCD, more nonpolar surface area (ΔASA_{non} = 334 – 367 Å^2) than polar surface area ($\Delta ASA_{pol} \approx$ 200 Å^2) is buried. Whereas ΔASA_{pol} does not depend much on either the type of BS or the CD involved in the complex, ΔASA_{non} systematically depends on the type of BS and in particular the number of HP-chains on the CD. The dependence of ΔASA_{non} on the DS of the CD is shown in Figure 15.

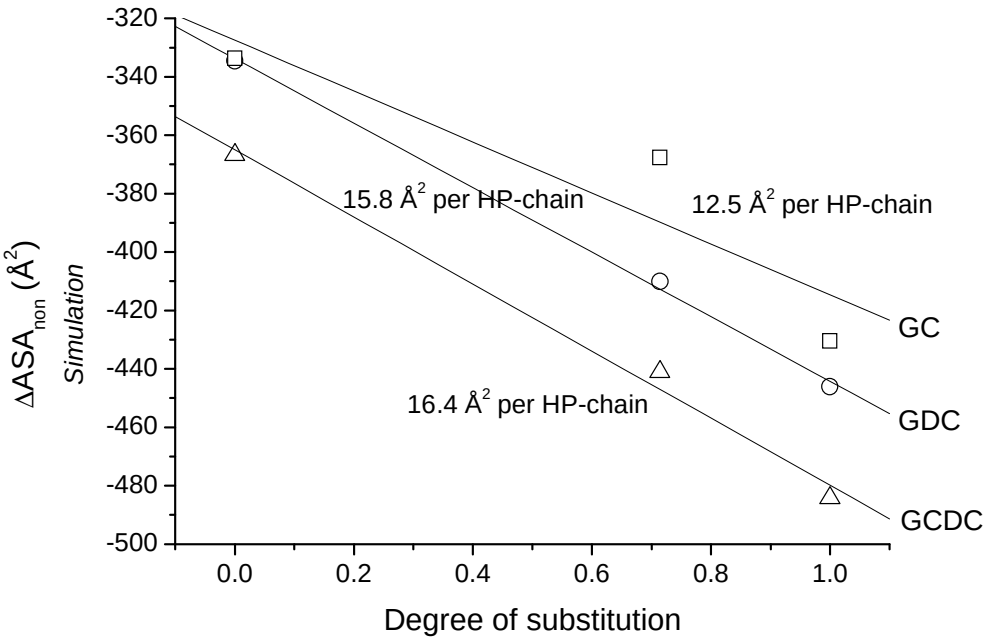

Figure 15: The buried nonpolar surface area increases with the number of HP-chains on the CD. The plotted data are for simulated complexes of βCD and two HPβCDs with GC (□) , GDC (○) and GCDC (△).

As calculated from the slopes of the plots, each HP-chain on the rim of the CD results in an additional dehydration, or burial, of 13 – 16 $Å^2$ of nonpolar surface. As shown on Figure 16 the CD resides at its usual site on the GCDC and the HP-chains extend the CD and thus bury a larger part of the predominantly nonpolar BS. As mentioned above, the only ROESY interactions observed between the HP-chains and the BSs are the weak interaction between Hb and P19. The distance between the HP-chains and the BS is apparently too large to result in significant ROESY peaks but still short enough to expel water molecules from the hydrophobic surfaces. Maybe the thermal motion of the HP-chains prevents a close contact with the BS. The HP-chains are mainly attached to O2 and could thereby point away from the BS, as is the case for methyl groups at O2.

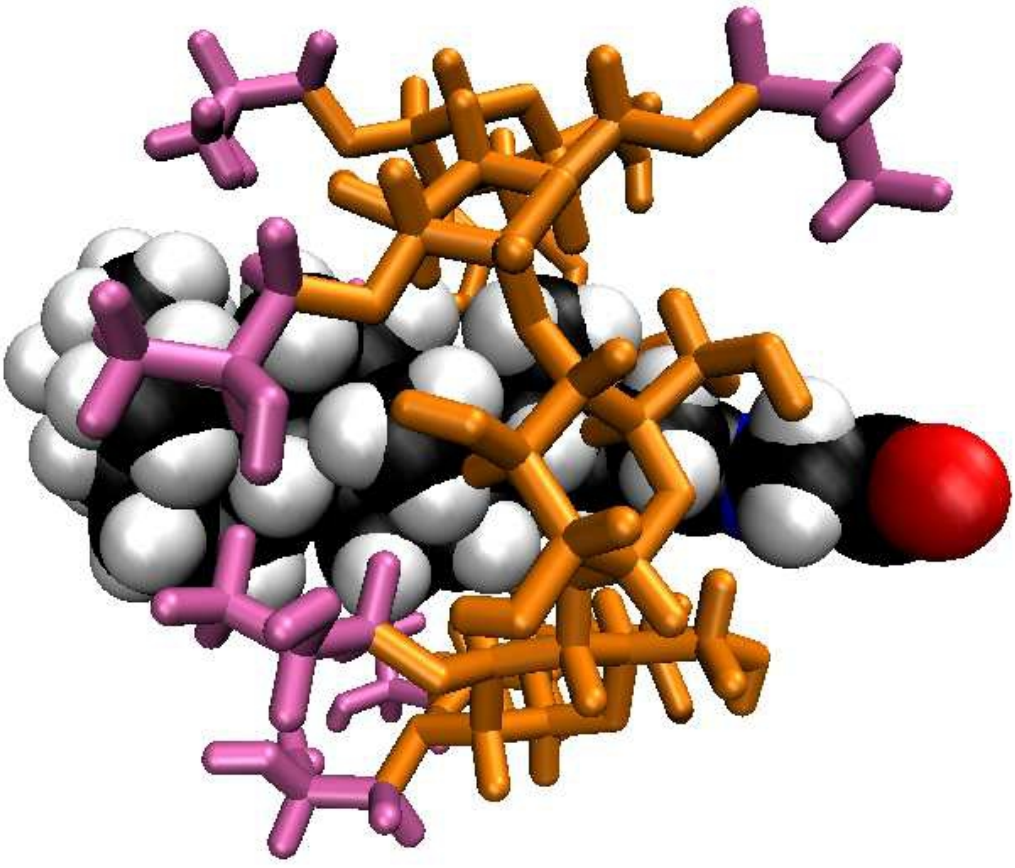

Figure 16: Snapshot from the MD simulation of GCDC complexed with a highly substituted HPβCD (DS = 1). The basic CD structure is shown in orange and the HP-chains are colored pink.

Another interesting observation from Figure 15 is that ΔASA_{non} for the GCDC complexes are consistently numerically larger than for the GC and GDC complexes. This is most likely related to the lack of a polar hydroxyl group on C12 of GCDC.

3.3.5 Summary of complex structures

I. The number and position of hydroxyl groups on the BSs only have a minor influence on the structures of the complexes,[ii] although the absence of a hydroxyl group on C7 of GDC results in a second binding site for βCDs. The primary binding site, however, is the same as on the other BSs.
II. The diameter of the CD ring strongly influence how deep the BS is included in the CD. Only the conjugation tail is included in αCD, the D-ring is accommodated in βCDs, while it is possible for γCD to encroach all the way to the B- and C-rings.
III. The BS conjugation tail protrudes from the primary rim of the CDs, with the possible exception of some of the γCD complexes, where it can not be excluded that the tail protrudes from the secondary rim.
IV. The number and type of substituents at the rim of βCD do not seem to affect the structure of the complexes, except in the case of mβ300 which might not form an inclusion complex with GC and could have a different binding mode towards GDC.
V. Methyl groups at O3 seem to point inwards towards the BS whereas methyl groups on O2 points away from the opening of the CD. For complexes with HPβCDs, the close proximity between the HP-substituents and the BS results in an additional burial of hydrophobic surface upon complexation – around 13 -16 $Å^2$ per HP-chain. No additional polar surface is buried by the substituents.

[ii] There are indications that the absence of a hydroxyl group on C12 of GCDC leads to a slightly deeper inclusion of this BS.

Chapter 4: Methods for determination of binding thermodynamics

The most important thermodynamic property to be experimentally determined is the association constant, K, for the binding of BS to CD. Once the association constants for the relevant complexes are known, together with K for a given drug:CD complex, the equilibrium concentration of free drug in a mixture of various BSs and CDs can be calculated, provided that the total concentration of each chemical component is known.

K is directly related to the standard change in Gibbs free energy, $\Delta G°$, associated with the complexation reaction. In principle, all other thermodynamic properties can be calculated from derivatives of $\Delta G°$ but are often determined directly by experiment. In the present work we will limit ourselves to the changes in enthalpy, H, entropy, S, and isobaric heat capacity, C_p, associated with the formation of complexes. Out of these, only ΔH is directly measured and the remaining two are calculated from ΔH and $\Delta G°$.

Although only knowledge of K is necessary to calculate the concentration of free drug, the other thermodynamic functions may provide valuable insight into the mechanisms driving the formation of the complexes.

Three experimental techniques have been employed to determine the thermodynamics for the binding of BSs to CDs. Binding constants for the relatively weak complexes formed with αCD and HPαCD was obtained by Affinity Capillary Electrophoresis (ACE). Isothermal titration calorimetry provided K, ΔH and $\Delta S°$ for the complexes of βCDs and γCD, and experiments were conducted at a range of temperatures to yield ΔC_p for some complexes. Finally, a ^{13}C NMR titration was conducted to verify the binding constants for the 2:1 βCD:GDC complex.

A common mathematical formalism is used to analyse the data from the three experimental techniques, and the equations are derived in the present chapter. The obtained binding thermodynamics for all investigated complexes are compiled in Table 4 at the end of the chapter.

Section 4.1: Direct determination of K and ΔH

All methods for the determination of binding constants relies on varying the concentrations of the binding species and observing the concomitant change in one or more observables that are sensitive to complex formation. Plotting the observable as a function of the concentrations generates a binding isotherm, which is fitted by a binding model to yield the binding constant. In NMR, the observable is the chemical shift, in ITC it is the complexation heat, and in ACE the electrophoretic mobility.

In the following, two binding models are derived. The 1 sites model describes a system where only one type of interaction is possible, and the 2 sites model incorporates the presence of a second type of non-cooperative interaction. Subsequently, the models are linked to the observables of the three methods to yield the actual fitting equations.

4.1.1 Binding models

In this subsection the 1 sites and 2 sites binding models are derived and linked to the observables of NMR, ITC and ACE, and examples of the fits are shown. Only the ITC data were analyzed with both models. The ACE data were analyzed using the 1 sites model and the NMR titration was fitted by the 2 sites model.

<u>1 sites model (one type of binding sites)</u>

For notational simplicity the binding site on the BS is denoted A and the CD B. Then the simple equilibrium in which a CD binds to a binding site on the BS is:

$$A + B \leftrightarrow AB \qquad [4.1]$$

with the binding constant

$$K = \frac{[AB]}{[A][B]} \qquad [4.2]$$

The conservation of mass requires that

$$NA_t = [A] + [AB] \qquad [4.3]$$

$$B_t = [B] + [AB] \qquad [4.4]$$

in which N is the number of identical binding sites on each BS molecule and A_t is the total concentration of BS. Note that N does not appear in the expression for the binding constant in equation 4.2 since this binding constant is defined using the

concentration of free binding sites instead of the concentration of free BS. In the studied systems N deviates slightly from unity, but this does not mean that a non-integer number of CDs bind to each BS. Rather than denoting the number of identical binding sites on each BS molecule, N is a measure of errors in the concentrations of the interacting species.

From these 3 equations one may solve for [A], [B] and [AB] as a function of K, N, A_t and B_t. However, it is more convenient to introduce the fractional saturation f_1:

$$f_1 = \frac{[AB]}{NA_t} \qquad [4.5]$$

Using equations 4.2, 4.3 and 4.5, K is expressed as a function of f_1 and [B]:

$$K = \frac{f_1}{(1-f_1)[B]} \qquad [4.6]$$

And equation 4.4 is written as:

$$B_t = [B] + f_1 NA_t \qquad [4.7]$$

Combining equations 4.6 and 4.7 a second order equation in f_1 is obtained:

$$f_1^2 - f_1\left(1 + \frac{B_t}{NA_t} + \frac{1}{KNA_t}\right) + \frac{B_t}{NA_t} = 0 \qquad [4.8]$$

which has the physically meaningful solution:

$$f_1 = \frac{1}{2}\left\{1 + \frac{B_t}{NA_t} + \frac{1}{KNA_t} - \sqrt{\left(1 + \frac{B_t}{NA_t} + \frac{1}{KNA_t}\right)^2 - \frac{4B_t}{NA_t}}\right\} \qquad [4.9]$$

As shown below, the fractional saturation is directly related to the observables in the NMR, ITC and ACE titrations.

2 sites model (2 types of binding sites)

In the 2 sites model each BS molecule contains two types of independent (non-cooperative) binding sites and there are N of each type of binding site on each BS molecule. Thus, two equilibria and equilibrium constants are required in the description of this system:

$$A1 + B \leftrightarrow A1B \qquad K1 = \frac{[A1B]}{[A1][B]} \qquad [4.10]$$

$$A2 + B \leftrightarrow A2B \qquad K2 = \frac{[A2B]}{[A2][B]} \qquad [4.11]$$

where [A1] and [A2] are the concentrations of unoccupied type 1 and type 2 binding sites on the BS molecule, respectively.

Conservation of mass requires that:

$$NA_t = [A1] + [A1B] \quad [4.12]$$

$$NA_t = [A2] + [A2B] \quad [4.13]$$

$$B_t = [B] + [A1B] + [A2B] \quad [4.14]$$

From these 5 equations the 5 unknowns [A1], [A2], [B], [A1B] and [A2B] may be determined. As before, it is convenient to introduce the fractional saturation of the 2 binding sites:

$$f_{11} = \frac{[A1B]}{NA_t} = \frac{K1[B]}{1 + K1[B]} \quad [4.15]$$

$$f_{12} = \frac{[A2B]}{NA_t} = \frac{K2[B]}{1 + K2[B]} \quad [4.16]$$

These 2 equations and equation 4.14 may be used to derive a cubic equation in [B]:

$$[B]^3 + a_2[B]^2 + a_1[B] + a_0 = 0 \quad [4.17]$$

with the coefficients:

$$a_0 = -\frac{B_t}{K1K2} \quad [4.18]$$

$$a_1 = \left(\frac{1}{K1} + \frac{1}{K2}\right)(NA_t - B_t) - \frac{1}{K1K2} \quad [4.19]$$

$$a_2 = \frac{1}{K1} + \frac{1}{K2} + 2NA_t - B_t \quad [4.20]$$

As shown by Wang[50] the only physically meaningful solution to the cubic equation describing this system is given by:

$$[B] = \frac{2\sqrt{a_2^2 - 3a_1}\cos(\theta/3) - a_2}{3} \quad [4.21]$$

where

$$\theta = \arccos\left(\frac{-2a_2^3 + 9a_1a_2 - 27a_0}{2\sqrt{(a_2^2 - 3a_1)^3}}\right) \quad [4.22]$$

Once [B] is calculated f_{11} and f_{12} are determined from equations 4.15 and 4.16.

4.1.2 Modelling the NMR titration

Under fast exchange conditions the observed chemical shift, δ, of a nucleus is the weighted average of the chemical shift of the nucleus in the free and the bound species. Assuming that a nucleus on site 1 of the BS is only affected by the degree of saturation of site 1 and not of site 2, its chemical shift is:

$$\delta = f_{01}\delta_{A1} + f_{11}\delta_{A1B} \qquad [4.23]$$

where δ_{A1} is the chemical shift of the nucleus in the free species, f_{11} is the previously described fractional saturation of site 1 and f_{01} is the fraction of unsaturated sites[iii]:

$$f_{01} = \frac{[A1]}{NA_t} \qquad [4.24]$$

The change in the observed chemical shift, Δδ, upon fractional saturation of site 1 is:

$$\Delta\delta = \delta - \delta_{A1} = f_{11}(\delta_{A1B} - \delta_{A1}) = f_{11}\Delta\delta_{\max} \qquad [4.25]$$

$\Delta\delta_{max}$ is the maximum change in the chemical shift corresponding to complete saturation of the binding site and is unique for each nucleus.
Likewise, the change in the observed chemical shift of a site 2 nucleus upon fractional saturation of site 2 is:

$$\Delta\delta = f_{12}\Delta\delta_{\max} \qquad [4.26]$$

Now the observable, Δδ, is related to the known variables, A_t and B_t, by equations 4.15 – 4.22 and the model may be fitted to the experimentally determined values of Δδ yielding N, K1, K2 and $\Delta\delta_{max}$ as best fit values.

In Figure 17 Δδ for carbon C4, which is located at the secondary site on GDC, is plotted as a function of the ratio B_t/A_t, called the molar ratio of CD to BS. At low molar ratios there is a large surplus of BS and only a small fraction of the BS molecules are complexed. The averaged chemical shifts of the BS nuclei are very close to their chemical shifts in the free BS, and Δδ, which is proportional to the degree of saturation, is very small. As the concentration of βCD increases, the majority of the βCDs bind to the stronger primary binding site, and the GDC nuclei located at the secondary site only experience small Δδ. A further increase in the CD/BS molar ratio leads to saturation of the primary binding site and the βCDs start

[iii] A notational clarification: The first index in the subscript of f_{01} indicates the number of CDs binding to the site given by the second index number. Thus, f_{01} is the fraction of BSs containing 0 CDs on the 1st binding site. Likewise, f_{11} indicates 1 CD on the 1st binding sites and f_{12} indicates 1 CD on the 2nd binding site.

binding to the secondary site, resulting in a sharp increase in Δδ for nuclei at the secondary site. This leads to the S-shaped binding isotherm in Figure 17 which is characteristic for all secondary site nuclei. The fit of equations 4.16, 4.21 and 4.26 to the data in Figure 17 is obtained with the fitting parameters listed in the table in Figure 17.

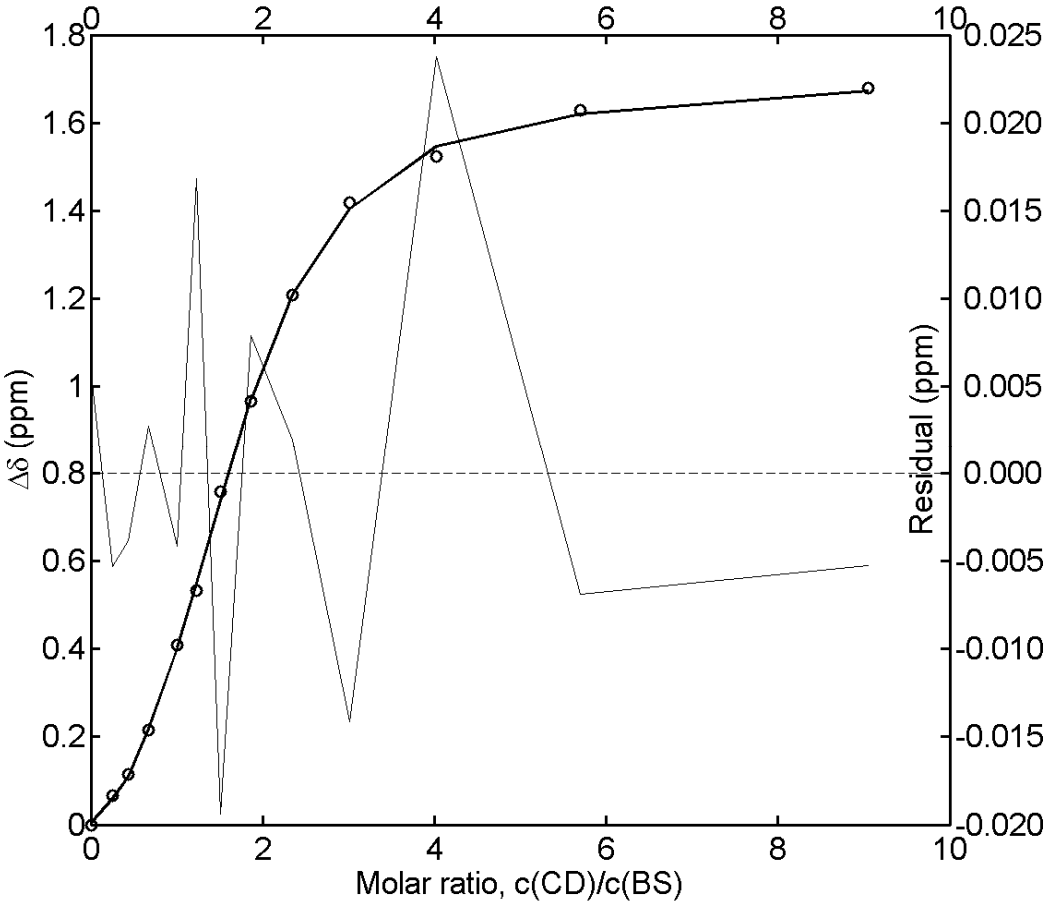

Parameter	Best fit value	Asymptotic 95% Error	Correlation Matrix			
N	1.01	0.12	1	-0.15	0.92	-0.81
K1 (M^{-1})	4708	1470		1	0.13	-0.34
K2 (M^{-1})	597	283			1	-0.95
$\Delta\delta_{max}$ (ppm)	1.93	0.13				1

Figure 17: Fitted binding isotherm for C4 on GDC, obtained from the titration with βCD. The thick line shows the best fit of the 2 sites model and the thin line shows the residuals (right axis).

In principle, binding isotherms for the nuclei at the primary binding site on GDC can also be used for determination of K1 and K2, but unfortunately the nuclei at the first binding site suffer from peak broadening (probably due to unfavourable exchange kinetics), such that a large part of the binding isotherm can not be determined, as

shown in Figure 18. Nevertheless, it is clear that the binding site is close to saturation at molar ratios slightly above 1, as expected for the stronger primary binding site.

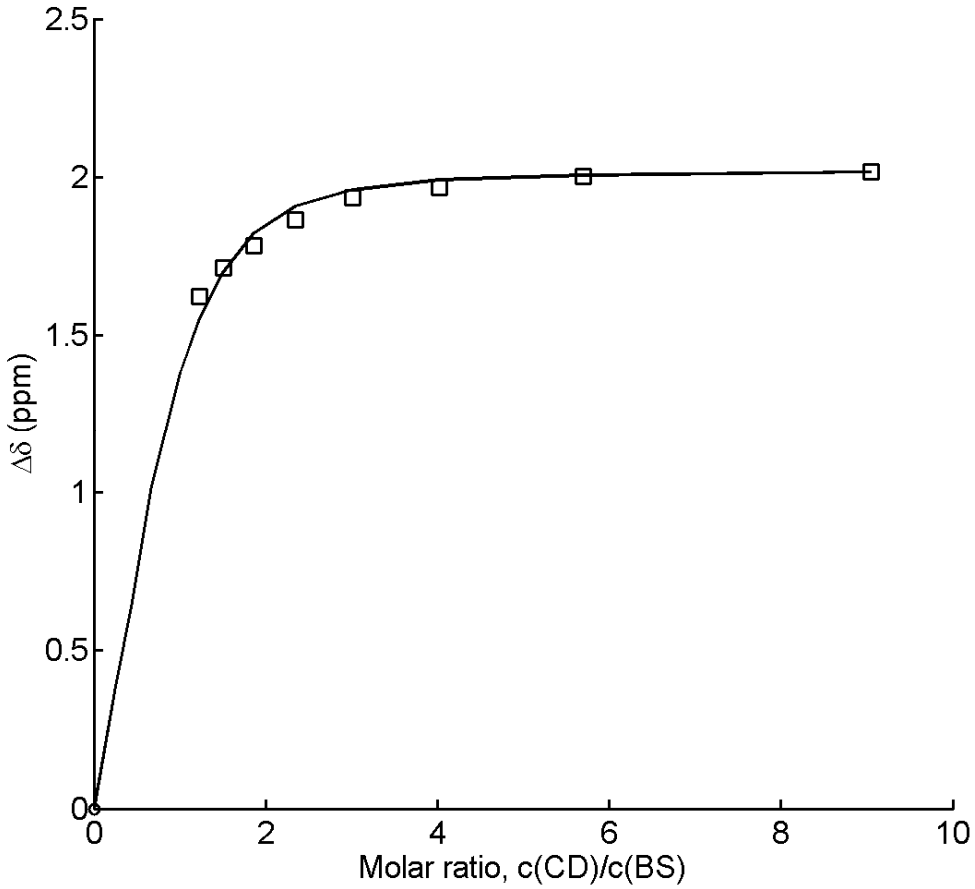

Figure 18: Partial binding isotherm for C21 which is located at the primary site of GDC. It was not possible to determine the chemical shifts at low molar ratios due to disappearance of the peak. Also at higher molar ratios there was considerable peak broadening and the shown data points are not very precise. The solid line shows the expected isotherm, calculated from the parameters in Table 4.

The BS nuclei 1-10 and 19 (see Figure 3) all exhibit secondary site behaviour while BS nuclei 13, 15-18 and 20-27 exhibit primary site behaviour. Nucleus 12 hardly seems to be affected while nuclei 11 and 14 are affected by binding of the CD to both sites. This gives a very clear picture of the location of the two binding sites, as illustrated in Figure 9.

Also the chemical shifts of the CD nuclei are affected by the complexation and may be used to determine the binding constants. The chemical shift of a CD nucleus is the

weighted average of its chemical shifts in the 3 states where it is free (δ_B), bound to site 1 (δ_{A1B}) and bound to site 2 (δ_{A2B}):

$$\delta = f_B\delta_B + f_{A1B}\delta_{A1B} + f_{A2B}\delta_{A2B} \quad [4.27]$$

where

$$f_B = \frac{[B]}{B_t} \quad [4.28]$$

$$f_{A1B} = \frac{[A1B]}{B_t} \quad [4.29]$$

$$f_{A2B} = \frac{[A2B]}{B_t} \quad [4.30]$$

Equation 27 may be rewritten as:

$$\Delta\delta = f_{A1B}\Delta\delta_{A1B,\max} + f_{A2B}\Delta\delta_{A2B,\max} \quad [4.31]$$

where

$$\Delta\delta_{A1B,\max} = \delta_{A1B} - \delta_B \quad [4.32]$$

$$\Delta\delta_{A2B,\max} = \delta_{A2B} - \delta_B \quad [4.33]$$

The concentrations [A1B] and [A2B] needed to calculate f_{A1B} and f_{A2B} are easily calculated from equations 4.15 and 4.16 and so $\Delta\delta$ for the CD nuclei may be fitted using N, K1, K2, $\Delta\delta_{A1B,\max}$ and $\Delta\delta_{A2B,\max}$ as fitting parameters.

Two examples of characteristic binding isotherms for βCD nuclei, created by binding to the two sites of GDC, are shown in Figure 19 and Figure 20. The nuclei are expected to experience different chemical shifts, depending on whether the CD binds to the primary or the secondary site. Consequently, the binding isotherms for the CD nuclei are fitted with 5 parameters whereas only 4 parameters were required to fit the BS nuclei. Most of the CD nuclei behave as C1 in Figure 19 and are shifted downfield upon binding to each of the GDC binding sites (both $\Delta\delta_{A1B,\max}$ and $\Delta\delta_{A2B,\max}$ are positive). It is therefore difficult to distinguish between the two binding events, and as a result, the errors on the binding constants are very large. The only CD nucleus that provides a reasonable precision on the binding parameters is C6 (Figure 20). In this single case, binding to the primary site induces an upfield shift whereas the usual downfield shift is observed for binding to the secondary site. These opposite shifts

lead to a better resolution of the two binding events and a better estimate of the binding parameters.

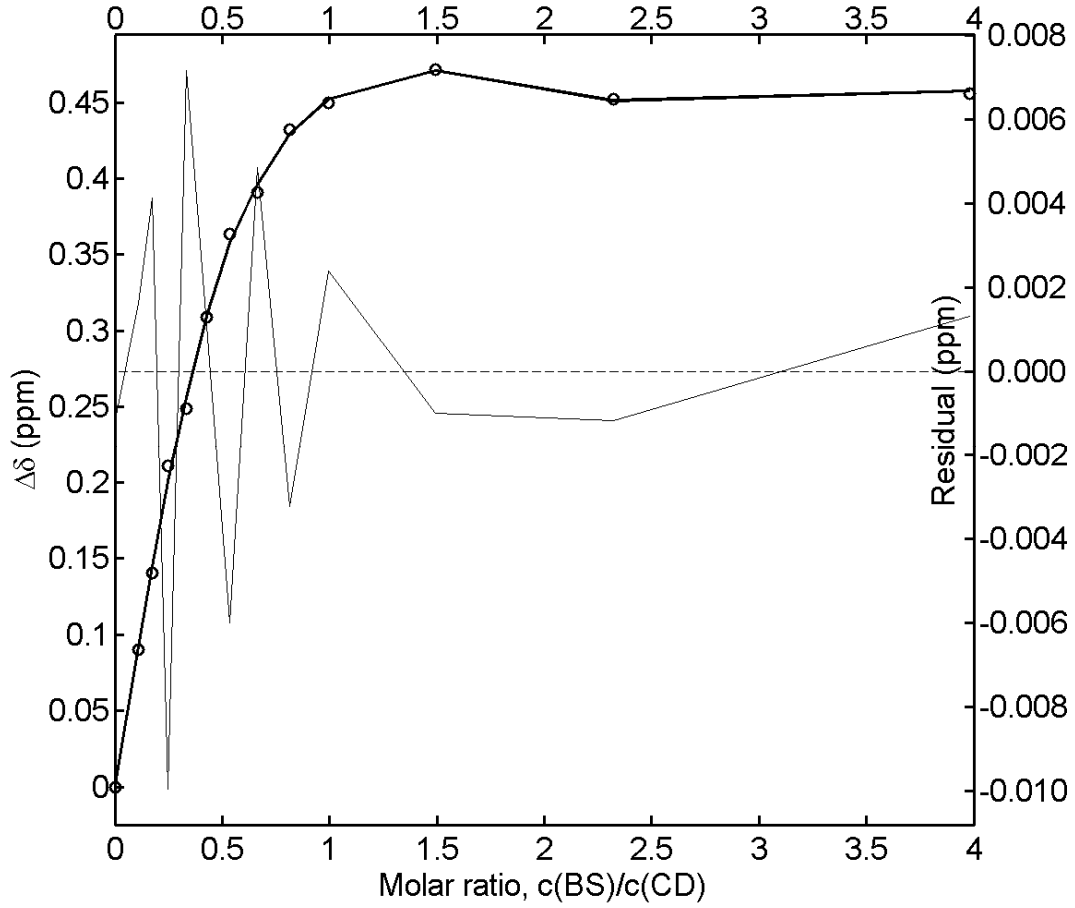

Parameter	Best fit value	Asymptotic 95% Error	Correlation Matrix				
N	0.71	0.490	1	-0.91	0.88	0.88	-0.99
K1 (M^{-1})	17257	57244		1	-0.75	-0.97	0.90
K2 (M^{-1})	443	507			1	0.65	-0.93
$\Delta\delta_{A1B,\max}$ (ppm)	0.48	0.072				1	-0.85
$\Delta\delta_{A2B,\max}$ (ppm)	0.84	1.235					1

Figure 19: Fitted binding isotherm for C1 on βCD for the titration with GDC. The thick line shows the best fit of the 2 sites model and the thin line shows the residuals (right axis). Note that the decrease in Δδ at high molar ratios is due to the low concentrations of binding species and consequently a shift in the equilibrium towards the free species. Such low concentrations were required to keep the concentration of BS below CMC.

It is obvious that the BS nuclei provide much more precise values of the binding parameters than the CD nuclei. This is despite that the chemical shifts of the CD nuclei can be determined more reliably due to the sevenfold symmetry of βCD, which

leads to stronger peak intensities. Further, the chemical shifts of the BS nuclei are severely affected by even slight tendencies of micellization and are also broadened upon complexation. These reasons may have led Cabrer *et al.*,[19] who also conducted a NMR titration of exactly the same system, to only use the CD nuclei to determine the binding constants. Consequently, their results are associated with large errors compared to the ones presented here.

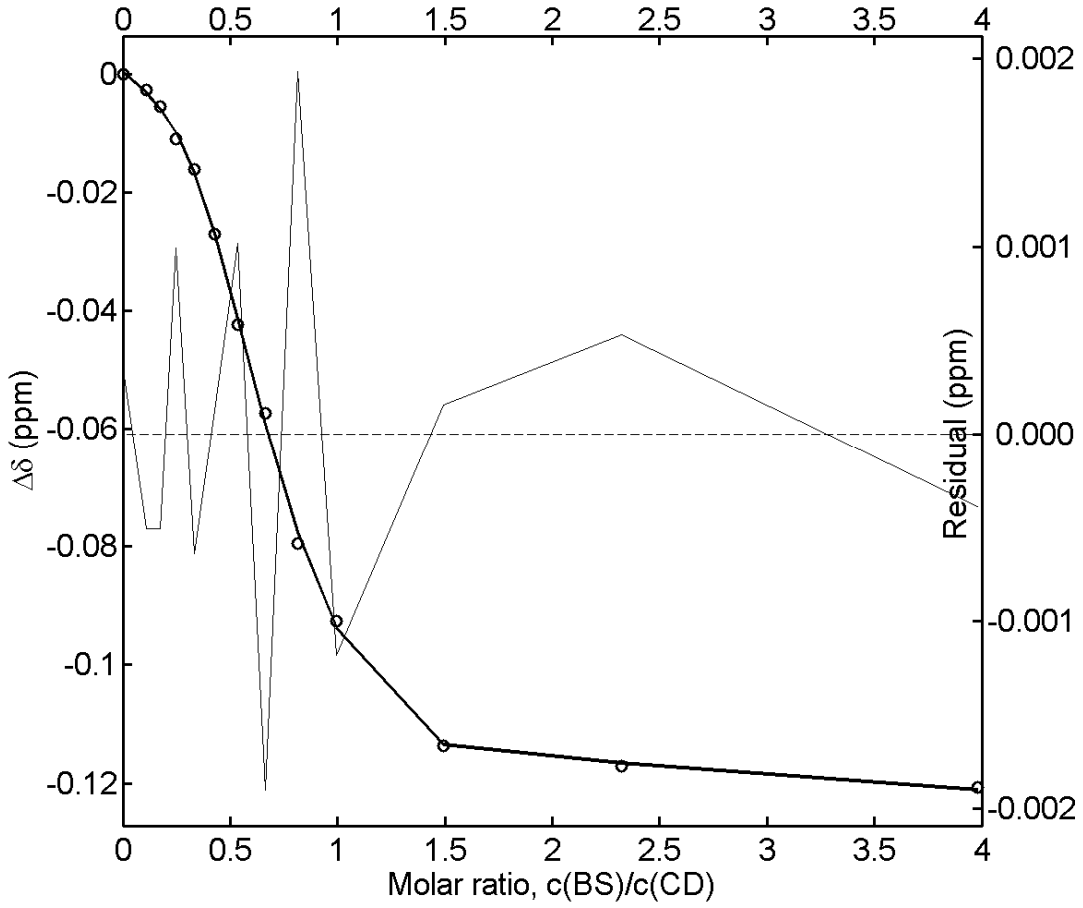

Parameter	Best fit value	Asymptotic 95% Error	Correlation Matrix				
N	0.99	0.080	1	0.24	0.76	-0.23	-0.22
K1 (M^{-1})	9300	8875		1	0.62	0.77	-0.94
K2 (M^{-1})	438	495			1	-0.01	-0.70
$\Delta\delta_{A1B,\max}$ (ppm)	-0.15	0.022				1	-0.61
$\Delta\delta_{A2B,\max}$ (ppm)	0.14	0.054					1

Figure 20: Fitted binding isotherm for C6 on βCD for the titration with GDC. The thick line shows the best fit of the 2 sites model and the thin line shows the residuals (right axis).

4.1.3 Modelling the ITC titration

The total amount of released/absorbed heat at any point during the titration is proportional to the number of bound CDs and thereby proportional to the degree of saturation of the binding sites. If the enthalpy of binding 1 mole of CDs to a site on the BS is denoted by ΔH_{CD}, the released heat due to the partial saturation of this site is given as:

$$Q = [AB]\Delta H_{CD} V = f_1 N A_t \Delta H_{CD} V \qquad [4.34]$$

where V is the cell volume. For the 1 sites model, this equation may be used together with equation 4.9 to fit the ITC data using N, K and ΔH as fitting parameters. However, more precise results are obtained if the model is fitted to the directly measured observable which is the *increment* in Q, q, upon injection of an aliquot of CD solution.

$$q = Q(i) - Q(i-1) \qquad [4.35]^{iv}$$

For the 2 sites model Q is calculated as:

$$Q = VNA_t(f_{11}\Delta H1 + f_{12}\Delta H2) \qquad [4.36]$$

where ΔH1 and ΔH2 are the enthalpies for the binding of 1 mole of CDs to site 1 and site 2, respectively. As for the 1 sites model, the 2 sites model is also fitted to measured values of q yielding N, K1, K2, ΔH1 and ΔH2 as the best fit values of the fitting parameters.

Both models fit q as a function of A_t and B_t. These are the total concentrations of BS and CD in the titration cell, but due to dilution and displacement of the solution in the cell the calculation of these concentrations is not trivial. In the subsequent data analysis these concentrations are obtained from the Microcal application for Origin 7.0 that was supplied with the calorimeter and used for standard analysis of ITC data.

A fit of the 1 sites model to an enthalpogram[v], which is a plot of q as a function of the molar ratio, is shown in Figure 21. For this particular complex the binding constant is relatively large and results in a characteristic S-shaped plot. Weaker complexes give rise to a curve without an inflexion point.

[iv] This is a simplification of the actual method used to calculate q. The actual calculation of q takes into account the effect of displacing some of the volume upon each injection as described in the ITC manual "ITC Data Analysis in Origin" supplied with the calorimeter.

[v] All enthalpograms have been corrected for heat of dilution by subtraction of a reference experiment in which the CD solution is titrated into buffer.

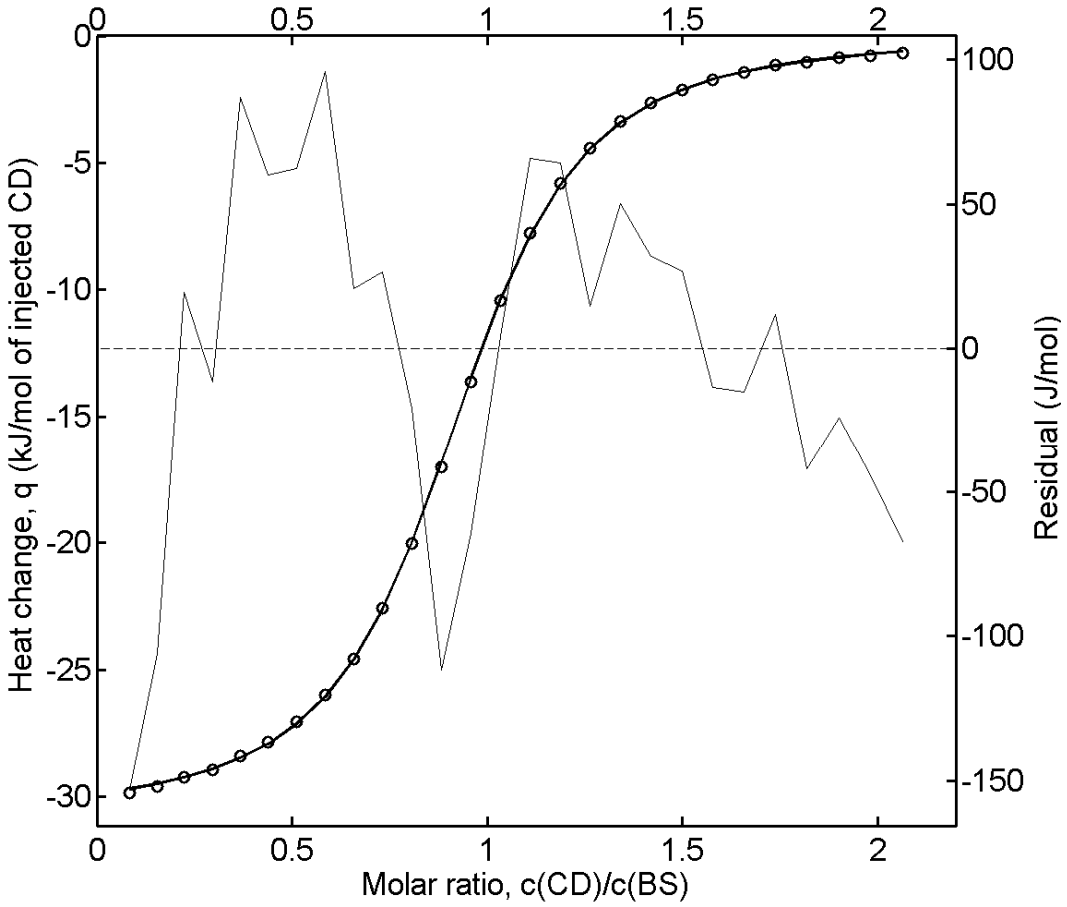

Parameter	Best fit value	Asymptotic 95% Interval	Correlation Matrix		
N	0.92	0.002	1	0.20	0.53
K (M^{-1})	134856	2433		1	0.68
ΔH (kJ/mol)	-30.77	0.07			1

Figure 21: Fit of the 1 sites model to the enthalpogram for the titration of 2.5 mM βCD into 0.25 mM GCDC at 25°C. The thin line shows the residuals (right axis).

4.1.4 Modelling the ACE titration

In ACE, the observable to be fitted by the binding model is the electrophoretic mobility, μ, of the BS. A fixed amount of BS is injected into the capillary which contains buffer with varying concentrations of CD. The observed electrophoretic mobility of the BS depends on the fraction of complexed BS:

$$\mu = (1 - f_1)\mu_A + f_1\mu_{AB} \qquad [4.37]$$

where μ_A and μ_{AB} are the electrophoretic mobilities of the free BS and the complex, respectively. Although an exact expression of μ can be derived by insertion of

equation 4.9, an approximate expression is derived by combining equation 4.37 with equation 4.6:

$$\mu = \frac{\mu_A + \mu_{AB} K[B]}{1 + K[B]} \qquad [4.38]$$

Under the employed experimental conditions the concentration of bound CD is very low compared to the total concentration of CD, and [B] is approximated by B_t in equation 4.38. Thus the measured electrophoretic mobility may be fitted by equation 38 using μ_A, μ_{AB} and K as fitting parameters. However, since the viscosity of the buffer in the capillary depends significantly on the CD concentration it is necessary to correct the measured electrophoretic mobility,[51] and the mobility fitted by equation 4.38 is actually the corrected mobility. The correction factors were determined by an internal and an external standard as described in Paper III. An example of a corrected mobility isotherm is shown in Figure 22.

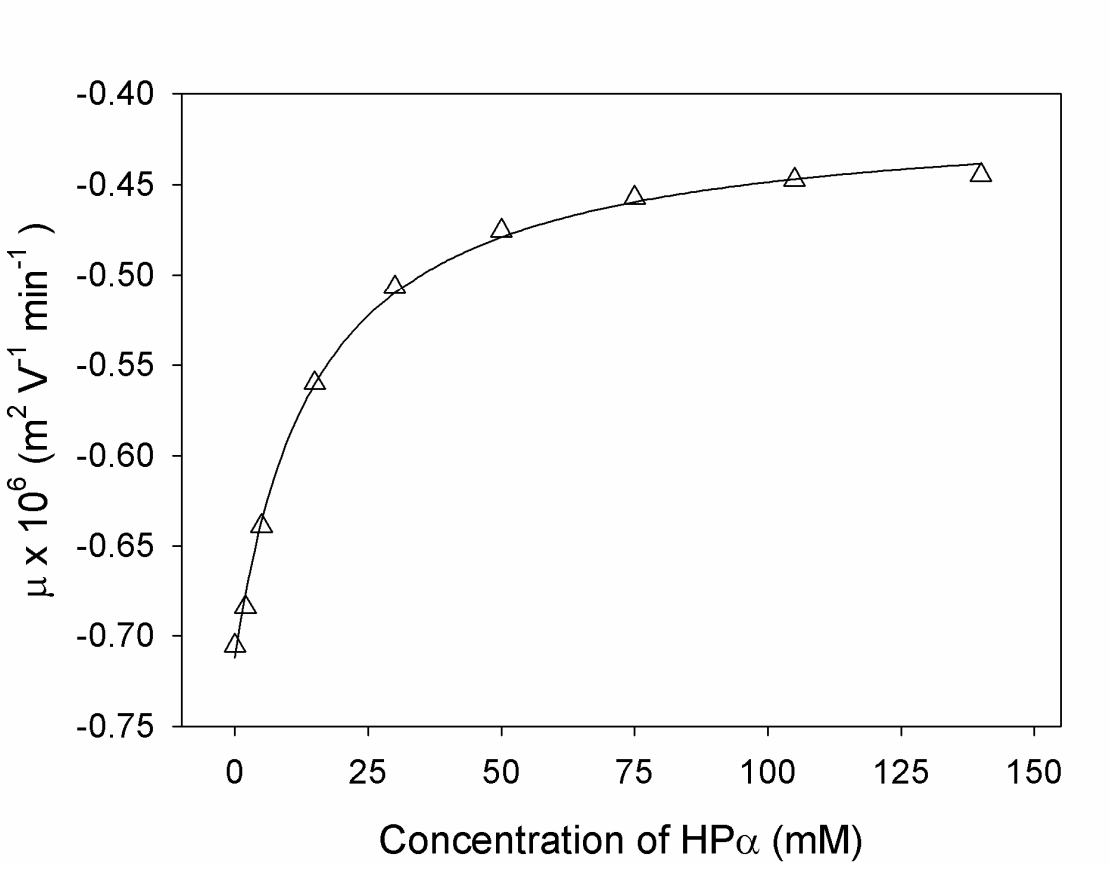

Figure 22: ACE binding isotherm for the HPα:GCDC complex. The plotted mobility has been corrected using an internal standard (Paper III).

Section 4.2: Calculation of ΔG°, ΔS° and ΔC_p

The ACE and NMR titrations were only conducted at a single temperature (25°C) and K is thus the only obtainable thermodynamic parameter from those experiments, in contrast to the calorimetric titrations which provide both K and ΔH. From K one may calculate ΔG°, and also ΔS° if ΔH is known:

$$\Delta G^\circ = -RT\ln(K) = \Delta H - T\Delta S^\circ \qquad [4.39]$$

Conducting the titrations at a range of temperatures allows for calculation of ΔC_p, according to the definition:

$$\Delta C_P = \left.\frac{\partial \Delta H}{\partial T}\right|_P \qquad [4.40]$$

As mentioned above, all thermodynamic functions may be calculated from the derivates of ΔG°. Thus, ΔH and ΔS° are given as:[52]

$$\frac{\Delta H}{T^2} = -\left.\frac{\partial}{\partial T}\frac{\Delta G^\circ}{T}\right|_P \qquad [4.41]$$

$$\Delta S^\circ = -\left.\frac{\partial \Delta G^\circ}{\partial T}\right|_P \qquad [4.42]$$

From these thermodynamic relations the temperature dependence of K (or ΔG°) is expressed as:[53]

$$\ln(K(T)) = \frac{\Delta H_0 - T_0\Delta C_P}{R}\left[\frac{1}{T_0} - \frac{1}{T}\right] + \frac{\Delta C_P}{R}\ln\left(\frac{T}{T_0}\right) + \ln(K_0) \qquad [4.43]$$

where ΔH_0 and K_0 are reference values measured at temperature T_0. Once ΔH_0, K_0 and ΔC_p are found at a single temperature, K may be calculated at any temperature. Alternatively, the expression may be fitted to a plot of ln(K) versus 1/T to provide values of ΔH and ΔC_p. It is often assumed that ΔC_p is negligible and a simpler version of equation 43, in which ΔC_p is set to zero, is used for non-calorimetric determination of ΔH.[54-57] Enthalpies determined from the temperature dependence of K are termed van't Hoff enthalpies (ΔH_{vH}) to distinguish them from directly measured enthalpies, termed calorimetric enthalpies (ΔH_{cal}). Although there are numerous examples of discrepancies between ΔH_{vH} and ΔH_{cal},[58,59] the two values should be equal. Discrepancies may arise from imprecise values of K, problems with the experimental equipment, or application of an improper binding model. Regarding the latter, I have

shown that comparison of ΔH_{vH} and ΔH_{cal} is a useful tool for selecting the proper binding model (Paper IV).

Section 4.3: Non-linear regression analysis

Regression is the process of fitting a mathematical expression to a dataset by finding the right set of fitting parameters that produces the best fit to the data. The best fit is the one that results in the smallest residuals, that is, the vertical distance between the fit and the experimental data. If the mathematical expression is linear, the parameters corresponding to the best fit can be calculated using linear algebra, but fitting a non-linear equation requires the use of an iterative procedure. One of the challenges inherent in non-linear regression is that one can never be sure that the regression produces the best fit. The iterative procedure may converge at a local minimum or it may stop before a minimum has been found. Another challenge is that it is difficult to determine the exact confidence intervals of the best fit parameters. Most software provides socalled approximate or asymptotic confidence intervals but these may give a very misleading picture of the exact confidence intervals.[60,61] To obtain reliable estimates of the fitting parameters it is necessary to do a parameter analysis in which the correlations between the parameters are checked, and, if necessary, exact confidence intervals are calculated. This is described in the next section followed by the analysis of some of my own data. For a general introduction to non-linear regression and its concepts, the reader is referred to the excellent book by Motulsky and Christopoulos,[62] which is available free of charge via the Internet at www.graphpad.com.

4.3.1 Parameter analysis and exact confidence intervals

Even if the iterative regression procedure finds the global minimum on the p-dimensional error surface spanned by the p fitting parameters, the best fit parameters corresponding to this minimum may not be the true parameters. First of all, there is a certain error associated with each data point. Such errors are mostly assumed to be random and are also called noise. Second, the fitting model may not be adequately describing the system under investigation. In the present case there are interactions between the molecules which are not accounted for by the binding models. Noisy data results in non-systematic variations of the residuals while the use of an inadequate fitting model results in systematic variations. Thus, plotting the residuals is a first step

in assessing the quality of the fit. The residuals shown on the plots above (residual axis is to the right) show no significant systematic variations, meaning that the intermolecular interactions described by the binding model constitute the dominant contributions to the observable. In contrast, the fit of the 1 sites model to the enthalpogram in Figure 23 show systematic variations of the residuals.

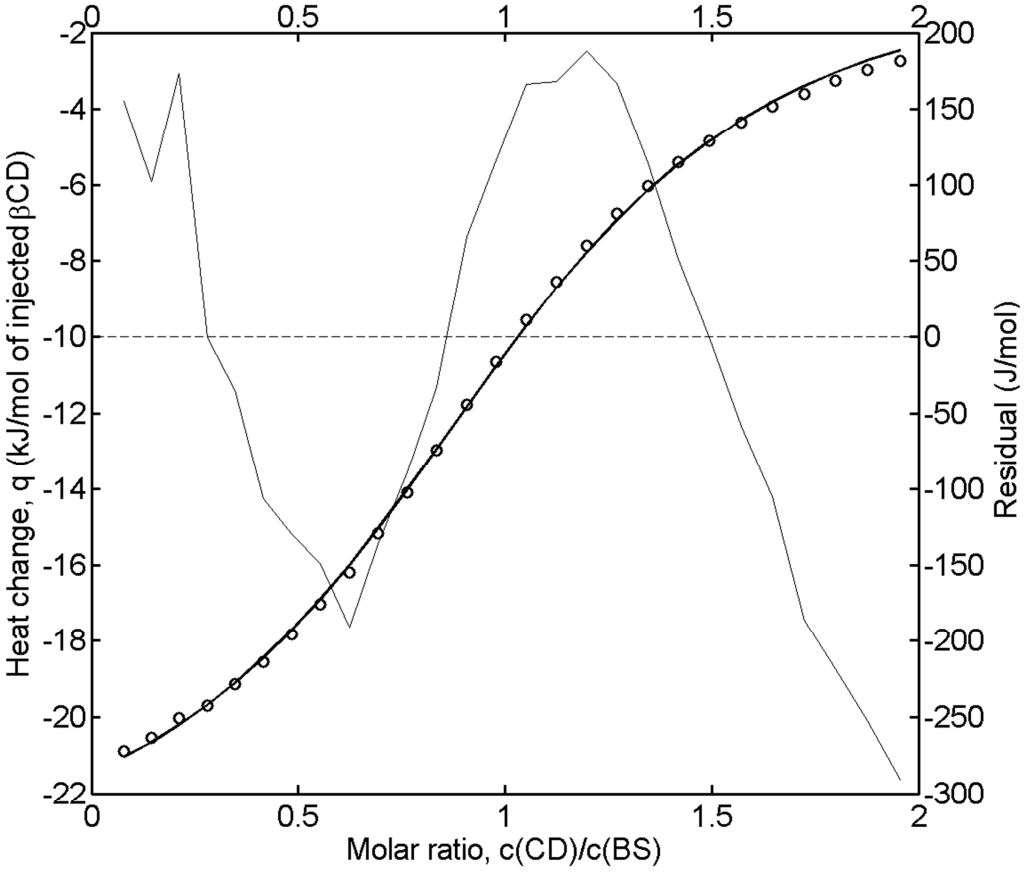

Parameter	Best fit value	Asymptotic 95% Error	Correlation Matrix		
N	1.04	0.010	1.00	0.43	0.71
K (M^{-1})	6260	380		1.00	0.87
ΔH (kJ/mol)	-24.41	0.37			1.00

Figure 23: Fit of the 1 sites model to the enthalpogram for the titration of 10 mM βCD into 1 mM GDC at 5°C. The residual (thin line and right axis) show systematic variations).

Despite the systematic variations, the errors on the parameters are relatively small but these errors can not be trusted since they are based on the assumption that the residuals are randomly distributed, which is clearly not the case. There might be several reasons for the systematic variations. The residuals are actually quite small and could be caused by many factors. The obvious explanation for the inability of the

model to account for the data is that the heat of dilution contributes significantly to the measured heat. The heat of dilution, measured in a reference experiment, has been subtracted from the raw data before fitting the model, but this may not completely eliminate the contribution from the heat of dilution in the real experiment. Another explanation is that the CD and BS may interact in a more complex way than described by the 1 sites model. The next step is thus to fit the data with the 2 sites model, which assumes the presence of a second binding site on the BS. The result is shown in Figure 24.

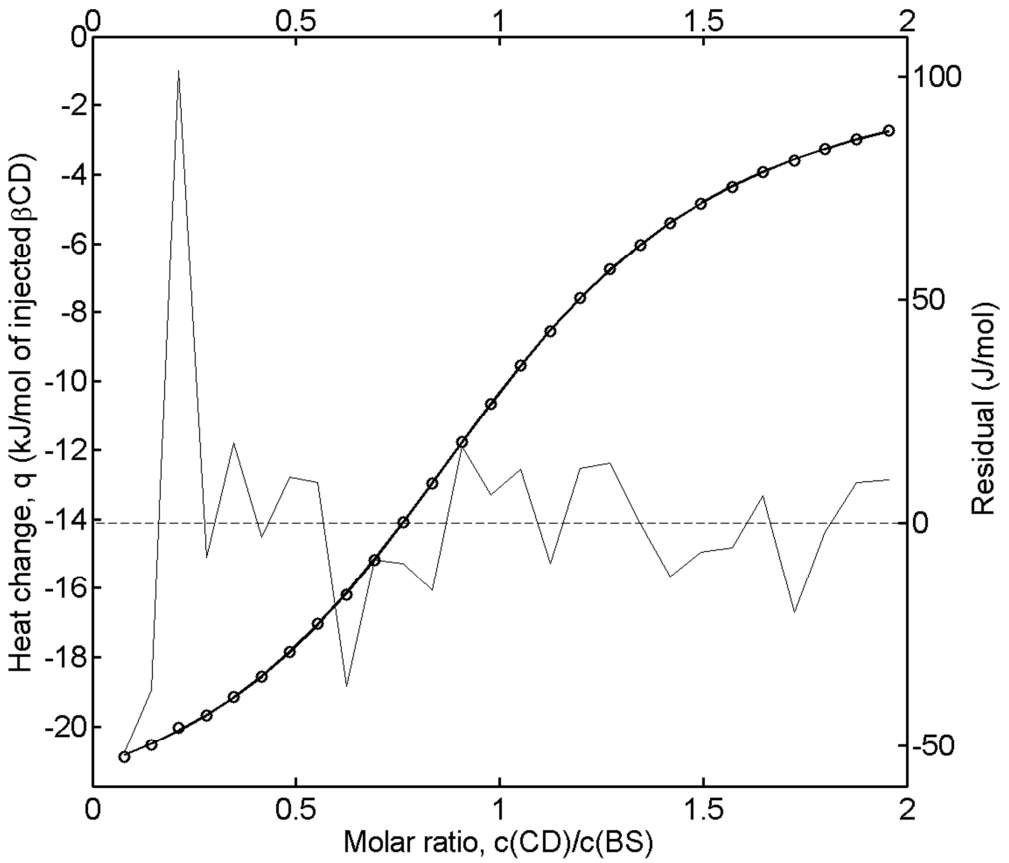

Parameter	Best fit value	Asymptotic 95% Error	Correlation Matrix				
N	0.97	0.031	1	-0.99	-0.99	-0.49	-0.98
K1 (M^{-1})	9997	3126		1	1.00	0.49	0.99
K2 (M^{-1})	216	370			1	0.43	1.00
ΔH1 (kJ/mol)	-23.34	0.11				1	0.38
ΔH2 (kJ/mol)	-10.03	10.14					1

Figure 24: Fit of the 2 sites model to the enthalpogram for the titration of 10 mM βCD into 1 mM GDC at 5°C. The residuals (thin line and right axis) are randomly distributed.

It is clear that the 2 sites model gives a much better fit to the data. The residuals are much smaller and are randomly distributed, but this should not lead to the conclusion that there is a second binding site. It is no surprise that the 2 sites model gives a better fit than the 1 sites model since it employs two additional fitting parameters, which are adjusted to provide a good fit. Rather than describing the thermodynamics of a possible second binding site, these 2 additional parameters could very well be modelling an improper correction for the heat of dilution or some experimental artefacts. Even if we know that there *is* a second binding site that is correctly described by the 2 sites model, the best fit parameters obtained from the enthalpogram in Figure 24 are very imprecise, as seen from the listed errors. The correlation matrix shows that there is a strong correlation between many of the parameters. As a parameter is changed from its best fit value the fit gets worse, but if there is a strong correlation this can be compensated by changing another parameter such that the resulting fit is not significantly worsened. Entries in the correlation matrix close to 1 or -1 means strong correlations. The correlation matrix in Figure 24 shows several entries that are close to 1 or -1, for example the correlation between K2 and ΔH2 which has the value 1.00. This means that a good fit is maintained even if K2 is changed from its best fit value, as long as it is accompanied by a change in ΔH2. Consequently, neither K2 or ΔH2 can be precisely determined. Further, it turns out that the errors listed in Figure 24 can not be trusted. These errors are based on the linear approximation and may deviate significantly from the exact confidence intervals, depending on the non-linearity of the fitting function.

To illustrate the non-linearity of the fitting function and to calculate the exact confidence intervals of the parameters, I have used a graphical approach called a profile *t* plot, described by Bates and Watts in the book *Nonlinear regression analysis and its applications.*[61] The idea is to vary each parameter, one by one, within a specified interval, while letting all other parameters float to achieve the best fit. As the investigated parameter is "forced away" from its best fit value the residuals increase. The steeper the increase in the residuals, the narrower is the confidence interval of the parameter. A poorly determined parameter may be pulled far away from its best fit value without significantly worsening the fit.

Specifically, the profile t function, $\tau(\theta_p)$, in equation 4.44 is plotted versus the studentized parameter, $\delta(\theta_p)$, in equation 4.45.

$$\tau(\theta_p) = sign(\theta_p - \hat{\theta}_p)\sqrt{\{\tilde{S}(\theta_p) - S(\hat{\theta})\}/s} \qquad [4.44]$$

$$\delta(\theta_p) = (\theta_p - \hat{\theta}_p)/se(\hat{\theta}_p) \qquad [4.45]$$

in which θ_p is the investigated parameter fixed at a value different from its best fit value, $\hat{\theta}_p$ is the investigated parameter at its best fit value, $S(\hat{\theta})$ is the sum of squared residuals when all parameters are allowed to float and $\tilde{S}(\theta_p)$ is the sum of squared residuals when θ_p is fixed. s is the square root of the variance estimate and $se(\hat{\theta}_p)$ is the asymptotic standard error on θ_p. The *sign* operator yields the sign (plus or minus) of the bracketed expression.

In the case of a linear model the plot of $\tau(\theta_p)$ versus $\delta(\theta_p)$ yields a straight line with slope 1. Thus, the nonlinearity of the model is easily observed as the deviation from this line.

The exact confidence interval for θ_p is given as the interval for which:

$$-t(f;\alpha/2) \le \tau(\theta_p) \le t(f;\alpha/2) \qquad [4.46]$$

in which $t(f;\alpha/2)$ is Student's T distribution for f degrees of freedom. Thus, an additional y-axis may be constructed for the confidence limits corresponding to each value of $\tau(\theta_p)$. The desired confidence limit, e.g. the 95% upper confidence limit, can be read from the profile t plot as the parameter value where the 95% confidence limit intersects the t plot. The intersection with the straight line gives the asymptotic confidence intervals.

Examples of t plots based on the fit in Figure 24 are shown in Figure 25 and Figure 26. These show the t plots for the parameters K2 and ΔH2, which are the most problematic parameters. The t plot of K2 in Figure 25 only shows a slight non-linearity, so the exact upper 95% confidence limit is only a little higher than the linear approximation, which gives 586 M^{-1}. The lower 95% confidence limit (even the 80%

limit) is negative, which is unphysical. All that can be concluded about K2 from this enthalpogram is that it with 95% confidence is below 696 M^{-1}. It might even be zero, meaning that a secondary binding site is non-existent.

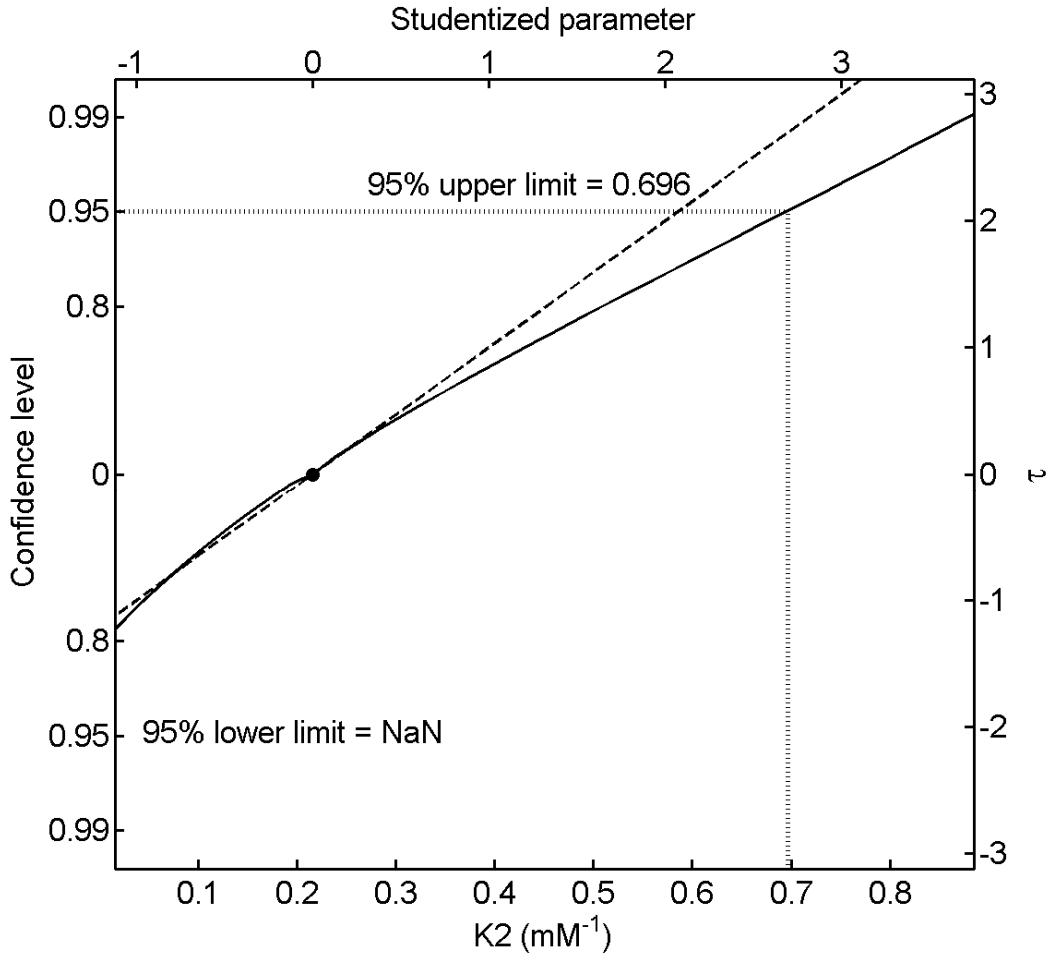

Figure 25: Profile t plot for K2 obtained from the fit of the 2 sites model to the titration of 1 mM GDC with 10 mM βCD at 5°C. Full line shows the profile t function, $\tau(\theta_p)$, broken line corresponds to the linear approximation and the dotted lines show the construction of exact 95% confidence limits. NaN means that no lower 95% confidence limit is found.

The t plot of ΔH2 (Figure 26), obtained from the same enthalpogram, shows severe non-linearity and the exact confidence intervals strongly deviate from the approximate intervals. Actually, the exact upper 95% confidence limit (-6.2 kJ/mol) is much lower than the approximate limit (0.1 kJ/mol). Conversely, the exact lower limit is much lower than the approximate limit, and can not be determined. This means that ΔH2 could be set to an extremely negative value without destroying the quality of the fit. The strong correlation between ΔH2 and K2 suggests that very negative values of ΔH2 are compensated for by letting K2 approach zero.

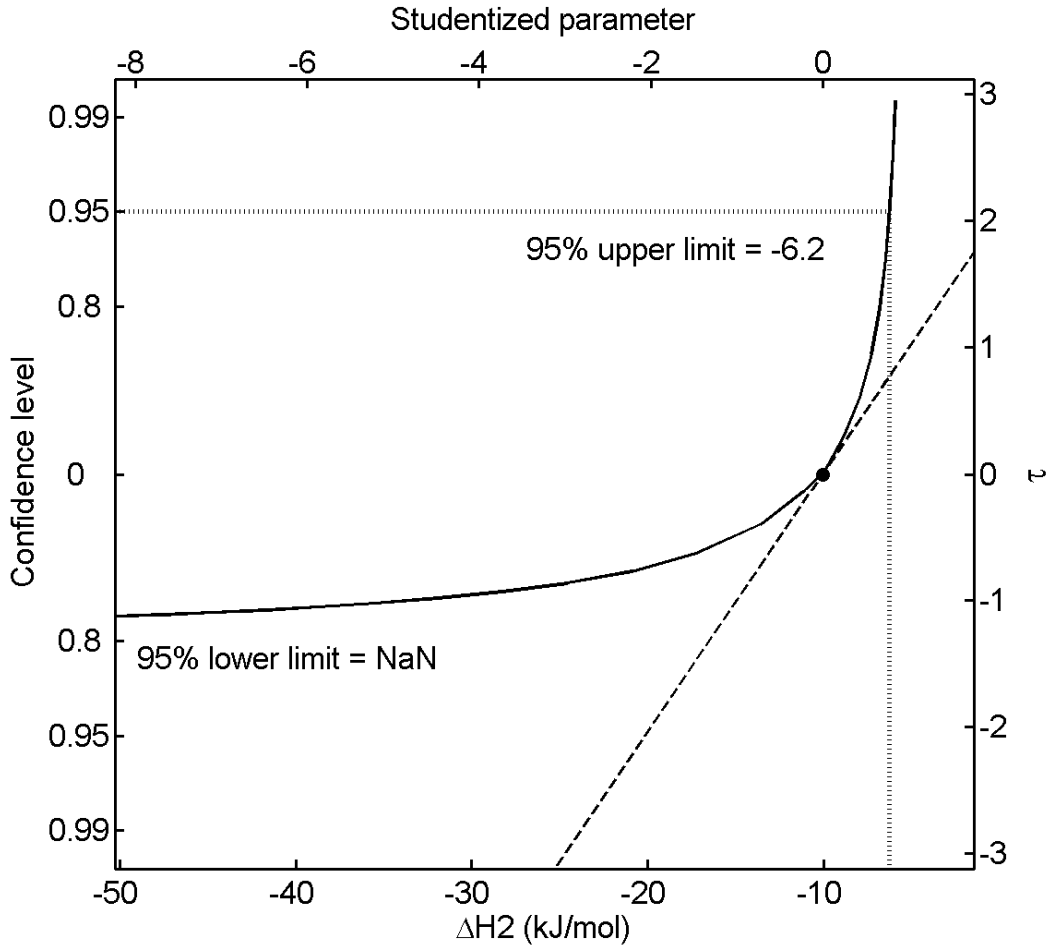

Figure 26: Profile t plot for ΔH2 obtained from the fit of the 2 sites model to the titration of 1 mM GDC with 10 mM βCD at 5°C. Full line shows the profile t function, $\tau(\theta_p)$, broken line corresponds to the linear approximation and the dotted lines show the construction of exact 95% confidence limits. NaN means that no lower 95% confidence limit is found.

The above example illustrates the problem of over-parameterization, a situation in which one or more of the parameters are redundant (or almost redundant) in the fit of a particular dataset. Similar problems arise when the NMR isotherms for the CD ^{13}C nuclei are fitted with the 2 sites model. The t plot of K1, as determined from the isotherm of C1 in Figure 19, is shown in Figure 27. The plot is highly non-linear and the asymptotic confidence intervals are extremely misleading. According to the linear approximation, K1 could easily be set to 0 without ruining the fit but the exact lower limit shows that K1 with 95% confidence is larger than 1230 M^{-1}. Conversely, there is no upper limit of K1. The t plot of K2 (not shown) is very similar and sets a lower limit of 205 M^{-1} but no upper limit is defined.

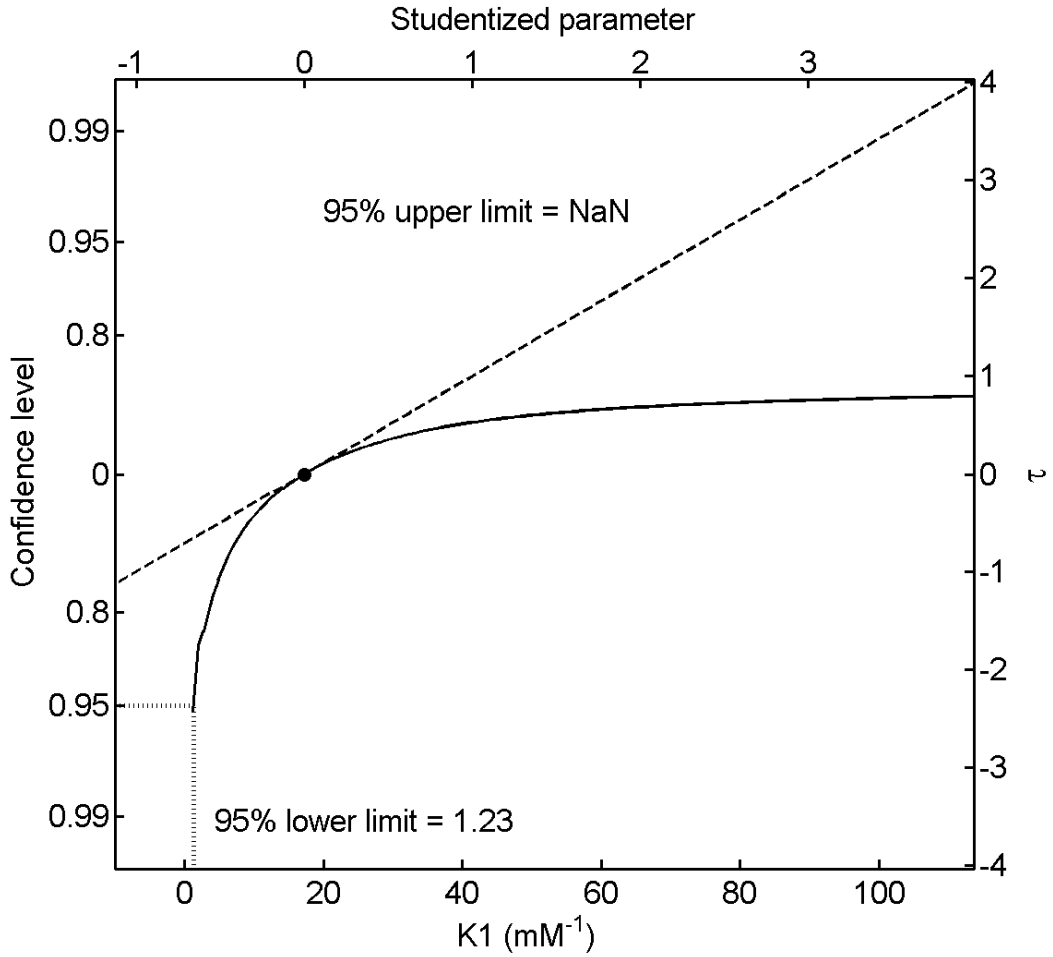

Figure 27: Profile t plot of K1 obtained from the fit of the 2 sites model to the NMR binding isotherm for the ^{13}C nucleus 1 on βCD upon complexation with GDC. Full line shows the profile t function, $\tau(\theta_p)$, broken line corresponds to the linear approximation and the dotted lines show the construction of exact 95% confidence limits. NaN means that no upper 95% confidence limit is found.

As mentioned above, the BS nuclei are much better suited for precise determination of the binding constants. This is also reflected in the t plots, an example is given in Figure 28, which show some non-linearity but not quite as much as observed for the CD nuclei.

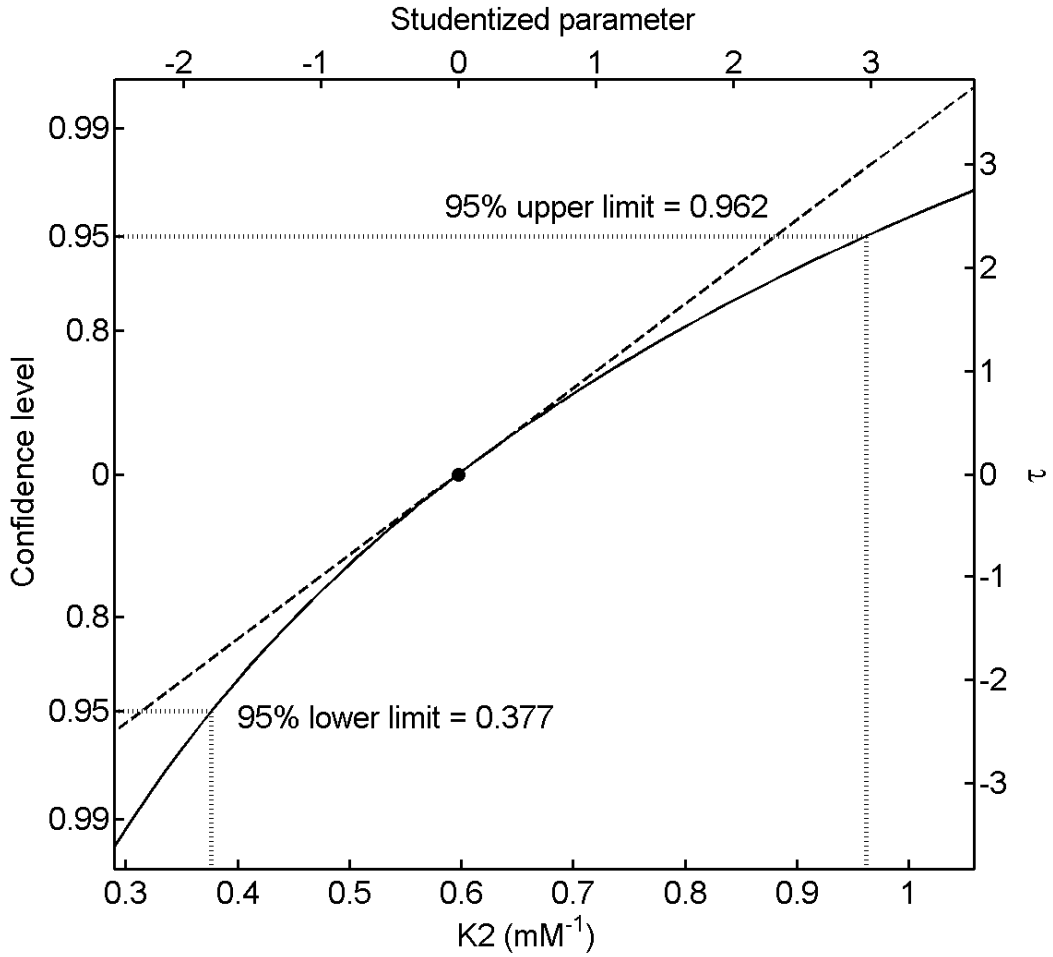

Figure 28: Profile t plot of K2 obtained from the fit of the 2 sites model to the NMR binding isotherm for the ^{13}C nucleus 4 on GDC upon complexation with βCD (see fit of the isotherm in Figure 17). Full line shows the profile t function, $\tau(\theta_p)$, broken line corresponds to the linear approximation and the dotted lines show the construction of exact 95% confidence limits.

4.3.2 Global fitting procedures

As illustrated by the above examples, the large number of fitting parameters in the 2 sites model leads to relatively large confidence intervals on the parameters describing the secondary site. The calorimetric titration can not even determine if there is a secondary site or not. So how can the confidence intervals be narrowed down? The obvious answer is to increase the accuracy and number of the individual datapoints that constitute the binding isotherm. Another solution is to improve the experimental design, for example by using other concentrations of the interaction species. In order to precisely characterize the secondary binding site on GDC, it would be beneficial to conduct the calorimetric titration to a higher molar ratio of CD/BS (it is only conducted to molar ratio 2 in Figure 24) to increase the number of CDs that bind to the weaker secondary site. By lowering the concentration of GDC in the sample cell I

have conducted titrations to molar ratios of 4 and 8. Although more precise parameters are obtained, it is still not convincing that the secondary site parameters actually describe a secondary binding site (Paper IV). They could just as well express some other heat effect, for example heat of dilution.

One way to increase the number of datapoints and at the same time take advantage of an improved experimental design, is to conduct a global fit of several titrations. Individual fits to each of the titrations provides an individual set of fitting parameters for each experiment. *E.g.*, three titrations would provide three different binding constant as well as three different values of N and ΔH. In a global fitting procedure all titrations are fitted simultaneously by one set of global fitting parameters. Fitting the 1 sites model to several titrations would thus yield the values of N, K and ΔH that provides the best fits to all of the experimental data. If designed correctly, global fits may strongly improve both precision and accuracy of the fitting parameters. For this reason, global fits have been used in a number of cases to determine binding constants and binding enthalpies from several calorimetric titration experiments, using both simple and more complex binding models.[63-65] Usually the concentration of the binding species are varied among the experiments, but in my study of the βCD:GDC complex, an extra dimension is added to the experimental parameter space by also varying the temperature. Global fits to titrations conducted at several concentrations and temperatures provide precise values of K, ΔH and ΔC_p for both binding sites on GDC. Further, the consistency with the basic thermodynamic relations given by equations 4.42 and 4.43, which are incorporated into the fitting equations, is a strong validation of the obtained binding parameters. All enthalpograms included in the global fit of the βCD:GDC titrations are shown in Figure 29 along with a table listing the binding parameters. In addition to the 6 fitting parameters shown in Figure 29, the stoichiometry N was employed as a local parameter. The resulting 18 values of N range from 0.89 to 0.95. Ideally, one would obtain the same value of N in all titrations but the deviation in N might be attributed to variations in the concentrations of the reactants. Generation of profile t plots (not shown) for each of the fitting parameters reveal that the exact confidence intervals are close to the approximate confidence intervals listed in the table in Figure 29.

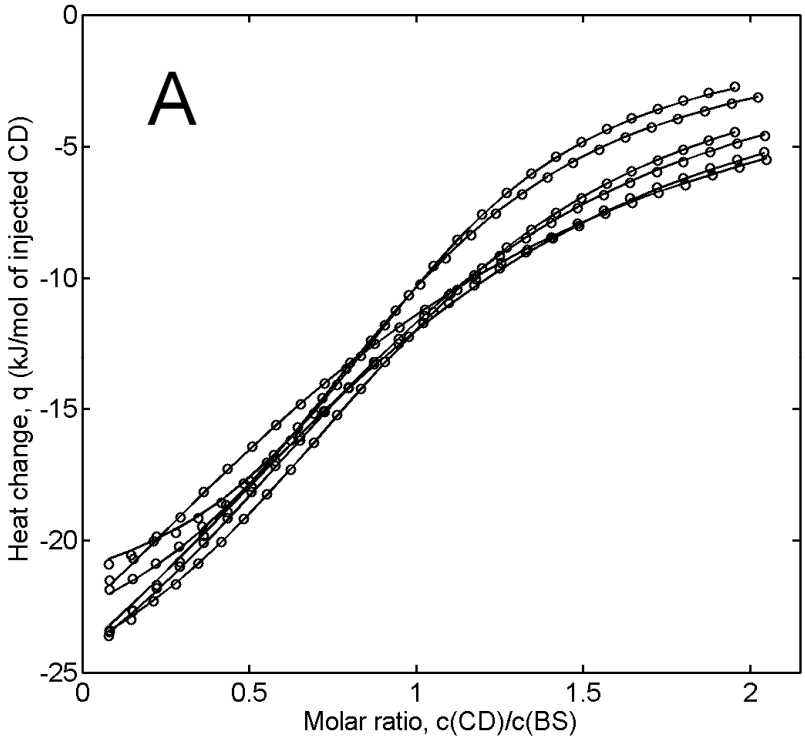
A
Heat change, q (kJ/mol of injected CD)
Molar ratio, c(CD)/c(BS)
0
-5
-10
-15
-20
-25
0
0.5
1
1.5
2

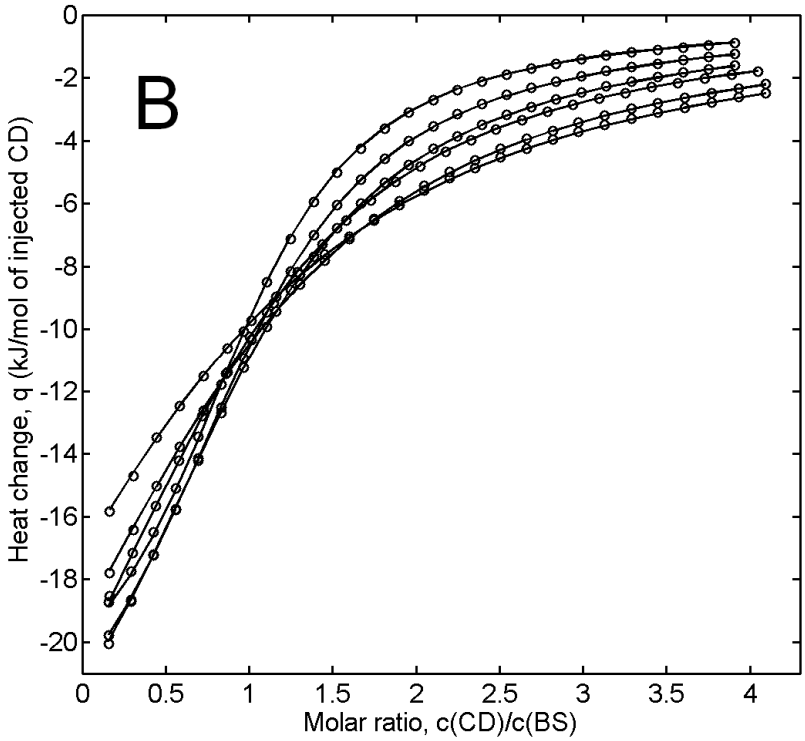
B
Heat change, q (kJ/mol of injected CD)
Molar ratio, c(CD)/c(BS)
0
-2
-4
-6
-8
-10
-12
-14
-16
-18
-20
0
0.5
1
1.5
2
2.5
3
3.5
4

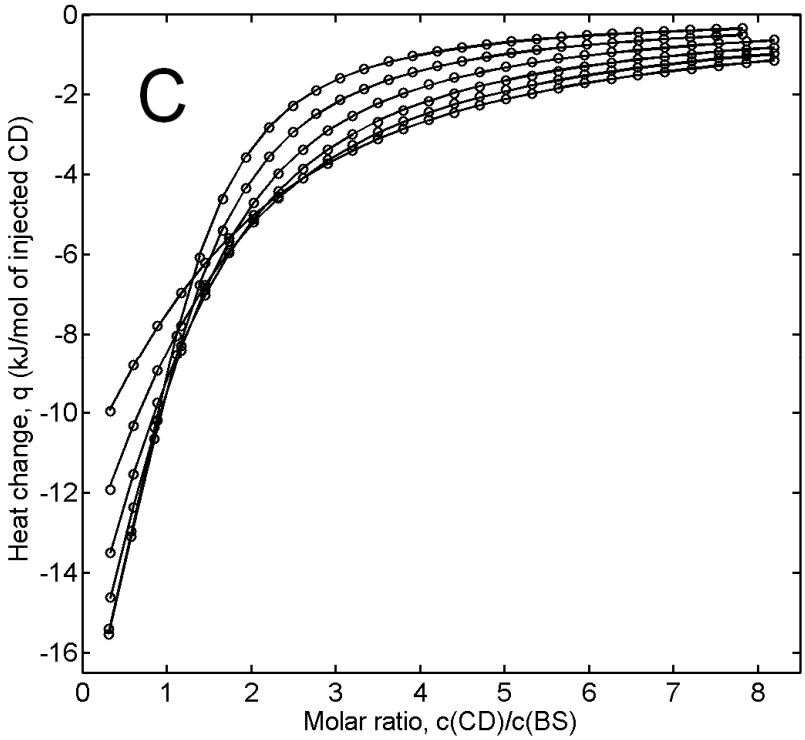

Parameter	Best fit value	Asymptotic 95% Interval	Correlation Matrix					
K1 (M^{-1})	5673	46	1	0.84	0.13	0.28	0.27	-0.07
K2 (M^{-1})	308	14		1	-0.34	0.59	-0.11	0.12
ΔH1 (kJ/mol)	-28.50	0.06			1	-0.46	0.79	-0.27
ΔH2 (kJ/mol)	-14.87	0.30				1	-0.33	0.65
ΔC_p1 (J/mol/K)	-271.14	2.82					1	-0.13
ΔC_p2 (J/mol/K)	-359.22	16.02						1

Figure 29: Global fit of the 18 enthalpograms shown in the three windows above. 10 mM βCD was injected into 1, 0.5 or 0.25 mM GDC, producing titrations to molar ratio 2 (window A), 4 (window B) or 8 (window C), respectively. Such experiments were conducted at 6 temperatures in the range 5-55°C. Experimental data are shown by circles and the best fit of the 2 sites model is shown by the line.

Recently, a global fit of calorimetric titrations conducted at different temperatures was used to determine both the thermodynamics and kinetics for the binding of a ligand to RNA and subsequent folding of the RNA,[66] thus illustrating the usefulness of including the temperature dimension in the global analysis.

Section 4.4: Results: Complexation thermodynamics of all investigated complexes

In the preceding parts of this chapter two different binding models were presented and the mathematical equations required for the analysis of experimental data from the ACE, NMR and ITC titrations were derived. Statistical tools for the analysis of the obtained fitting parameters were presented and a global fitting procedure was employed to improve the precision of the fitting parameters when the 2 sites model was used (Paper IV). The global fitting procedure is also used to determine ΔC_p (Paper VII). The results for all of the investigated complexes of glycoconjugated BSs are presented in Table 4. Most of the corresponding complexes with tauroconjugated BSs have also been characterized but since the thermodynamics are very similar to the glycoconjugated counterparts the data are not shown in the table but can be found in Paper I and II.

Most of the thermodynamic data in Table 4 was obtained by analyzing the titration with the 1 sites model. The 2 sites model was only employed for the βCD:GDC complex. However, the structural analysis in Section 3.3 suggests that not only the natural βCD but also the methylated βCDs bind to a secondary site on GDC. Global temperature fits of the 2 sites model to calorimetric titrations of these complexes did not yield significantly better fits than the 1 sites model, and in some cases the 2 sites model provided fitting parameters that were not meaningful. These titrations were only conducted to molar ratio 2 and therefore it is difficult to detect and characterize a weaker secondary site. Further, the 2 sites model assumes non-cooperativity between the sites. This seems to be a valid assumption for the 2:1 βCD:GDC complex, but the extended cavity of the methylated βCDs is expected to result in severe repulsion between the two CDs.

Table 4: Compilation of thermodynamic data for the studied complexes. Only thermodynamic data for glycoconjugated BSs are shown. Most of the corresponding complexes with tauroconjugated BSs have also been characterized but since the thermodynamics are very similar to the glycoconjugated counterparts the data are not shown.

BS	CD	Method	K (M^{-1})	ΔH (kJ/mol)	TΔS° (kJ/mol)	ΔC_p (J/mol/K)
GC	αCD	ACE	12	-	-	-
	HPα	ACE	46	-	-	-
	βCD	ITC	2960	-25.2	-5.4	-318
	mβ067	ITC	2902	-19.2	0.6	-
	mβ069	ITC	3464	-20.0	0.2	-
	mβ117	ITC	2262	-13.7	5.4	-
	mβ163	ITC	1809	-12.4	6.2	-
	mβ167	ITC	1742	-12.5	6.0	-
	mβ209	ITC	2474	-16.0	3.4	-
	mβ212	ITC	2716	-15.1	4.5	-
	mβ300	ITC	NA[1]	NA[1]	NA[1]	-
	HPβ054	ITC	2141	-13.6	5.4	-
	HPβ063	ITC	2084	-11.5	7.4	-413
	HPβ082	ITC	1229	-6.8	10.8	-
	HPβ102	ITC	1162	-3.5	14.0	-494
	HPβ106	ITC	669	-4.3	11.8	-
	SBβ091[2]	*ITC*	*1520*	*-13.4*	*4.8*	-
	γCD[3]	*ITC*	*5030*	*-13.13*	*8.0*	-
GDC	αCD	ACE	21	-	-	-
	HPα	ACE	93	-	-	-
	βCD	ITC	5673	-28.5	-7.1	-271
	mβ067	ITC	5711	-20.9	0.5	-396
	mβ069	ITC	7374	-22.3	-0.2	-
	mβ117	ITC	4825	-12.9	8.1	-
	mβ163	ITC	4265	-10.6	10.1	-
	mβ167	ITC	3883	-11.1	9.4	-534
	mβ209	ITC	7514	-20.4	1.7	-
	mβ212	ITC	7481	-20.1	2.0	-432
	mβ300	ITC	NA[1]	NA[1]	NA[1]	-
	HPβ054	ITC	4326	-16.3	4.5	-
	HPβ063	ITC	4677	-13.3	7.6	-458
	HPβ082	ITC	3284	-7.8	12.3	-
	HPβ102	ITC	3348	-4.2	15.9	-574
	HPβ106	ITC	2405	-4.0	15.3	-
	SBβ091	ITC	4160	-11.7	9.0	-584

	γCD[3]	*ITC*	*14,400*	*-10.4*	*13.4*	-
GCDC	αCD	ACE	10	-	-	-
	HPα	ACE	68	-	-	-
	βCD	ITC	156,226	-30.9	-1.3	-484
	mβ067	ITC	174,490	-27.3	2.6	-518
	mβ069	ITC	191,200	-28.6	1.5	-
	mβ117	ITC	152,767	-23.0	6.6	-
	mβ163	ITC	123,967	-22.2	6.9	-
	mβ167	ITC	137,163	-21.4	7.9	-650
	mβ209	ITC	141,100	-27.7	1.7	-
	mβ212	ITC	135,929	-26.8	2.5	-598
	mβ300	ITC	2634	-33.6	-14.1	-564
	HPβ054	ITC	84,657	-22.4	5.7	
	HPβ063	ITC	74,465	-20.2	7.6	-615
	HPβ082	ITC	41,935	-16.1	10.3	-
	HPβ102	ITC	35,430	-13	13.0	-702
	HPβ106	ITC	22,617	-12.8	12.1	-
	SBβ091	ITC	112,978	-22.2	6.6	-669
	γCD[3]	*ITC*	*95,067*	*-13.9*	*14.5*	-
GDC 2nd site	βCD	ITC	308	-14.9	-0.7	-359
	βCD	NMR	546	-	-	-

1: The association between the CD and the BS is too weak to be reliably determined by ITC.
2: The data are from Paper VI.
3: The data are from Paper V.

Chapter 5: Relations between structure and thermodynamics

In Section 3.3 the structures of the complexes were derived and the complexation thermodynamics were determined by the techniques described in Chapter 4. This large pool of structural and thermodynamic data allows for a detailed comparative analysis of the relations between the thermodynamics of binding and the structures of the binding species and their complexes. The elucidation of these relations between structure and properties may benefit the rational design of new modified CDs, and may also contribute to the understanding of intermolecular interactions.

Section 5.1: Binding constants

It is apparent from Table 4 that the investigated complexes exhibit very different thermodynamic stabilities. Many of these differences are explained on the basis of the known molecular structures.

5.1.1 Effect of the CD cavity size

The diameter of the CD cavity is crucial for the stabilities of the complexes.[4] The small diameter of the αCDs limits the inclusion of the BS and only the conjugation tail is included. Apparently, this is not a very favourable structure and the binding constants are in the range of 10-20 M^{-1} for the complexes with the natural αCD. Straight-chain guests fit well into the cavity of αCD and complexes with alkanols exhibit binding constants up to several thousand M^{-1}, increasing with the length of the carbon chain.[4] The low affinity towards BSs is probably due to the hydrophilic groups on the conjugation tail.

As shown in Section 3.3, the larger cavity diameter of βCDs and γCD allows the inclusion of the more bulky steroid body of the BSs. This results in larger binding constants, which could be explained by increased van der Waals attractions. The binding constants of natural βCD and γCD are similar in magnitude although βCD

binds stronger to GCDC while γCD binds stronger to GC and GDC. The smaller diameter of βCD probably gives a tighter fit with GCDC and a stronger binding.

5.1.2 Effect of the BS structure

The structures of the investigated BSs differ in the type of conjugation, which is either glycine or taurine, and the number and position of hydroxyl groups on the steroid body. In agreement with previous observations[7] the type of conjugation only play a minor role, with the glycoconjugated BSs having a slightly higher affinity towards βCDs. Even in the complexes with αCDs, where the conjugation tail is partially included in the CD cavity, only small differences between the glyco- and tauroconjugated BSs are observed.

The number and position of hydroxyl groups on the steroid body is a much more important factor, even in the complexes with the αCDs, which are located at a reasonable distance from the hydroxyl groups. The importance of the hydroxyl groups on the BS was first noted by Tan and Lindenbaum who observed that the presence of a hydroxyl or carbonyl group at C12 results in reduced binding affinity towards natural βCD.[67] They speculated that the presence of such groups at C12 hinder βCD binding beyond the D ring. Such observations and a similar interpretation are found in a number of later works on complexes with natural βCD[7,68] and modified βCDs[15,41]. My results are in line with these observations and show that the presence of a hydroxyl group on C12 decreases the binding constants of the βCDs 30-80 times, depending on the modification of the βCD. The analysis of the complex structures in Section 3.3 only revealed minor structural differences in the binding to GC and GCDC with a slightly deeper inclusion of GCDC, and it is interesting that these minor structural differences have such a marked impact on the binding constants. In addition to sterically preventing the deep inclusion of the BS, the hydrophilicity of the 12-OH group is probably also an important factor, making it less favourable for the βCDs to reside on the D-ring. The small structural differences of the complexes induced by the 12-OH group suggest that the hydrophilicity rather than the bulkiness of this group is the more important factor. This tentative conclusion is to some extent corroborated by the impact on the binding to γCD. The bulkiness of the 12-OH group can not prevent the wider γCD from moving from the D-ring onto the B- and C-rings and there do not

seem to be significant differences in the binding modes of the three investigated BSs. Still, as shown in Table 4 and in a previous investigation of γCD and HPγCD[16] the 12-OH group has a significant impact on the association constants. The numbers in Table 4 show that the binding constants for GCDC are almost 20 times large than for GC. This difference is not as large as for the βCDs and might be related to the ability of the γCD to move back and forth along the steroid body and thus avoid unfavourable binding positions. In this way, the 12-OH on GC and GDC does not destabilize the γCD complexes to the same extent as for the βCD complexes.

The impact of the hydroxyl group on C7 has also been studied previously, and shows a much smaller impact on the binding affinity, which is usually slightly higher in the absence of 7-OH.[7,17,19,69,70] Again, my results confirm that this trend is valid for all types of modified βCDs which bind 2-3 times stronger to GDC than to GC. The structural analysis shows that 7-OH is not included in the cavity of the βCDs but its proximity to the binding site apparently still has a destabilizing effect. Surprisingly, even though γCD resides closer to 7-OH, the effect is of the same size as for the βCDs - the binding constant of GDC towards γCD is just three times larger than GC.

5.1.3 Effect of substituents on modified CDs

The substituents at the rims of the CDs may affect the ability of the CD to form complexes with guest molecules through several mechanisms. The partial substitution of hydroxyl groups at the secondary rim of the CDs results in a disruption of the hydrogen bond network that is thought to stabilize the circular structure of the CD. Consequently, the shapes of substituted CDs may differ from the natural CDs,[71,72] although a NMR study claims that conformational changes of the CD torus only take place in peralkylated CDs.[73] A distortion of the CD structure will inevitably affect the inclusion of the guest. Various kinds of direct interactions between the substituents and the guest may also affect the complex stabilities. Depending on the site of substitution the substituent may block the cavity opening or the substituent may engage in favourable interactions with the guest.

The association constants for complexes of HPβCDs are shown in Figure 30. It is clear that the HP-substituents have a destabilizing effect on complexes with the three

types of BSs. In all three cases the stabilities of the complexes decrease in a similar way with the number of HP-chains attached to the rims of the CD. The reason for this destabilization is not clear and can only be speculated about. The MD simulations showed that HP-substitution results in an increased burial of non-polar surface upon complexation (Section 3.3), but this should *stabilize* the complexes through increased hydrophobic interactions.

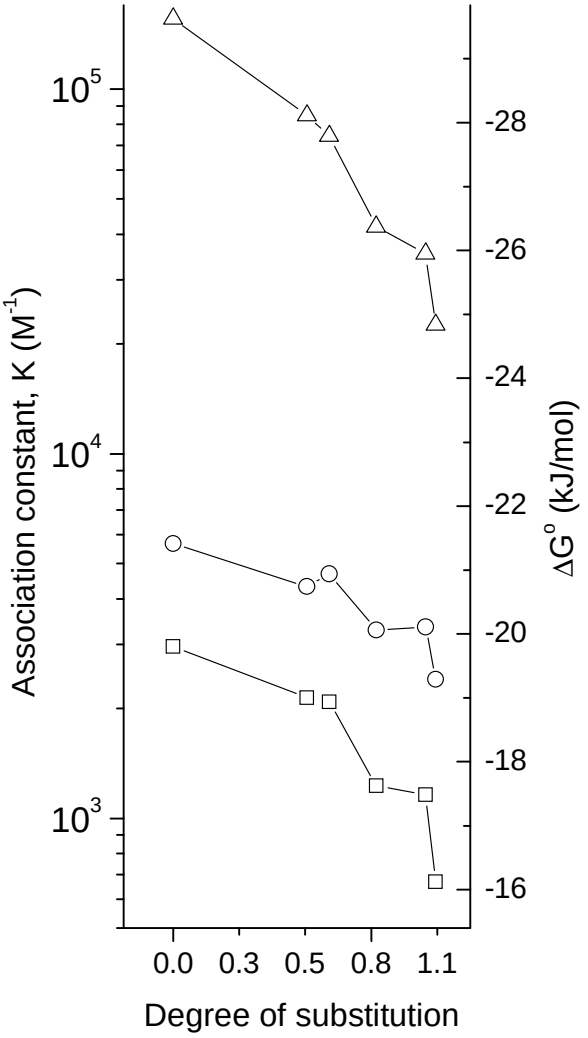

Figure 30: Association constants from Table 4 for complexes of HPβCDs plotted as a function of the number of HP-substituents per glucose unit. □: GC, ○: GDC, △: GCDC.

So what could be the reason for the destabilizing effect of the HP-substituents? It is not hard to imagine that the HP-substituents occasionally move in front of the cavity of an empty CD and prevent an approaching BS from entering. Thermodynamically, this amounts to an entropic destabilization. This hypothesis is purely speculative and

there could be other destabilizing effects such as the increased flexibility of the CD upon substitution.

Although the present study shows that an increased number of HP-substituents decrease the formation of inclusion complexes with all of the investigated BSs, the effect is different towards other guests. In the literature there are many examples of HPβCDs forming either stronger[74,75] or weaker[76-78] complexes than the natural βCD, depending on the type of guest molecule but also on the number and position of HP-substituents.[32]

As in the case of the HPβCDs, the effect of methylation depends on the degree of substitution of the CD but hardly depends on the type of BS. Further, the effect of methyl groups depends on the site of substitution and since the pattern of substitution varies among the investigated samples of mβCDs, no simple trend is observed when the association constant is plotted against the DS (see Figure 6 in Paper II). However, since the substitution patterns of the methylated samples have been established (Table 3) it is possible to discern the effects of substituting the various sites (O2, O3 and O6) (Paper II). It seems that methylation at O6 only has a minor effect which is not so surprising since it is situated at the primary rim from which the conjugation tail protrudes. The more bulky steroid body protrudes from the secondary opening and may thus interact with the methyl groups at O2 and O3. Methyl groups at O3 decrease the stability, probably by steric repulsion as they point inwards towards the guest (Section 3.3). Even though the BS still manage to enter the cavity of the CD, the steric repulsion between the methyl groups and the BS energetically destabilizes the complex. The methyl groups at O2, on the other hand, point away from the guest and cause more stable complexes. This could be explained by increased hydrophobic interactions between the methyl groups and the BS. It seems that the O2 methyls are too far away from the BS to disturb the inclusion but still close enough to engage in hydrophobic interactions.

Finally, the increased flexibility and structural distortion of the methylated CDs also seem to be of importance, especially in the complexes of the per-substituted mβ300, which form surprisingly weak complexes with all BSs (too weak to be detectable by ITC in the case of GDC and GC). It seems to be a general trend that complete methylation at O2 and O6 improves the affinity of the CD towards hydrophobic guest

molecules, but further methylation at O3 severely disturbs the complexation.[4,79,80] This is not always the case, however. For some guests, complexation is favoured by the flexible structure of CDs that are completely methylated at the secondary rim. The induced fit of these CDs leads to large van der Waals interactions with the guest and consequently large binding constants.[45,46]

Section 5.2: Enhalpic and entropic contributions

As expressed by equation 4.39, the overall binding affinity given by the binding constant, K, or the difference in standard Gibbs free energy, $\Delta G°$, can be divided into contributions from enthalpy, ΔH, and entropy, $\Delta S°$. Enthalpic contributions arise from the formation or breaking of non-covalent "bonds". Such bonds include hydrogen bonds, coulombic interactions and van der Waals interactions. Entropy is a measure of the disorder of the system and contributes positively to the stability of the complex if the complexation results in a more disordered system. The relative values of ΔH and $\Delta S°$ are often interpreted in terms of the forces and mechanisms driving the complexation. Negative contributions to ΔH are often taken as an indication of van der Waals interactions or hydrogen bonding, while positive contributions to $\Delta S°$ are interpreted in terms of hydrophobic interactions. [55,81-85] The interpretation of ΔH and $\Delta S°$, however, is being complicated by the fact that many individual interactions between the molecules contribute to the observed values of ΔH and $\Delta S°$. Further, the formation of a single bond may be accompanied by both structural changes and hydration changes whose contributions to ΔH and $\Delta S°$ overshadows the thermodynamic fingerprint of the bond formation itself. For example, the attachment of positively charged NH_3^+ groups to βCD dramatically improves its affinity towards negatively charged guest molecules, but ΔH is not becoming more negative as would be expected from the increased coulombic interactions. On the contrary, ΔH changes sign from negative to positive and the complex is stabilized by a large increase in $T\Delta S°$, which the authors ascribe to an extensive dehydration of the ions.[86]

In the following, the experimentally determined enthalpies and entropies for the formation of CD:BS complexes are primarily interpreted in terms of dehydration of the host and guest molecules. These are surrounded by a hydration layer in which the water molecules are structurally more ordered than in the bulk water. Upon

complexation some of these water molecules are released into the disordered bulk phase, resulting in a positive contribution to both ΔS° and ΔH. As was shown in Section 3.3, the buried surface area, which is proportional to the number of released water molecules, increase linearly with the DS of the CD. The thermodynamic impact of this dehydration of host and guest molecules will be explored in the following. It should be noted that the water molecules residing in the cavity of the CD experience a more confined environment than the rest of the hydration waters and may contribute in a thermodynamically different way when excluded from the cavity. The thermodynamics of the cavity-bound waters will not be discussed.

5.2.1 Variation in ΔH and ΔS°with the number of substituents

As shown in Figure 31 the number of HP-substituents results in a moderate increase in ΔG°, but the impact on ΔH and ΔS° is much larger. Both ΔH and ΔS° for the complexation with all 6 bile salts exhibit an almost linear increase with increased number of HP-substituents (only the glycoconjugated BSs are shown in Figure 31). As discussed in more detail later, this is interpreted in terms of an increased dehydration of hydrophobic surface, induced by the interaction of the HP-substituents with the parts of the BS that protrudes from the CD (see illustration in Figure 16).

Similar plots are shown in Figure 32 for the complexes of mβCDs. At low DS (<1.5) a similar, but less pronounced, increase in ΔH and ΔS° is observed, which is again interpreted as resulting from an increased burial of hydrophobic surface. Because the smaller methyl groups cause less dehydration than the larger HP-chains the increase in ΔH and ΔS° is less pronounced. At higher DS both ΔH and ΔS° decrease rather steeply. The reasons for this are not clear. It could be caused by a more shallow inclusion of the BS, and concomitant less extensive dehydration, due to steric repulsion with the O3 methyls, or as a consequence of an increasingly distorted CD. A more shallow inclusion is not supported, however, by the structural analysis in Section 3.3, which does not reveal any significant differences in the topologies of the complexes. Neither do the heat capacity changes (see below) fully support such interpretation. Another possible cause is the increased flexibility of the CD caused by the partial or complete disruption of the H-bond belt. A highly flexible CD possesses a large conformational entropy in its unbound state and will experience a large loss of

entropy as it binds to the BS. However, this interpretation is not in line with the suggestion in Section 3.3, that mβ167 undergoes larger conformational changes upon complexation than mβ209. It seems plausible, though, that the turning points in ΔH and ΔS° at around DS 1.5 are related to conformational changes of the CD structure caused by disruption of the H-bond belt, and a similar trend might be observed for the series of HPβCDs if extended to a larger DS.

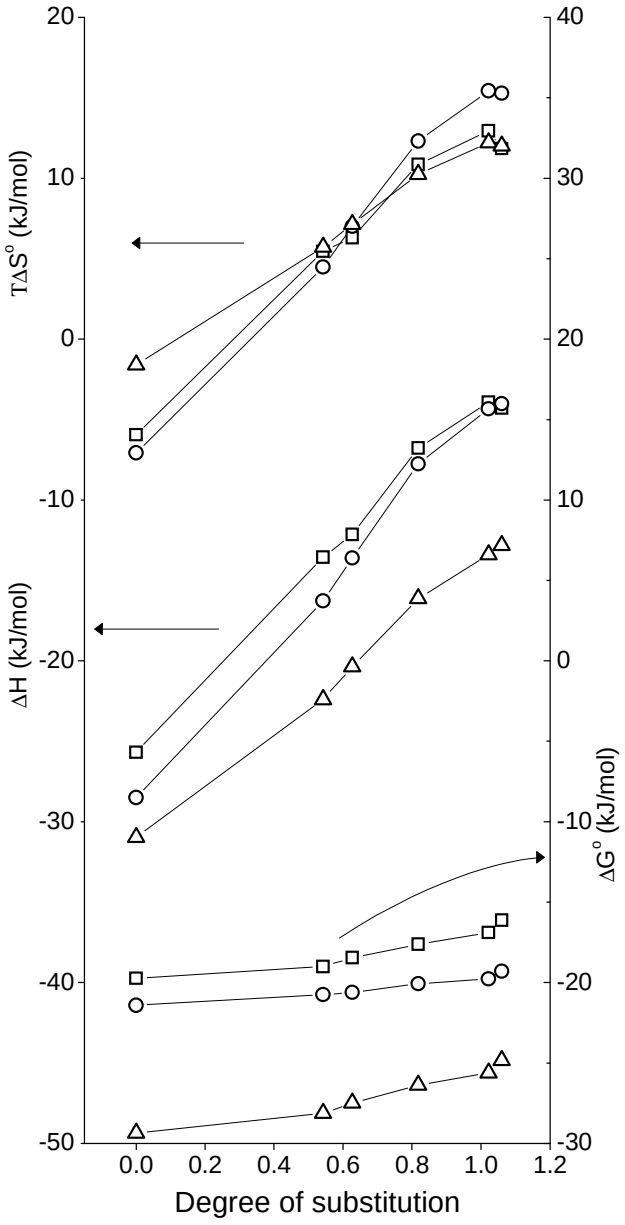

Figure 31: Changes in entropy, enthalpy (left axis) and Gibbs free energy (right axis) upon complexation with GC (□) , GDC (○) and GCDC (△), plotted as a function of DS for HPβCDs (Paper I) and natural βCD (Paper II and IV).

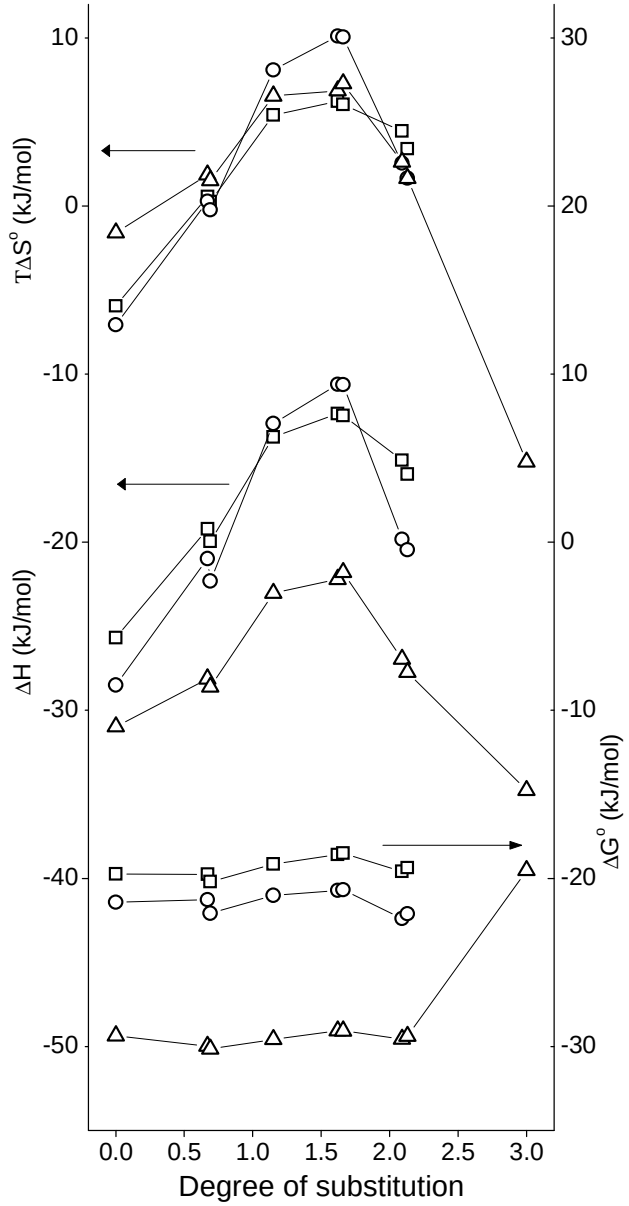

Figure 32: Changes in entropy, enthalpy (left axis) and Gibbs free energy (right axis) upon complexation with GC (□) , GDC (○) and GCDC (△), plotted as a function of DS for mβCDs (Paper II) and natural βCD (Paper II and IV).

5.2.2 Enthalpy-entropy compensation

The relatively small variation in ΔG° as compared to the large variation in ΔH is a consequence of enthalpy-entropy (H-S) compensation in which an increase (or decrease) in ΔH is compensated by a similar increase (decrease) in TΔS°, such that the resulting change in ΔG° (see equation 4.39) is relatively small. Even though the presence of substituents at the rim of the CD has a large impact on the enthalpy and

entropy of binding to the BSs, the stability of the complexes is affected to a much smaller extent.

H-S compensation is commonly observed among CD inclusion complexes and is often illustrated by plotting $T\Delta S°$ as a function of ΔH,[4,33,57,82] or sometimes by plotting ΔH as a function of $\Delta S°$.[7,87,88] In both cases the datapoints should lie on straight lines, with slopes being close to 1 or the experimental temperature, T, respectively. The first type of H-S compensation plot is constructed in Figure 33 using the experimentally determined thermodynamic data for all investigated complexes of βCDs – natural βCD, HPβCDs, mβCDs and SBβCD. It turns out that the data fall into three groups depending on the type of guest molecule: Complexes of GC and TC form one group, GDC and TDC another and GCDC/TCDC a third group. The broken lines in the figure indicate the linear regression to each of the groups and show that all of the data fall on three straight lines (R^2 = 0.99, 0.99 and 0.97) with slopes slightly below unity (α = 0.82, 0.90 and 0.75). The interpretation of the H-S compensation plot is discussed in subsection 5.2.5.

It is noteworthy that the complexes are divided into three groups according to the identity of the guest molecule rather than the character of the host molecule. After all, the structural differences between the three groups of BSs are minor compared to the CDs which differ in both type, position and number of substituents. In terms of complex stabilities, the position of a single hydroxyl group on the BS is a much more important factor than the numerous substituents at the rim of the CD.

A second observation is that all complexes of modified βCDs, with the exception of mβ300 which is not shown in the plot, are shifted towards the upper right corner. The complexes of the highest substituted HPβCDs are found in the upper right corner of the H-S compensation plot. This indicates that all investigated types of substituents fundamentally behave the same way in the complexes and cause an increased dehydration (see next subsection).

In other calorimetric studies the same effect is observed: The substituted CDs results in increased values of ΔH and $\Delta S°$, as compared to complexes of the natural βCD.[57,82,83,88] This indicates that increased dehydration is a general consequence of substituted CDs. The opposite trend has also been reported but the authors concluded that this was due to self-inclusion of the substitutent.[89]

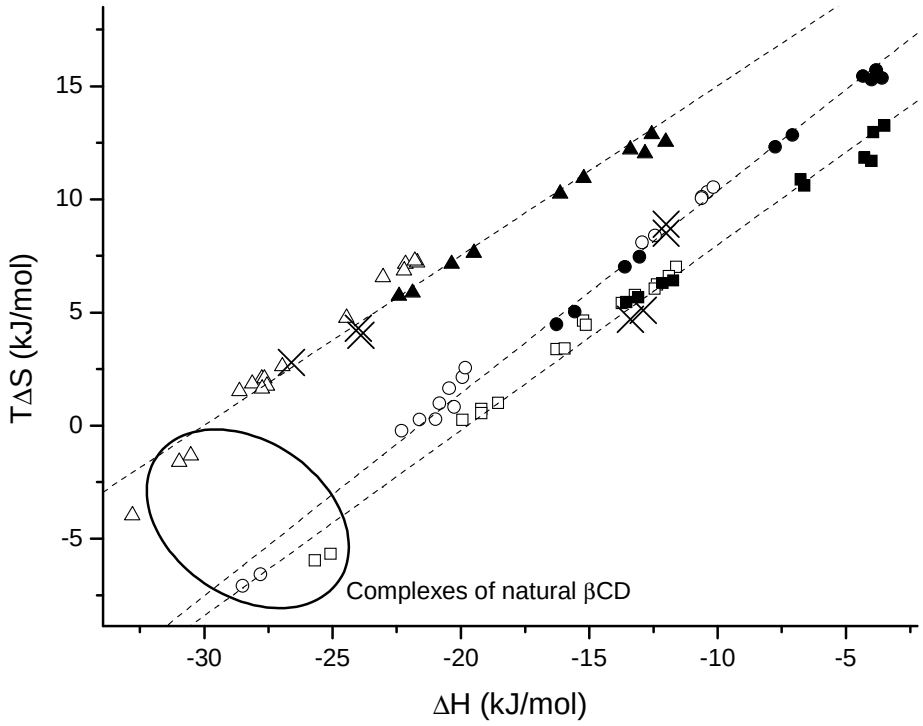

Figure 33: Global enthalpy-entropy compensation plot for the interaction of BSs with natural (Paper II and IV), sulfobutylated (Paper VI) (crosses), methylated (Paper II) (open symbols) and hydroxypropylated (Paper I) (closed symbols) βCDs. Nonpublished values for the binding of natural βCD to the primary site of TDC (ΔH = -27.8 kJ/mol and TΔS° = -6.6 kJ/mol) are also included. Squares denote complexes with TC and GC, circles with TDC and GDC and triangles with TCDC and GCDC. Complexes of mβ300 with GCDC and TCDC are not shown. Dashed lines show the linear regression to each of the three groups of BSs.

5.2.3 Enthalpy, entropy and dehydration of hydrophobic surface

In the above discussion, the thermodynamic data have mainly been interpreted in terms of hydration differences. But what about other contributions from the substituents to the thermodynamics of complexation, why are they ignored? For example, the motion of the HP-substituents is probably restricted upon complex formation, causing a loss of configurational entropy. Or the intermolecular hydrogen bonds between the HP-hydroxyls and the C3 hydroxyls on the CD[71] may be broken upon complexation, giving a positive contribution to ΔH and ΔS°, in accordance with the experimental observations. These effects, and others, may also contribute to the thermodynamics but it is estimated that hydration differences is the primary reason for the large range of measured ΔH and ΔS°. Several considerations lead to this conclusion:

i) *The strong H-S compensation observed within each of the groups of complexes*. As the complex is formed, water molecules from the hydration layers of the host and guest molecules are released into the bulk water, a process termed solvent reorganization. The release of ordered water contributes positively to $\Delta S°$ and also to ΔH since the hydrogen bonds between the water molecules in the hydration layer are stronger than in the bulk phase.[vi] In fact, both Ben-Naim[93] as well as Grunwald and Steel[87] have on theoretical grounds shown that solvent reorganization is associated with exact H-S compensation such that it contributes equally to $T\Delta S°$ and ΔH. This leads to straight lines with unity slopes in the H-S compensation plot.

ii) *Large range of ΔS° which is quantitatively accounted for by buried surface area*. The substituents at the rim of the CD result in a strong increase in $\Delta S°$ of complexation, most notably in the case of HP-substituents. Linear regression to the data plotted in Figure 31 shows that each HP-substitutent contributes with 2.5, 3.1 and 1.9 kJ/mol to $T\Delta S°$, upon complexation with GC, GDC and GCDC, respectively. The MD simulations described in Section 3.3: suggest that each HP-substituent increase the dehydrated hydrophobic surface area by 12.5, 15.8 and 16.4 $Å^2$ in complexes of GC, GDC and GCDC, respectively. Assuming that dehydration of hydrophobic surface is the sole contributor to the HP-induced increments in $T\Delta S°$, one obtains that the dehydration of one $Å^2$ of hydrophobic surface area adds 0.20, 0.20 and 0.12 kJ/mol to $T\Delta S°$ (using the data for complexes with GC, GDC and GCDC, respectively). Errors associated with the theoretical determination of ΔASA_{non} may explain the variation in these values.
From the literature, it is possible to obtain similar values for the dehydration of one $Å^2$ of hydrophobic surface. Based on thermodynamic data for the dissolution of alkylbenzenes into water, the model developed by Costas *et al.* predicts that dehydration of one $Å^2$ contributes with 0.231 kJ/mol to $T\Delta S°$.[94] This value is close to the 0.20 kJ/mol obtained from the GC and GDC complexes. From the linear relationship between surface areas[95] and hydration entropies[96] of 5 linear alkanes (ethane to hexane) one obtains the value 0.120 kJ/mol per $Å^2$, which is close to the value obtained from the GCDC complexes. Apparently, it is hard to find a precise

[vi] These thermodynamic consequences are based on the iceberg model. The organization of water around hydrophobic surfaces and the impact on solubility and hydrophobic interactions is a complex and much debated topic.[90-92]

value for the proportionality constant between dehydrated surface area and TΔS° and maybe it is wrong to assume that such simple relation actually exists. However, the fact that the values obtained from the complexes of HPβCDs show some similarity to those from the literature, shows that it is not unreasonable to assume that the observed increment in TΔS° is caused by the increased dehydration of hydrophobic surface.

iii) *Similar results for the three types of substituents*. Independent of whether the CDs are methylated, hydroxypropylated or sulfobutylated their complexes with BSs lie on the same straight lines in the H-S compensation plot. Further, increased substitution shifts the complexes towards the upper right corner in the plot (with the exception of complexes of mβ209, mβ212 and mβ300 in which increased flexibility of the CD is an important factor). If a substituent-specific property, like the formation of intra-molecular hydrogen bonds between the HP-substituent and C3 hydroxyls at the rim of the CD, is dominating the thermodynamic fingerprint, such similarity between complexes of differently substituted CDs would not be seen.

iv) *Experimental determination of ΔC_p confirms that the HP-substituents cause an increased burial of hydrophobic surface area.* As shown below this estimation of dehydrated surface corresponds well to the areas estimated from the MD simulations.

5.2.4 Effect of CD cavity size on complexation thermodynamics

Enthalpy and entropy changes have only been measured for the complexes of β- and γCD but not for αCD, so the present discussion rests on a weak empirical foundation. However, clear trends are still identified. As discussed above, the larger cavity of γCD, as compared to natural βCD, does not result in major differences in the affinity towards BSs, but the enthalpic and entropic contributions are very different. All complexes of natural βCD are characterized by large negative values of ΔH and small negative values of ΔS°. Conversely, complexes of natural γCD are stabilized by moderately negative values of ΔH and positive values of ΔS°. As for the substituted βCDs, this difference in enthalpic and entropic contributions may be interpreted in terms of dehydration effects. The larger cavity of the γCD accommodates a large part of the bulky steroid body of the BS and thereby dehydrates a larger hydrophobic surface than βCD. MD simulations of the γCD:BS complexes have not been

conducted and it is thus not possible to further validate this hypothesis. The increase in ΔH and ΔS° observed for the complexes of γCD, as compared to the complexes of βCD, could also be explained by assuming a less tight fit in the case of the γCD complexes. Fewer van der Waals interactions would lead to a less negative ΔH and the greater rotational freedom of the guest residing in the larger cavity would lead to an increase in ΔS°. There is no experimental evidence, however, that the fit is less tight in the γCD complexes. The larger radius of γCD could lead to a less tight fit but γCD resides at the more bulky steroid body so there is no reason to believe that the intermolecular distances are larger, and the van der Waals interactions weaker, in the complexes of γCD.

5.2.5 Criticism of conventional interpretation of H-S compensation plots

In the discussion above it is argued that the solvent reorganization that follows from the burial of hydrophobic surface leads to positive contributions to ΔH and ΔS° that are similar, if not equal, in magnitude. If this is true, then it is in conflict with the conventional interpretation of H-S plots introduced and propagated by Inoue *et al.*[4,97,98] According to this often encountered interpretation of H-S compensation plots,[17,99-101] the slope, α, and the intercept, $T\Delta S_0$, are measures of the conformational change and the extent of desolvation, respectively, that takes place upon complexation. An increased binding strength (more negative ΔH) restricts the configurational space of the complex, thereby leading to a decrease in entropy, which to some extent cancels out the negative enthalpic contribution to ΔG°. The magnitude of this entropic penalty, and thereby α, depends on the conformational changes that the complexing molecules undergo. Flexible molecules typically undergo large conformational changes resulting in values of α being close to unity, while rigid pre-organized molecules experience much lower entropic penalties. According to the same interpretation scheme, host and guest molecules undergoing extensive desolvation upon complexation are characterized by large values of $T\Delta S_0$.

The present interpretation is not consistent with these interpretations of α and $T\Delta S_0$. First of all, complexes that lie on the same straight line, and thereby share the same values of $T\Delta S_0$, are characterized by a large variation in the extent of dehydration.

Complexes at the lower left end of the line are characterized by a low degree of dehydration while complexes at the upper right end experience an extensive dehydration upon formation. According to the conventional interpretation all these complexes experience the *same* degree of dehydration. This is in direct conflict with the present interpretation that variations in the extent of desolvation is the primary *difference* between the complexes. Further, complexes on the same line share the same value of α and should therefore, according to the conventional interpretation, all be equally flexible and experience the same degree of conformational changes. The present data cast doubt on the soundness of this interpretation as complexes of both natural βCD and highly substituted HPβCDs are found on the same line. It seems unreasonable to postulate that natural βCD undergoes the same extent of conformational changes as a HPβCD possessing 7 flexible HP-substitutents.

A much more sound interpretation of the presently observed H-S compensation plot is achieved if it is analyzed within the framework of solvent reorganization as formulated by Grunwald and Steel.[87] They divide the overall enthalpy and entropy changes, which are those measured by experiment, into a nominal and an environmental part. The nominal contribution is associated with the interacting host and guest molecules while the environmental part stems from the changes experienced by the solvent (solvent reorganization). Mathematically speaking:

$$\Delta H = \Delta H_{nom} + \Delta H_{env} \qquad [5.1]$$

$$\Delta S^{\circ} = \Delta S_{nom} + \Delta S_{env} \qquad [5.2]$$

Only the environmental part is subject to H-S compensation such that $\Delta H_{env} = T\Delta S_{env}$. As a consequence, if the only difference between the complexes is the extent of solvent reorganization, then α = 1. Thus, values of α close to 1 indicate that the differences in complexation thermodynamics mainly stems from differences in the environmental contributions, while the nominal contributions are more or less constant for all complexes on the same line. This means that the large variations in ΔH and ΔS° observed for CD:BS complexes can be ascribed to differences in the extent of dehydration. That said, one should bear in mind that also the nominal part may experience some degree of H-S compensation and H-S compensation is therefore

not a proof that the primary difference between the complexes is the extent of dehydration.

The intersection, $T\Delta S_0$, is not a direct measure of some physical property. It depends on both the nominal contributions and α. Rather than being a measure of the extent of dehydration, it will often show some correlation with ΔG°. A negative shift in ΔG° can be accomplished by shifting the data points in the plot leftwards towards more negative ΔH (keeping ΔS° fixed) or upwards towards more positive ΔS° (keeping ΔH fixed). Both shifts will produce a more positive $T\Delta S_0$.

Section 5.3: Heat capacity changes

As shown in Table 4, the change in heat capacity, ΔC_p, was determined for a number of complexes. The water in the hydration shells of hydrophobic molecules are thought to have a higher heat capacity than the bulk water, and a reduction of the hydration shell upon complex formation will thus results in a negative ΔC_p. Inclusion of a hydrophobic guest molecule into the CD cavity results in a burial of hydrophobic surface and is thus expected to exhibit a negative ΔC_p, in agreement with what is generally observed for CD inclusion complexes.[102-105vii] The presently investigated complexes also show considerable negative ΔC_ps. For the HPβCDs, excellent linear relations are observed when ΔC_p is plotted as a function of DS (Figure 34). Remembering the almost linear relation between ΔASA_{non} and DS, it is tempting to interpret this increase in (negative) ΔC_p as stemming from increased dehydration of hydrophobic surface, induced by the HP-substituents. This interpretation is in *qualitative* agreement with the conventional knowledge that dehydration of hydrophobic surface gives a negative contribution to ΔC_p, but is the increment in ΔC_p also in *quantitative* agreement with what is observed for related phenomena? In Paper VII I have used experimental data from the literature, for various kinds of experiments involving hydration/dehydration of hydrophobic surface, to calculate proportionality constants between ΔC_p and ΔASA_{non}. The proportionality constants fall in a rather wide range, having an average value of 1.8 J/mol/K/Å^2 with a standard deviation of

[vii] Examples of large positive values of ΔC_p for formation of CD complexes do exist but the authors claim that these are due to dehydration of charged groups and ordering of water inside the CD cavity in the complex.[106]

0.4 (upon dehydration both ΔASA_{non} and ΔC_p are negative, so the proportionality constant is a positive number). Plotting the experimental values of ΔC_p from Table 4 versus the values of ΔASA_{non} obtained from the MD simulations, the data lie on three more or less straight lines, a line for each of the BSs (Figure 35).

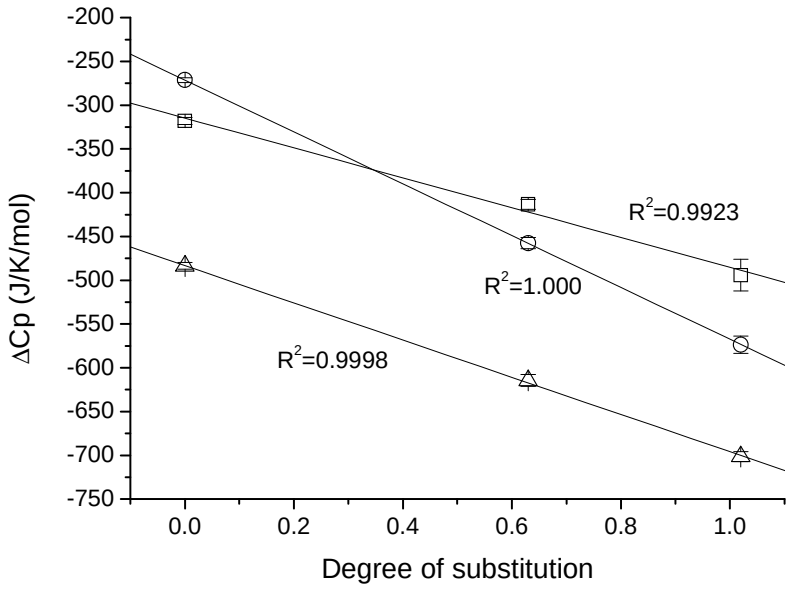

Figure 34: Values of ΔC_p from Table 4 for complexes of HPβCDs plotted as a function of the number of HP-substituents per glucose unit. □: GC, ○: GDC, △:GCDC

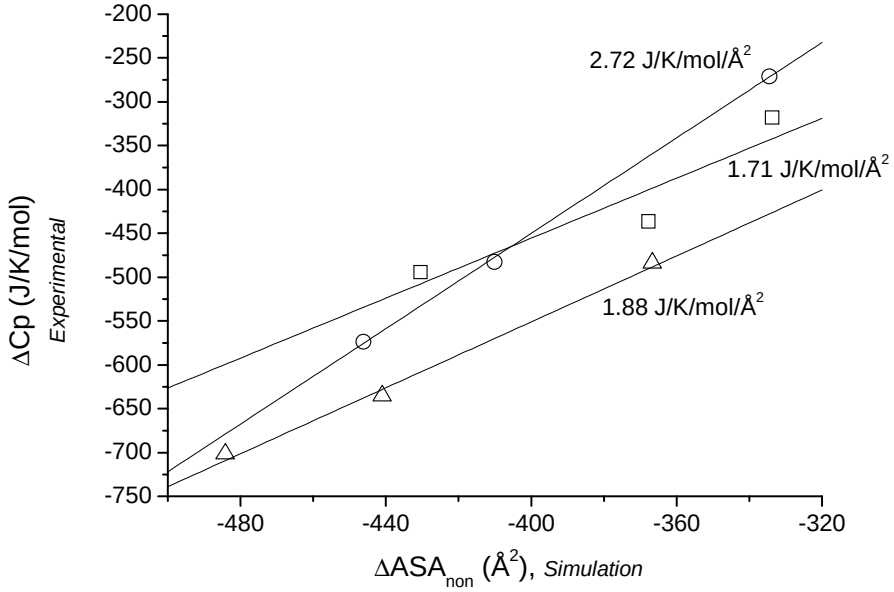

Figure 35: Values of ΔC_p from Table 4 for complexes of HPβCDs plotted as a function of the change in water accessible surface area, determined from the MD simulations. □: GC, ○: GDC, △: GCDC.

If dehydration of hydrophobic surface is the sole contributor to ΔC_p one would expect all datapoints to lie on the same straight line passing through origo of the coordinate system. This is not the case, however. The intercepts with the y-axis are all large and positive and may indicate that dehydration of the cavity contributes to ΔC_p in an unusual way. In fact, Olvera *et al.* finds that the release of water molecules from the CD cavity contributes positively to ΔC_p.[103] The fact that the datapoints lie on three distinct lines indicates that complexes of the three BSs differ by more than just hydration differences and that these differences also contribute to ΔC_p. The slopes of the three lines in Figure 35 are related to the dehydration of the HP-chains and the parts of the BSs that protrudes from the cavity. Each dehydrated $Å^2$ of these hydrophobic surfaces contributes with 1.71, 2.72 and 1.88 J/K/mol in the case of GC, GDC and GCDC, respectively. Two of these values are close to the abovementioned proportionality factor (1.8 J/mol/K/$Å^2$) and it certainly seems likely that increased dehydration is responsible for the increasingly negative values of ΔC_p in complexes of HP-substituted CDs.

Values of ΔC_p for the complexes of mβCDs are plotted in Figure 36 as a function of DS. Up to DS ≈ 1.5 a monotonous and almost linear decrease is observed for ΔC_p but at higher DS ΔC_p starts to increase. This turning point around DS 1.5 resembles the plot of ΔH and TΔS° versus DS, and may again be related to the disruption of the H-bond network. Nevertheless, all of the methylated CD complexes show significantly more negative values of ΔC_p than the complexes of natural βCD, indicating that the methyl substituents, like the HP-substituents, increase the hydrophobic contacts with the BS. Due to the smaller size of the methyl groups, they cause a smaller decrease in ΔC_p than the HP-substituents. Unfortunately, this explanation can not be quantitatively tested since ΔASA_{non} have not been determined for the complexes of mβCDs

ΔC_p for the complexes of SBβ091 with GDC and GCDC are also very negative, close to the values observed for the complexes with the highly substituted HPβ102. MD simulations show that ΔASA_{non} is -500 and -498 $Å^2$ for the binding of SBβ091 to GDC and GCDC, respectively. This is slightly more negative than for the complexes of HPβ102 and again demonstrates that ΔC_p is a reliable measure of buried hydrophobic surface area.

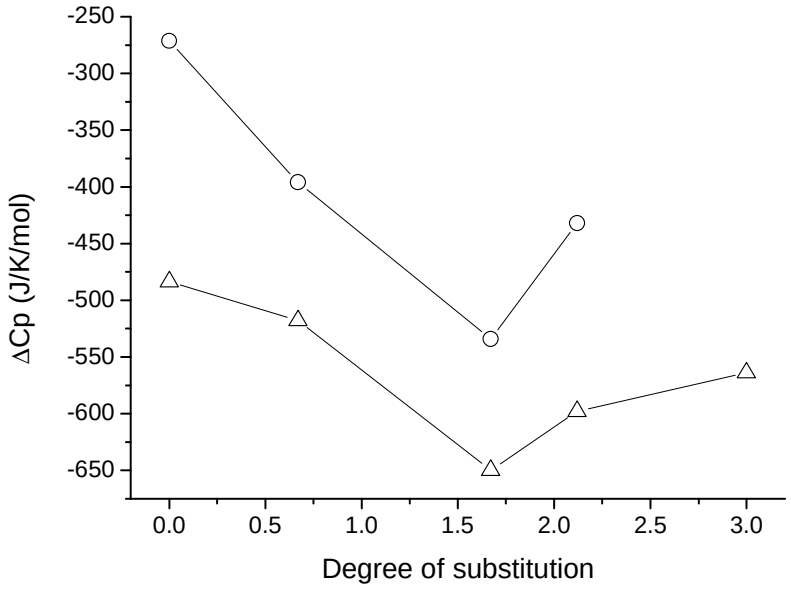

Figure 36: Values of ΔC_p from Table 4 for complexes of mβCDs plotted as a function of the number of methyls per glucose unit. ○: GDC, △:GCDC

5.3.1 Isoentropic and isoenthalpic temperatures

Once ΔC_p has been determined it is in principle possible to extrapolate the thermodynamic parameters, K, ΔH and ΔS° to any temperature, assuming that ΔC_p is constant throughout the relevant temperature range. This is in general not the case when hydrophobic surfaces are exposed to water and ΔC_p often shows a slight temperature dependence,[107-109] so the isentropic and isoenthalpic temperatures discussed in the following should be viewed as hypothetical temperatures rather than real temperatures.

The enthalpies and entropies are extrapolated using the following equations:

$$\Delta H(T) = \Delta H_0 + \Delta C_P (T - T_0) \qquad [5.3]$$

$$\Delta S^\circ(T) = \Delta S_0 + \Delta C_P \ln\left(\frac{T}{T_0}\right) \qquad [5.4]$$

This results in the following graphs:

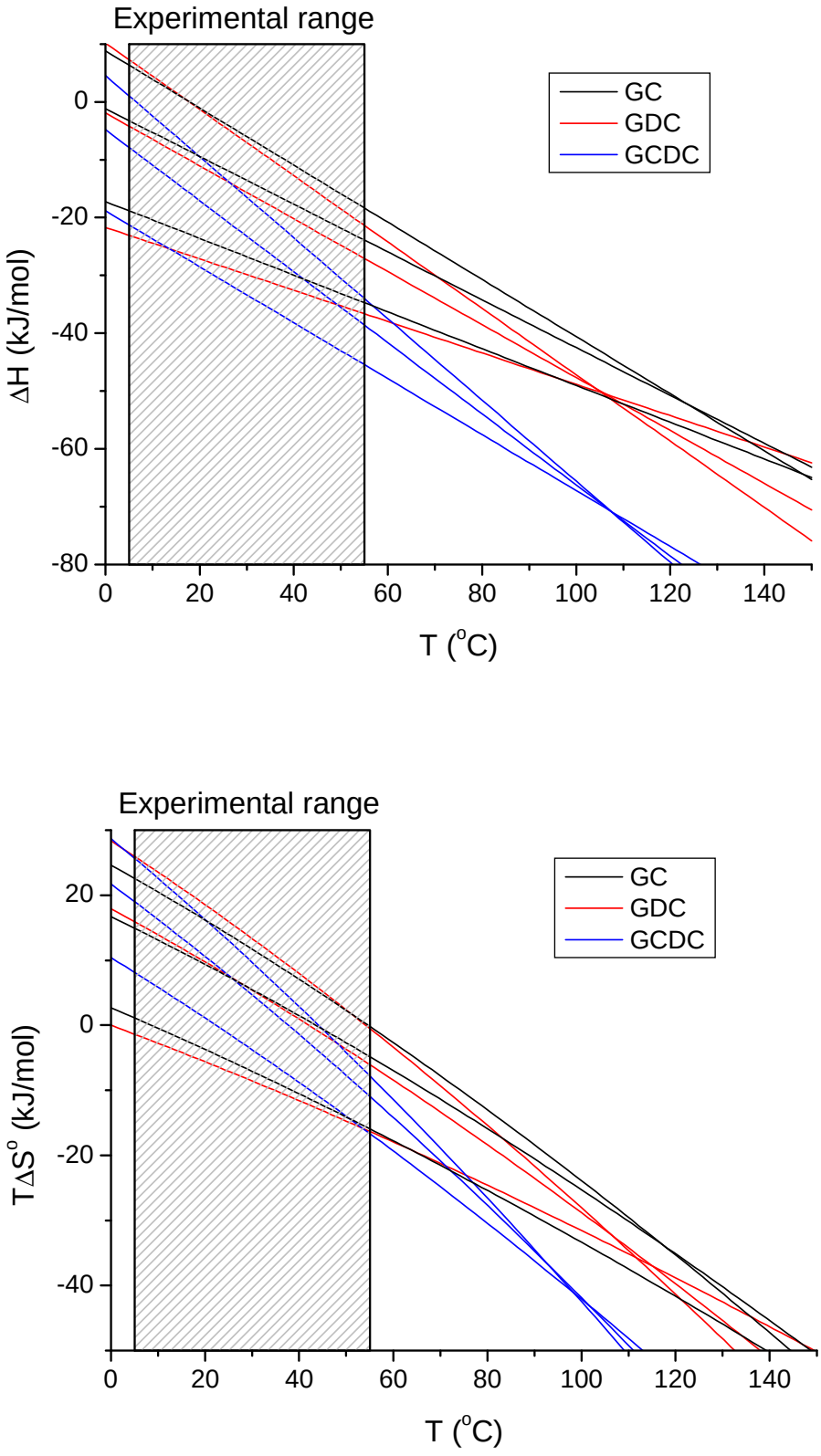

Figure 37: Extrapolation of the experimentally measured ΔH and ΔS° for the complexes of natural βCD, HPβ063 and HPβ102. The extrapolated enthalpies and entropies for the complexes of these three CDs with each type of BS tend to intersect at high temperatures. Complexes of βCD have the smallest slopes while complexes of HPβ102 have the largest slopes.

The extrapolated enthalpies for the three GCDC complexes intersect very precisely at 107.4 °C. At this temperature the enthalpies for the three complexes are equal, independent of the number of HP-substituents. The enthalpies for the three GDC complexes also show a clear intersection around 105 °C. For the GC complexes no clear isoenthalpic point is observed although the enthalpies tend to be similar at temperatures around 120 °C. It is possible that the lack of a clear isoenthalpic temperature for the GC complexes is due to imprecision in the experimental determination of ΔH and ΔC_p, resulting from the challenges of using ITC to determine binding thermodynamics in weak complexes. Extrapolation of the entropies gives rise to similar isoentropic temperatures although they are not as clear-cut as the isoenthalpic temperatures, probably due to larger errors in the experimental determination of $\Delta S°$.

The existence of isoenthalpic and isoentropic temperatures, or convergence temperatures as they are often called, has previously been reported in the literature. The phenomenon has been observed for unfolding of proteins,[110] dissolution of small hydrocarbons,[111] hydration of n-alcohols[112] and seems to be a general feature of processes in which predominantly hydrophobic molecular surfaces are exposed to water.[113] Isoentropic temperatures always seem to be in the vicinity of 110 °C but isoenthalpic temperatures vary between room temperature for dissolution of hydrocarbons and 110 °C for unfolding of globular proteins.

A convenient way of analyzing for isoenthalpic and –entropic temperatures is by plotting ΔH and $\Delta S°$ as a function of ΔC_p, resulting in socalled MPG plots, named after the inventors Murphy, Privalov and Gill.[113] If the reference enthalpies, entropies and temperatures in equations 5.3 and 5.4 are chosen to be the enthalpies and entropies, ΔH^* and ΔS^*, at the isoentropic and isoenthalpic temperatures, T_H^* and T_S^*, we get:

$$\Delta H(T) = \Delta H^* + \Delta C_p \left(T - T_h^*\right) \qquad [5.5]$$

$$\Delta S^\circ(T) = \Delta S^* + \Delta C_p \ln\left(T/T_s^*\right) \qquad [5.6]$$

Linear regression of equation 5.5 to a MPG enthalpy plot yields $T-T_H^*$ as the slope and ΔH^* as the intercept. Likewise, $\ln(T/T_S^*)$ and ΔS^* are given as the slope and intercept of a MPG entropy plot.

MPG plots for all the complexes in Table 4 for which ΔC_p is known are shown in Figure 38. The complexes formed with natural βCD, HPβ063 and HPβ102 fall on three straight lines in both the enthalpy and the entropy plot. Isoenthalpic and isoentropic temperatures for these series of complexes are obtained from the linear regression of equations 5.5 and 5.6 to these data and listed in Table 5 along with the extrapolated values of ΔH and $\Delta S°$ at these temperatures. For the GDC and GCDC complexes T_S^* is close to the "universal" isoentropic temperature of 110 °C,[113] but analysis of the GC complexes yields a T_S^* that is higher than what is usually observed, but this is possibly due to imprecise experimental determination of $\Delta S°$ and ΔC_p.

The isoenthalpic temperatures are quite close to the isoentropic temperatures. This is not a general observation – isoenthalpic temperatures seem to be less common and no "universal" value of T_H^* is found. To my knowledge, the only system in which T_H^* is close to T_S^* is the unfolding of a series of globular proteins.[110] It can be shown that the similar values of T_H^* and T_S^* is mathematically linked to the strong H-S compensation observed for the CD complexes.[viii]

The complexes of mβCDs and SBβCD do not fall on straight lines, meaning that no isoenthalpic and isoentropic temperatures are found. The deviations from the straight lines spanned by the HPβCDs are not that large, however, when the weakly substituted mβCDs are considered.

Table 5: Isoentropic and isoenthalpic temperatures for the complexes of βCD, HPβ063 and HPβ102 with the three BSs. ΔH^* and ΔS^* are the hypothetical enthalpic and entropic contributions at these temperatures.

BS	T_S^* (°C)	ΔS^* (J/mol/K)	T_H^* (°C)	ΔH^* (kJ/mol)
GC	159	-134	149	-64
GDC	112	-93	106	-50
GCDC	99	-111	107	-71

[viii] Without going into the mathematical derivations, this statement can be justified by looking at Figure 37. The temperature at which the lines intersect are governed by the values of ΔH (or $T\Delta S°$) at 25 °C and the slopes. H-S compensation links the values of ΔH and $T\Delta S°$ at 25 °C and the slopes are determined by the values of ΔC_p (see equations 5.3 and 5.4), which are the same in both plots.

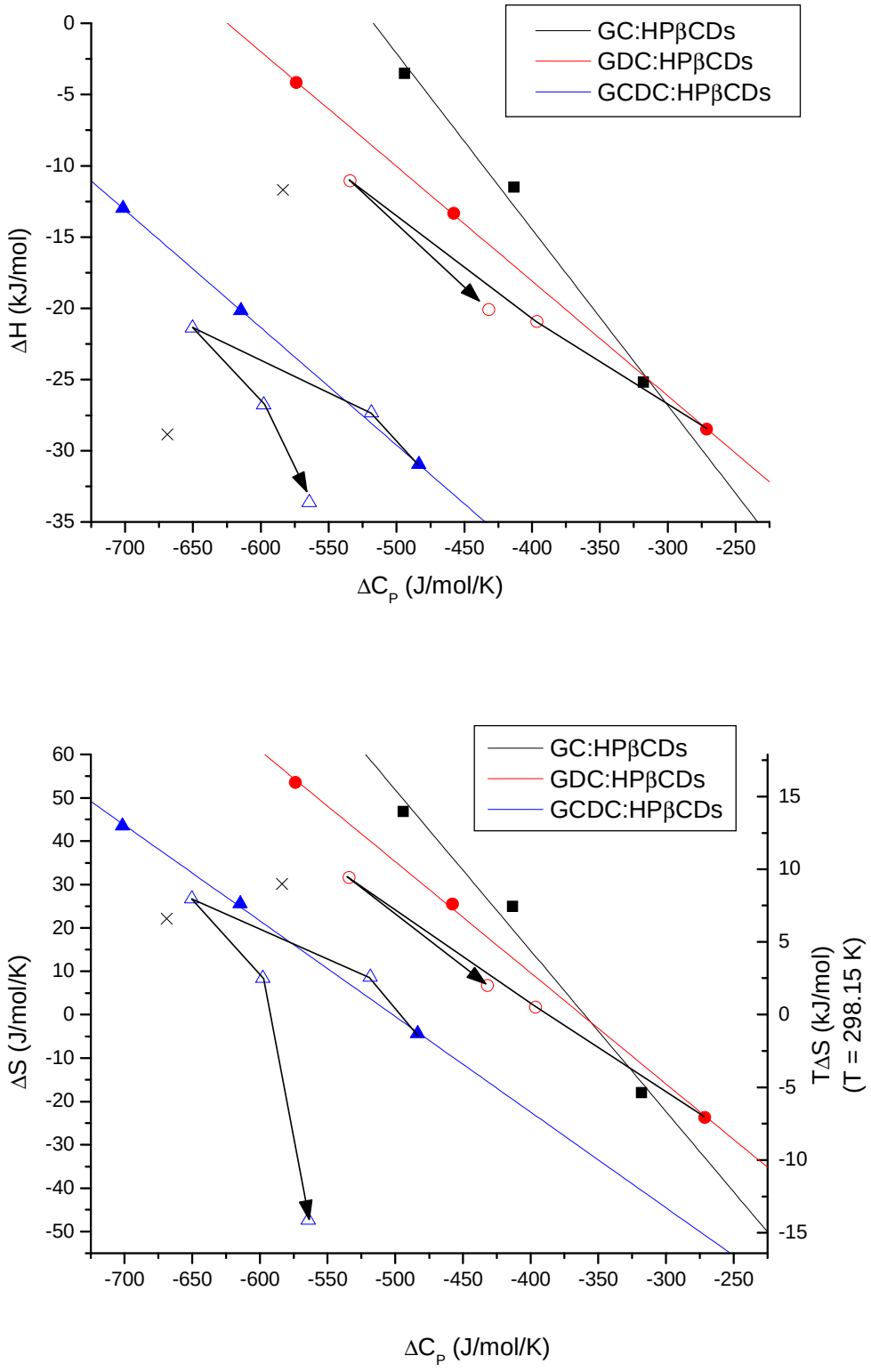

Figure 38: MPG enthalpy and entropy plots. Complexes of HPβCDs and natural βCD are shown with closed symbols, mβCDs with open symbols and SBβ091 with crosses. The type of guest molecule is given by the colour and shape: GC = Black squares, GDC = red circles, GCDC = blue triangles. The straight lines are the linear regressions to the complexes of HPβCDs and natural βCD. The two black arrows connect the complexes of mβCDs in the direction of increased methylation.

5.3.2 The meaning of isoenthalpic and isoentropic temperatures

So what is the interpretation of these isoenthalpic and isoentropic temperatures? And what does the occurrence of these temperatures tell about the thermodynamic consequences of HP-substitution? It has been suggested, that at T_S* the hydrophobic contribution to ΔS° is zero,[111,113] but it has later been noted that the occurrence of isoenthalpic and isoentropic temperatures is merely a mathematical consequence of ΔS° and ΔH being linearly dependent on a molecular property, such as the number of polar and nonpolar groups.[114,115] The following interpretation of T_S* will use the latter view as a starting point.

The contribution of HP-substituents to the thermodynamic functions are additive such that the increments in ΔH, ΔS° and ΔC_p are constant for each HP-substituent that is attached to the CD. These linear relations are apparent from the plots in Figure 31 and Figure 34. Since these three thermodynamic functions are linearly dependent on the DS, it is not surprising that the plots of TΔS° vs ΔH (Figure 33), ΔH vs ΔC_p or ΔS° vs ΔC_p (Figure 38) are linear. What is surprising, however, is the slopes of these plots. Why are the slopes of the H-S compensation plot so close to unity and why do the slopes in the MPG entropy plot translate into values of T_S* that are close to the "universal" value of 110 °C? An answer to the first question has been proposed in subsection 5.2.5 and the answer to the second question might also be related to the dehydration of hydrophobic surface. Such dehydration gives a characteristic contribution to ΔC_p and may also be associated with a characteristic contribution to ΔS°. Expressed mathematically:

$$\Delta C_p = \Delta C_{nom} + k_C \cdot \Delta ASA_{non} \qquad [5.7]$$

$$\Delta S^\circ = \Delta S_{nom} + k_S \cdot \Delta ASA_{non} \qquad [5.8]$$

ΔS_{nom} and ΔC_{nom} denotes, as defined by Grunwald and Steele and expressed in equations 5.1 and 5.2, the entropy and heat capacity of complexation in the absence of contributions from solvent reorganization. The characteristic contributions from dehydration are given by the proportionality factors k_S and k_C. For example, as calculated in Section 5.2 and Section 5.3, k_S and k_C for the GCDC complexes are

-0.40 J/K/mol/Å^2 (-0.12 kJ/mol/Å^2 divided by 298.15 K) and 1.88 J/K/mol/Å^2. From equations 5.6, 5.7 and 5.8 it can be shown that the slope in the MPG entropy plot is given by the ratio of k_S over k_C:

$$\ln(T/T_s^*) = \frac{k_S}{k_C} \qquad [5.9]$$

Using the values of k_S and k_C for the GCDC complexes one obtains T_S^* = 96 °C which is equal to the value determined from the MPG plot and presented in Table 5 (the small discrepancy is due to round-off errors).

The point is that dehydration of hydrophobic surface results in characteristic contributions to ΔC_p and $\Delta S°$, such that the ratio of these contributions always has the same value. Then, if the variation in ΔC_p and $\Delta S°$ in a series of processes is caused by hydration differences, then a hypothetical isoentropic temperature around 110 °C is observed. For example, according to this interpretation the dissolution of hydrocarbons considered by Baldwin[111] all share the same values of ΔS_{nom} and ΔC_{nom} but differ in ΔASA_{non}. Since the contributions from hydration to ΔC_p and $\Delta S°$ are both proportional to ΔASA_{non}, the ratio of these contributions is independent of the hydrocarbon and has a characteristic value that translates into $T_S^* \sim 110$ °C.

Similarly, the complexes of βCD, HPβ063 and HPβ102 with a given BS share common values of ΔS_{nom} and ΔC_{nom}, but the measured values of ΔC_p and $\Delta S°$ differ widely due to differences in the extent of dehydration. But since ΔS_{nom} and ΔC_{nom} is the same in the three complexes, the extrapolated enthalpies intersect at $T_S^* \sim 110$ °C. The conclusion from the H-S compensation plot is in line with the occurrence of an isoentropic temperature around 110 °C: The predominant effect of the HP-substitutents is to alter the hydration state.

Even though it is argued that the existence of an isoentropic temperature for a series of processes mean that they all share common values of ΔS_{nom} and ΔC_{nom}, this statement should be softened a bit. ΔS_{nom} and ΔC_{nom} need not be exactly the same in all of the processes. For the complexes of HPβCDs, for example, the restrictions in the movements of the HP-substitutents upon complexation will most likely contribute to ΔS_{nom}, which will therefore depend on the number of HP-substitutents. These contributions to the measured entropies, however, are much smaller than the contributions from hydration. The effect of HP-substituents on $\Delta S°$ is therefore dominated by dehydration and the same is probably valid for ΔC_p. The large

contributions from dehydration, relative to other contributions, are probably related to the small molecular size and the high density of H-bonds in water.

So what about the other complexes, those of mβCDs and SBβCD? Why do they not fall on straight lines? Some of the complexes actually lie quite close to the lines spanned by the HPβCDs and βCD, while others deviate significantly. According to the above interpretation the thermodynamics of all complexes falling on the same straight line, having a characteristic slope, are dominated by hydration differences. The primary reason why the complexation thermodynamics of HPβ102 differ so markedly from βCD, is because of the larger dehydration. For complexes that deviate from these lines other effects than just hydration differences are responsible for the variation in complexation thermodynamics. The largest deviations are observed for the highly methylated βCDs and SBβCD. As speculated in Section 5.2, the increased flexibility of the highly methylated βCDs leads to a large loss of conformational entropy upon complexation. This is in line with the deviations in the MPG entropy plot where especially the complex of mβ300 is found way below the straight line. In the complexes of SBβCD, some dehydration of the charged sulfo groups may take place. This has another thermodynamic profile than dehydration of nonpolar surface and consequently these complexes deviate from the straight lines.

Section 5.4: Hydrophobic interaction and hydrophobic hydration

The complexation thermodynamics of the HPβCDs and the interpretation of these give rise to what seems to be a paradox. All experimental and theoretical (MD simulations) results indicate that the HP-substituents cause an increased burial of hydrophobic surface by interacting with the parts of the BS that protrudes from the CD cavity. Increased hydrophobic contacts are expected to favour the formation of complexes but instead the HP-substituents slightly destabilize the complexes. To explain this paradox it is necessary to take a closer look at the hydrophobic effect.

The insertion of a hydrophobic molecule into water is often divided into several theoretical steps.[94] Although more steps are required for a complete description, the

two most important steps for the present purpose are the ones illustrated in Figure 39. First, a cavity is created in the water to accommodate the solute. Due to the large number of H-bonds that must be broken, this is an endothermic process. In the second step the water molecules around the solute relaxes and reorganize to form new H-bonds. This is en exothermic process but due to the high degree of order in the hydration shell, it is also characterized by a considerable loss of entropy as well as a large increase in heat capacity.

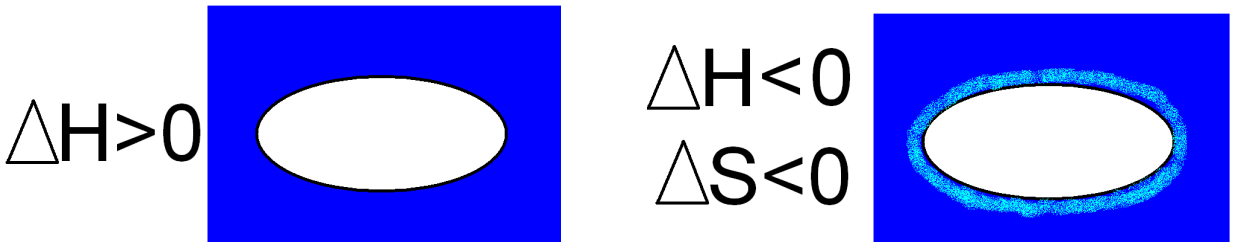

Figure 39: Illustration of the hydrophobic effect. Left: Creation of a cavity in water to accommodate a solute. Right: Relaxation of water molecules in the hydration shell around the hydrophobic solute. Creation of the cavity is an endothermic process while the relaxation of water is an exothermic process. The large entropy loss comes from the second order-creating step.

In hydrophobic interaction, defined as the water-mediated attractive interaction between nonpolar surfaces, both steps are involved. As two or more solutes form an aggregate their individual water cavities merge into a single cavity (step 1) and at the same time ordered water molecules from the eliminated hydration shells are released into the bulk water (step 2). Step 2 will here be termed hydrophobic hydration. Somehow these two steps are decoupled for the interaction of the HP-substituents with the BSs. Most of the thermodynamics of this interaction resembles what is expected for a hydrophobic interaction (positive $\Delta S°$ and negative ΔC_p) but these characteristics originate from step 2, the hydrophobic dehydration. While hydrophobic interaction entails hydrophobic dehydration, hydrophobic interaction is not a prerequisite for hydrophobic dehydration. In the HPβCD complexes the hydrophobic dehydration is caused by the conformational and steric restrictions of the HP-substituents which tend to position themselves so close to BS that the hydration shells of both entities are disrupted. There is no attraction between the HP-substituents and the BS, the dehydration is due to the random movements of the HP-substituents.

But why is it not favourable to merge the water cavities of the HP-substituents and the BS? The answer might lie in the small size of the substituents. In a review of the hydrophobic effect, Chandler[91] focuses on the importance of the length scale. Small molecules (radius < 1 nm) can to some extent be accommodated into the hydrogen bond network of water and therefore the creation of a cavity is not that energetically expensive. Maybe the HP-substituents, which also contain a hydroxyl group, fit so well into the water structure that nothing is gained by "sticking" to the hydrophobic BS.

Section 5.5: General interpretation of aqueous solution thermodynamics

The sign and magnitude of ΔH and ΔS° are often used to draw conclusions about the underlying driving forces and mechanisms for a given process. This might be a reasonable approach for processes taking place in the gas phase or in non-hydrogen-bonding solvents, but if the conclusions of the current work are correct, it is very difficult to apply to processes taking place in aqueous solution. The reorganization of water, which due to H-S compensation does not constitute a driving force, contributes significantly to the measured ΔH and ΔS°. As a consequence, the thermodynamics of the driving forces are masked by the large contributions from solvent reorganization (step 2 in Figure 39). For example, the complexation of GDC with βCD is enthalpy-driven and disfavoured by entropy while the complexation with HPβ102 mainly is driven by entropy and only to a smaller extent by enthalpy. Does this mean that the two complexes are driven by fundamentally different forces? No. The different thermodynamic fingerprints of these two complexes are caused by differences in the extent of hydrophobic dehydration, which hardly contributes to the complex stabilities.

Similar conclusions regarding the interpretation of ΔH and ΔS° are briefly expressed in the literature.[5,116]

Chapter 6: Conclusions

All investigated CDs, except the permethylated βCD, form complexes with the 6 investigated BSs. The αCDs are the least investigated but seem to form 1:1 inclusion complexes in which the αCD is located at the conjugation tail of the BS. The structures of the complexes of βCDs and γCD are much better characterized. All βCDs form 1:1 complexes with the BSs GC, TC, TCDC and GCDC in which the CD is located at the D-ring of the BS. Due to the lack of a hydroxyl group at C7, the BSs GDC and TDC possess a weaker secondary binding site on the A-ring, in addition to the primary site on the D-ring. The natural βCD and the methylated βCDs bind to the secondary site but it is not clear whether the hydroxypropylated βCDs do. The larger diameter of γCD allows a deeper inclusion of the bulky steroid body of the BSs such that this CD resides on the B- and C-rings of the BSs, forming 1:1 complexes.

The αCDs form much weaker complexes than the βCDs and γCD, which do not differ strongly in their affinities for BSs. The number and position of hydroxyl groups on the BS is the most important factor regarding the complex stabilities, despite a weak influence on the complex structures. The lack of a hydroxyl group at C12 leads to formation of very stable complexes.
Relative to this, the type, number and position of substituents at the rims of the CD are of secondary importance although clear trends are identified. Methyl substituents at O2 stabilize the complexes while methyls at O3 block the cavity entrance and disturb the inclusion of BSs. HP-substituents, which are primarily located at O2, destabilize the complexes.

The most striking feature of attaching substituents to the rims of the CDs is the impact on the thermodynamics of complexation. In general, the substituents lead to a large increase in ΔH and $\Delta S°$ as well as more negative values of ΔC_p. To clarify the underlying reasons for these thermodynamics changes, MD simulations of the HPβCD complexes were conducted. It turns out that the interaction between the HP-substituents and the parts of the BS that protrudes from the CD cavity leads to increased dehydration of hydrophobic surface area while not increasing the dehydrated polar surface area. The observed increments in $\Delta S°$ and ΔC_p with the

number of HP-substituents are quantitatively accounted for by the increased hydrophobic dehydration. This effect is not limited to the HP-substituents. All types of substituents are thought to cause increased hydrophobic dehydration leading to large changes in ΔH, $\Delta S°$, ΔC_p. It seems that differences in the extent of dehydration are responsible for the large variation in complexation thermodynamics observed for the substituted βCDs, and might also explain the different complexation thermodynamics of γCD vs. βCD. Dehydration of ionic groups in sulfobutylated βCD and the increased flexibility of highly methylated βCDs are also important factors contributing to the complexation thermodynamics.

Differences in the extent of (de)hydration is an important thermodynamic factor in the presently investigated system, and might be the cause of the commonly observed phenomenon of enthalpy-entropy compensation and the sporadic reports of entropy convergence temperatures around 110 °C.

Chapter 7: Suggestions for further work

The principal hypothesis presented in the present work is that the substituents increase the buried hydrophobic surface area. This hypothesis is experimentally supported by the thermodynamic parameters $\Delta S°$ and ΔC_p and theoretically by MD simulations. Other methods could be employed to probe and quantify the dehydrated hydrophobic surface area. Recently, I contributed to the Master Thesis of Pitchayanun Somprasirt in which salt effects on some of the same complexes were investigated.[117] Some ions are partially or wholly excluded from the hydration shells of hydrophobic surfaces[118] and the resulting osmotic pressure shifts the equilibrium towards the dehydrated state,[119] towards the complexed state. The increment in $\Delta G°$ with the salt concentration can then be used to quantify the number of water molecules released from the hydration shells upon complexation,[118,120] or equivalently, the dehydrated surface area. In Somprasirts work it appears that this area is around 1.5 times larger for the HPβ102:GCDC complex than for the βCD:GCDC complex, and this ratio is triply determined by the use of three different sodium salts. If the values of ΔC_p for the same two complexes (see Table 4) are compared, the ratio has the value 1.45. This similarity indicates that the creation of osmotic stress using ions is a promising technique for probing the extent of dehydration in the CD:BS complexes. A thorough study of more complexes by this technique would substantiate the discussions and conclusions of the present dissertation.
Not only ions but also electrically neutral molecules, for example polymers,[119] may be used to probe the extent of hydration through the creation of osmotic pressure, provided that they do not engage in specific interactions with the CD.

Pressure perturbation calorimetry is another technique to probe the extent of hydration in small, relatively inflexible molecules such as CDs and their complexes.[104] The pressure of the solution is varied in pulses and the resulting heat changes are measured and converted into molar thermal expansivity. This property might be a good measure of the size of the hydration layer in the free and complexed species.

These thermodynamic approaches could be complemented by a structural and dynamical investigation of the behaviour of water molecules in the hydration layer.

NMR techniques have been developed and used to study hydration waters in proteins[121] and small organic molecules.[122]

MD simulations of the free and complexed species were conducted to obtain the polar and non-polar surface areas. It is possible, however, to extract much more information from the simulations, both structural and thermodynamic information. MD simulations of methylated βCDs and their complexes with BSs could also clarify whether some of the structural interpretations in the present work are correct.

Chapter 8: References

1. Humphrey, W.; Dalke, A.; Schulten, K. VMD: Visual molecular dynamics. *J. Mol. Graphics* **1996,** *14* (1), 33-38.

2. Phillips, J. C.; Braun, R.; Wang, W.; Gumbart, J.; Tajkhorshid, E.; Villa, E.; Chipot, C.; Skeel, R. D.; Kale, L.; Schulten, K. Scalable molecular dynamics with NAMD. *J. Comput. Chem.* **2005,** *26* (16), 1781-1802.

3. Saenger, W. R.; Jacob, J.; Gessler, K.; Steiner, T.; Hoffmann, D.; Sanbe, H.; Koizumi, K.; Smith, S. M.; Takaha, T. Structures of the common cyclodextrins and their larger analogues - Beyond the doughnut. *Chem. Rev.* **1998,** *98* (5), 1787-1802.

4. Rekharsky, M. V.; Inoue, Y. Complexation thermodynamics of cyclodextrins. *Chem. Rev.* **1998,** *98*, 1875-1917.

5. Liu, L.; Guo, Q.-X. The driving force in the inclusion complexation of cyclodextrins. *J. Incl. Phenom. Macrocycl. Chem.* **2002,** *42*, 1-14.

6. Kraus, T. Modified Cyclodextrins with Pendant Cationic and Anionic Moieties as Hosts for Highly Stable Inclusion Complexes and Molecular Recognition. *Curr. Org. Chem.* **2011,** *15* (6), 802-814.

7. Holm, R.; Shi, W.; Hartvig, R. A.; Askjær, S.; Madsen, J. C.; Westh, P. Thermodynamics and structure of inclusion compounds of tauro- and glyco-conjugated bile salts and β-cyclodextrins. *Phys. Chem. Chem. Phys.* **2009,** *11*, 5070-5078.

8. Szejtli, J. Introduction and general overview of cyclodextrin chemistry. *Chem. Rev.* **1998,** *98*, 1743-1753.

9. Loftsson, T.; Brewster, M. E. Pharmaceutical applications of cyclodextrins: basic science and product development. *J. Pharm. Pharmacol.* **2010,** *62* (11), 1607-1621.

10. Rao.C.T.; Pitha, J.; Lindberg, B.; Lindberg, J. Distribution of substituents in O-(2-hydroxypropyl) derivatives of cyclomalto-oligosaccharides (cyclodextrins): influence of increasing substitution, of the base use in the preperation, and of macrocyclic size. *Carbohydr. Res.* **1992,** *223*, 99-107.

11. Westerberg, G.; Wiklund, L. β-cyclodextrin reduces bioavailability of orally administered [^{3}H]benzo[a]pyrene in the rat. *J. Pharm. Sci.* **2005,** *94*, 114-119.

12. Uekama, K.; Hirayama, F.; Irie, T. Cyclodextrin drug carrier systems. *Chem. Rev.* **1998,** *98*, 2045-2076.

13. Kalantzi, L.; Goumas, K.; Kalioras, V.; Abrahamsson, B.; Dressman, J. B.; Reppas, C. Characterization of the human upper gastrointestinal contents under conditions simulating bioavailability/bioequivalence studies. *Pharm. Res.* **2006,** *23*, 165-176.

14. de la Cruz Moreno, M.; Oth, M.; Deferme, S.; Lammert, F.; Tack, J.; Dressman, J.; Augustijns, P. Characterization of fasted-state human intestinal fluids collected from duodenum and jejunum. *J. Pharm. Pharmacol.* **2006,** *58* (8), 1079-1089.

15. Holm, R.; Madsen, J. C.; Shi, W.; Larsen, K. L.; Städe, L. W.; Westh, P. Thermodynamics of complexation of tauro- and glyco-conjugated bile salts with two modified β-cyclodextrins. *J. Incl. Phenom. Macrocycl. Chem.* **2011,** *69*, 201-211.

16. Holm, R.; Hartvig, R. A.; Nicolajsen, H. V.; Westh, P.; Østergaard, J. Characterization of the Complexation of Tauro- and Glyco-Conjugated Bile Salts with γ-Cyclodextrin and 2-Hydroxypropyl-γ-Cyclodextrin using Affinity Capillary Electrophoresis. *J. Incl. Phenom. Macrocycl. Chem.* **2008,** *61*, 161-169.

17. Liu, Y.; Yang, Y.-W.; Cao, R.; Song, S.-H.; Zhang, H.-Y.; Wang, L.-H. Thermodynamic origin of molecular selective binding of bile salts by animated β-cyclodextrins. *J. Phys. Chem. B* **2003,** *107*, 14130-14139.

18. Liu, Y.; Wu, H. X.; Chen, Y.; Chen, G. S. Molecular binding behaviours of bile salts by bridged and metallobridged bis(beta-cyclodextrin)s with naphthalenecarboxyl linkers. *Supramol. Chem.* **2009,** *21* (5), 409-415.

19. Cabrer, P. R.; Alvarez-Parrilla, E.; Al-Soufi, W.; Meijide, F.; Núñez, E. R.; Tato, J. V. Complexation of bile salts by natural cyclodextrins. *Supramol. Chem.* **2003,** *15*, 33-43.

20. Ghorab, M. K.; Adeyeye, M. C. Enhanced bioavailability of process-induced fast-dissolving ibuprofen cogranulated with β-cyclodextrin. *J. Pharm. Sci.* **2003,** *98*, 1690-1697.

21. Alvaro, D.; Cantafore, A.; Attili, A. F.; Gianni Corrandini, S.; De Luca, C.; Minervini, G.; Di Base, A.; Angelico, M. Relationships between bile salts hydrophilicity and phosphorlipid composition in bile of various animal species. *Comp. Biochem. Physiol.* **1986,** *83B*, 551-554.

22. Roda, A.; Hofmann, A. F.; Mysels, K. J. The influence of bile salt structure on self-association in aqueous solutions. *J. Biol. Chem.* **1983,** *258* (10), 6362-6370.

23. Tongiani, S.; Velde, D. V.; Ozeki, T.; Stella, V. J. Sulfoalkyl ether-alkyl ether cyclodextrin derivatives, their synthesis, NMR characterization, and binding of 6 alpha-methylprednisolone. *J. Pharm. Sci.* **2005,** *94* (11), 2380-2392.

24. Eskandani, Z.; Huin, C.; Guegan, P. Regioselective allylation of cyclomaltoheptaose (beta-cyclodextrin) leading to per(2,6-di-O-hydroxypropyl-3-O-methyl)-beta-cyclodextrin. *Carbohydr. Res.* **2011,** *346* (15), 2414-2420.

25. Tutu, E.; Vigh, G. Synthesis, analytical characterization and initial capillary electrophoretic use in an acidic background electrolyte of a new, single-isomer chiral resolving agent: Heptakis(2-O-sulfo-3-O-methyl-6-O-acetyl)-beta-cyclodextrin. *Electrophoresis* **2011,** *32* (19), 2655-2662.

26. Takeo, K.; Mitoh, H.; Uemura, K. Selective Chemical Modification of Cyclomalto-Oligosaccharides Via Tert-Butyldimethylsilylation. *Carbohydr. Res.* **1989,** *187* (2), 203-221.

27. Pavia, D. L.; Lampman, G. M.; Kriz, G. S. *Introduction to spectroscopy;* 3rd ed.; Thomson Learning: London, 2001.

28. Kay, L. E.; Keifer, P.; Saarinen, T. Pure Absorption Gradient Enhanced Heteronuclear Single Quantum Correlation Spectroscopy with Improved Sensitivity. *J. Am. Chem. Soc.* **1992,** *114* (26), 10663-10665.

29. Cicero, D. O.; Barbato, G.; Bazzo, R. Sensitivity enhancement of a two-dimensional experiment for the measurement of heteronuclear long-range coupling constants, by a new scheme of coherence selection by gradients. *J. Magn. Reson.* **2001,** *148* (1), 209-213.

30. Nyberg, N. T.; Duus, J. O.; Sorensen, O. W. Heteronuclear two-bond correlation: Suppressing heteronuclear three-bond or higher NMR correlations while enhancing two-bond correlations even for vanishing (2)J(CH). *J. Am. Chem. Soc.* **2005,** *127* (17), 6154-6155.

31. Pitha, J.; Rao, C. T.; Lindberg, B.; Seffers, P. Distribution of Substituents in 2-Hydroxypropyl Ethers of Cyclomaltoheptaose. *Carbohydr. Res.* **1990,** *200*, 429-435.

32. Yuan, C.; Jin, Z. Y.; Li, X. H. Evaluation of complex forming ability of hydroxypropyl-beta-cyclodextrins. *Food Chem.* **2008,** *106* (1), 50-55.

33. Liu, Y.; Yang, Y. W.; Yang, E. C.; Guan, X. D. Molecular recognition thermodynamics and structural elucidation of interactions between steroids and bridged bis(beta-cyclodextrin)s. *J. Org. Chem.* **2004,** *69* (20), 6590-6602.

34. Barnes, S.; Geckle, J. M. High-resolution nuclear magnetic-resonance spectroscopy of bile salts: individual proton assigment for sodium cholate in aqueous solution at 400 MHz. *J. Lipid Res.* **1982,** *23*, 161-170.

35. Campredon, M.; Quiroa, V.; Thevand, A.; Allouche, A.; Pouzard, G. NMR-studies of bile salts: 2D NMR studies of aqueous and methanolic

solutions of sodium cholate and deoxycholate. *Magn. Reson. Chem.* **1986,** *24*, 624-629.

36. Claridge, T. D. W. *High-Resolution NMR Techniques in Organic Chemistry;* 2nd ed.; Elsevier: Amsterdam, 2009.

37. Schneider, H.-J.; Hacket, F.; Rüdiger, V. NMR studies of cyclodextrins and cyclodextrin complexes. *Chem. Rev.* **1998,** *98*, 1755-1785.

38. Mucci, A.; Schenetti, L.; Vandelli, M. A.; Ruozi, B.; Salvioli, G.; Forni, F. Comparison between Roesy and ^{13}C NMR complexation shifts in deriving the geometry of inclusion compounds: A study on the interaction between hyodeoxycholic acid and 2-hydroxypropyl-β-cyclodextrin. *Supramol. Chem.* **2001,** *12*, 427-433.

39. Vandelli, M. A.; Salvioli, G.; Mucci, A.; Panini, R.; Malmusi, L.; Forni, F. 2-Hydroxypropyl-ß-cyclodextrin complexation with ursodeoxycholic acid. *Int. J. Pharm.* **1995,** *118*, 77-83.

40. Mucci, A.; Vandelli, M. A.; Salvioli, G.; Malmusi, L.; Forni, F.; Schenetti, L. Complexation of bile salts with 2-hydroxypropyl-β-cyclodextrin: a ^{13}C-NMR study. *Supramol. Chem.* **1996,** *7*, 125-127.

41. Mucci, A.; Schenetti, L.; Salvioli, G.; Ventura, P.; Vandelli, M. A.; Forni, F. The interaction of biliar acids with 2-hydroxypropyl-β-cyclodextrin in solution and in the solid state. *J. Incl. Phenom. Macrocycl. Chem.* **1996,** *26*, 233-241.

42. Tan, Z. J.; Zhu, X. X.; Brown, G. R. Formation of inclusion complexes of cyclodextrins with bile salt anions as determined by NMR titration studies. *Langmuir* **1994,** *10*, 1034-1039.

43. Funasaki, N.; Ishikawa, S.; Neya, S. 1 : 1 and 1 : 2 complexes between long-chain surfactant and alpha-cyclodextrin studied by NMR. *J. Phys. Chem. B* **2004,** *108* (28), 9593-9598.

44. Do Thi, T.; Nauwelaerts, K.; Froeyen, M.; Baudemprez, L.; Van Speybroeck, M.; Augustijns, P.; Annaert, P.; Martens, J.; Van Humbeeck, J.; Van den Mooter, G. Comparison of the Complexation between Methylprednisolone and Different Cyclodextrins in Solution by H-1-NMR and Molecular Modeling Studies. *J. Pharm. Sci.* **2010,** *99* (9), 3863-3873.

45. Kano, K.; Nishiyabu, R.; Doi, R. Novel behavior of O-methylated beta-cyclodextrins in inclusion of meso-tetraarylporphyrins. *J. Org. Chem.* **2005,** *70* (9), 3667-3673.

46. Kano, K.; Ishimura, T.; Negi, S. Mechanism for binding to the flexible cavity of permethylated alpha-cyclodextrin. *J. Inclusion Phenom. Mol. Recognit. Chem.* **1995,** *22* (4), 285-298.

47. Botsi, A.; Yannakopoulou, K.; Perly, B.; Hadjoudis, E. Positive Or Adverse-Effects of Methylation on the Inclusion Behavior of Cyclodextrins - A Comparative Nmr-Study Using Pheromone Constituents of the Olive Fruit-Fly. *J. Org. Chem.* **1995,** *60* (13), 4017-4023.

48. Shi, J.; Guo, D. S.; Ding, F.; Liu, Y. Unique Regioselective Binding of Permethylated beta-Cyclodextrin with Azobenzene Derivatives. *Eur. J. Org. Chem.* **2009,** (6), 923-931.

49. Harata, K.; Uekama, K.; Otagiri, M.; Hirayama, F. Conformation of permethylated cyclodextrins and the host-guest geometry of their inclusion complexes. *J. Incl. Phenom. Macrocycl. Chem.* **1984,** *1* (3), 279-293.

50. Wang, Z. X. An exact mathematical expression for describing competitive binding of two different ligands to a protein molecule. *FEBS Letters* **1995,** *360* (2), 111-114.

51. Østergaard, J.; Jensen, H.; Holm, R. Use of correction factors in mobility shift affinity capillary electrophoresis for weak analyte – ligand interactions. *J. Sep. Sci.* **2009,** *32*, 1712-1721.

52. Atkins, P.; de Paula, J. *Atkins' Physical Chemistry;* 7th ed.; Oxford University Press: New York, 200.

53. Clarke, E. C. W.; Glew, D. N. Evaluation of thermodynamic functions from equilibrium constants. *Trans. Faraday Soc.* **1966,** *62*, 539-547.

54. Jullian, C.; Orosteguis, T.; Perez-Cruz, F.; Sanchez, P.; Mendizabal, F.; Olea-Azar, C. Complexation of morin with three kinds of cyclodextrin - A thermodynamic and reactivity study. *Spectrochim. Acta, Part A* **2008,** *71* (1), 269-275.

55. Nishijo, J.; Moriyama, S.; Shiota, S. Interactions of cholesterol with cyclodextrins in aqueous solution. *Chem. Pharm. Bull.* **2003,** *51* (11), 1253-1257.

56. Matsui, Y.; Ono, M.; Tokunaga, S. NMR spectroscopy of cyclodextrin-inorganic anion systems. *Bull. Chem. Soc. Jpn.* **1997,** *70* (3), 535-541.

57. Zia, V.; Rajewski, R. A.; Stella, V. J. Thermodynamics of binding of neutral melecules to sulfobutyl ether β-cyclodextrins (SBE-β-CDs): the effect of total degree of substitution. *Pharm. Res.* **2000,** *17*, 936-941.

58. Mizoue, L. S.; Tellinghuisen, J. Calorimetric vs. van't Hoff binding enthalpies from isothermal titration calorimetry: Ba2+-crown ether complexation. *Biophys. Chem.* **2004,** *110* (1-2), 15-24.

59. Naghibi, H.; Tamura, A.; Sturtevant, J. M. Significant Discrepancies Between Vant Hoff and Calorimetric Enthalpies. *Proc. Natl. Acad. Sci. U. S. A.* **1995,** *92* (12), 5597-5599.

60. Johnson, M. L. Why, When, and How Biochemists Should Use Least-Squares. *Anal. Biochem.* **1992,** *206* (2), 215-225.

61. Bates, D. M.; Watts, D. G. *Nonlinear Regression Analysis and Its Applications;* Wiley: New York, 2007.

62. Motulsky, H. J.; Christopoulos, A. *Fitting models to biological data using linear and nonlinear regression. A practical guide to curve fitting;* Oxford University Press: New York, 2004.

63. Henzl, M. T.; Larson, J. D.; Agah, S. Estimation of parvalbumin Ca2+- and Mg2+-binding constants by global least-squares analysis of isothermal titration calorimetry data. *Anal. Biochem.* **2003,** *319* (2), 216-233.

64. Freiburger, L. A.; Auclair, K.; Mittermaier, A. K. Elucidating Protein Binding Mechanisms by Variable-c ITC. *ChemBioChem* **2009,** *10* (18), 2871-2873.

65. Houtman, J. C. D.; Brown, P. H.; Bowden, B.; Yamaguchi, H.; Appella, E.; Samelson, L. E.; Schuck, P. Studying multisite binary and ternary protein interactions by global analysis of isothermal titration calorimetry data in SEDPHAT: Application to adaptor protein complexes in cell signaling. *Protein Sci.* **2007,** *16* (1), 30-42.

66. Burnouf, D.; Ennifar, E.; Guedich, S.; Puffer, B.; Hoffmann, G.; Bec, G.; Disdier, F.; Baltzinger, M.; Dumas, P. kinITC: A New Method for Obtaining Joint Thermodynamic and Kinetic Data by Isothermal Titration Calorimetry. *J. Am. Chem. Soc.* **2012,** *134* (1), 559-565.

67. Tan, X.; Lindenbaum, S. Studies on complexation between β-cyclodextrin and bile salts. *Int. J. Pharm.* **1991,** *74*, 127-135.

68. Yim, C. T.; Zhu, X. X.; Brown, G. R. Kinetics of inclusion reactions of beta-cyclodextrin with several dihydroxycholate ions studied by NMR spectroscopy. *J. Phys. Chem. B* **1999,** *103* (3), 597-602.

69. Ollila, F.; Pentikäinen, O. T.; Forss, S.; Johnson, M. S.; Slotte, J. P. Characterization of bile salt/cyclodextrin interactions using isothermal titration calorimetry. *Langmuir* **2001,** *17*, 7107-7111.

70. Liu, Y.; Shi, J.; Guo, D. S. Novel permethylated beta-cyclodextrin derivatives appended with chromophores as efficient fluorescent sensors for the molecular recognition of bile salts. *J. Org. Chem.* **2007,** *72* (22), 8227-8234.

71. Yong, C. W.; Washington, C.; Smith, W. Structural behaviour of 2-hydroxypropyl-beta-cyclodextrin in water: Molecular dynamics simulation studies. *Pharm. Res.* **2008,** *25* (5), 1092-1099.

72. Botsi, A.; Yannakopoulou, K.; Hadjoudis, E.; Perly, B. Structural aspects of permethylated cyclodextrins and comparison with their parent oligosaccharides, as derived from unequivocally assigned H-1 and C-

13 NMR spectra in aqueous solutions. *Magn. Reson. Chem.* **1996,** *34* (6), 419-423.

73. Meieraugenstein, W.; Burger, B. V.; Spies, H. S. C.; Burger, W. J. G. Conformational-Analyses of Alkylated Beta-Cyclodextrins by Nmr-Spectroscopy. *Z. Naturforsch., B: J. Chem. Sci.* **1992,** *47* (6), 877-886.

74. Segura-Sanchez, F.; Bouchemal, K.; Lebas, G.; Vauthier, C.; Santos-Magalhaes, N. S.; Ponchel, G. Elucidation of the complexation mechanism between (+)-usnic acid and cyclodextrins studied by isothermal titration calorimetry and phase-solubility diagram experiments. *J. Mol. Recognit.* **2009,** *22* (3), 232-241.

75. Terekhova, I. V.; Obukhova, N. A.; Agafonov, A. V.; Kurochkina, G. I.; Syrtsev, A. N.; Gratchev, M. K. Thermodynamics of the effects of substituent, degree of substitution, and pH on complex formation of hydroxypropyl-alpha- and hydroxypropyl-beta-cyclodextrins with ascorbic acid. *Russ. Chem. Bull.* **2005,** *54* (8), 1883-1886.

76. Buvari-Barcza, A.; Barcza, L. Influence of the guests, the type and degree of substitution on inclusion complex formation of substituted beta-cyclodextrins. *Talanta* **1999,** *49* (3), 577-585.

77. Tee, O. S.; Fedortchenko, A. A.; Loncke, P. G.; Gadosy, T. A. Binding of aliphatic ketones to cyclodextrins in aqueous solution. *J. Chem. Soc., Perkin Trans. 2* **1996,** (6), 1243-1249.

78. Jullian, C.; Miranda, S.; Zapata-Torres, G.; Mendizabal, F.; Olea-Azar, C. Studies of inclusion complexes of natural and modified cyclodextrin with (+)catechin by NMR and molecular modeling. *Bioorg. Med. Chem.* **2007,** *15* (9), 3217-3224.

79. Thompson, D. O. Cyclodextrins-enabling excipients: their present and future use in pharmaceuticals. *Crit. Rev. Ther. Drug.* **1997,** *14*, 1-104.

80. Pattarino, F.; Giovannelli, L.; Giovenzana, G. B.; Rinaldi, M.; Trotta, M. Inclusion of methotrexate in alkyl-cyclodextrins: effects of host substitutents on the stability of complexes. *J. Drug Delivery Sci. Technol.* **2005,** *15* (6), 465-468.

81. Liu, Y.; Zhang, Q.; Guo, D. S.; Zhuang, R. T.; Wang, L. H. Thermodynamics of complexes between nucleobase-modified beta-cyclodextrins and bile salts. *Thermochim. Acta* **2008,** *470* (1-2), 108-112.

82. Castronuovo, G.; Niccoli, M.; Varriale, L. Complexation forces in aqueous solution. Calorimetric studies of the association of 2-hydroxypropyl-β-cyclodextrin with monocarboxylic acids or cycloalkanols. *Tetrahedron* **2007,** *63*, 7047-7052.

83. Zielenkiewicz, W.; Terekhova, I. V.; Wszelaka-Rylik, M.; Kumeev, R. S. Thermodynamics of inclusion complex formation of

hydroxypropylated alpha- and beta-cyclodextrins with aminobenzoic acids in water. *J. Therm. Anal. Calorim.* **2010,** *101* (1), 15-23.

84. Rekharsky, M. V.; Mori, T.; Yang, C.; Ko, Y. H.; Selvapalam, N.; Kim, H.; Sobransingh, D.; Kaifer, A. E.; Liu, S. M.; Isaacs, L.; Chen, W.; Moghaddam, S.; Gilson, M. K.; Kim, K. M.; Inoue, Y. A synthetic host-guest system achieves avidin-biotin affinity by overcoming enthalpy-entropy compensation. *Proc. Natl. Acad. Sci. U. S. A.* **2007,** *104* (52), 20737-20742.

85. Ma, B.; Shen, Y. B.; Fan, Z.; Zheng, Y.; Sun, H.; Luo, J. M.; Wang, M. Characterization of the inclusion complex of 16,17 alpha-epoxyprogesterone with randomly methylated beta-cyclodextrin in aqueous solution and in the solid state. *J. Incl. Phenom. Macrocycl. Chem.* **2011,** *69* (1-2), 273-280.

86. Kano, K.; Kitae, T.; Shimofuri, Y.; Tanaka, N.; Mineta, Y. Complexation of polyvalent cyclodextrin ions with oppositely charged guests: Entropically favorable complexation due to dehydration. *Chem.--Eur. J.* **2000,** *6* (15), 2705-2713.

87. Grunwald, E.; Steel, C. Solvent reorganisation and thermodynamic enthalpy-entropy compensation. *J. Am. Chem. Soc.* **1995,** *117*, 5687-5692.

88. Bertrand, G. L.; Faulkner, J. R.; Han, S. M.; Armstrong, D. W. Substituent Effects on the Binding of Phenols to Cyclodextrins in Aqueous-Solution. *J. Phys. Chem.* **1989,** *93* (18), 6863-6867.

89. Inoue, Y.; Lin, Y.; Tong, L.-H.; Shen, B.-J.; Jin, D.-S. Thermodynamics of molecular recognition by cyclodextrins. 2. Calorimetric titration of inclusion complexation with modified β-cyclodextrins. Enthalpy-entropy compensation in host-guest complexation: from ionophone to cyclodextrin and cyclophane. *J. Am. Chem. Soc.* **1993,** *115*, 10637-10644.

90. Blokzijl, W.; Engberts, J. B. F. N. Hydrophobic Effects - Opinions and Facts. *Angew. Chem., Int. Ed. Engl.* **1993,** *32* (11), 1545-1579.

91. Chandler, D. Interfaces and the driving force of hydrophobic assembly. *Nature* **2005,** *437* (7059), 640-647.

92. Southall, N. T.; Dill, K. A.; Haymet, A. D. J. A view of the hydrophobic effect. *J. Phys. Chem. B* **2002,** *106* (3), 521-533.

93. Ben-Naim, A. Hydrophobic interaction and structural changes in the solvent. *Biopolymers* **1975,** *14* (7), 1337-1355.

94. Costas, M.; Kronberg, B.; Silveston, R. General Thermodynamic Analysis of the Dissolution of Nonpolar Molecules Into Water - Origin of Hydrophobicity. *J. Chem. Soc. Faraday Trans.* **1994,** *90* (11), 1513-1522.

95. Gallicchio, E.; Kubo, M. M.; Levy, R. M. Enthalpy-entropy and cavity decomposition of alkane hydration free energies: Numerical results and implications for theories of hydrophobic solvation. *J. Phys. Chem. B* **2000,** *104* (26), 6271-6285.

96. Plyasunov, A. V.; Shock, E. L. Thermodynamic functions of hydration of hydrocarbons at 298.15 K and 0.1 MPa. *Geochim. Cosmochim. Acta* **2000,** *64* (3), 439-468.

97. Inoue, Y.; Hakushi, T. Enthalpy-Entropy Compensation in Complexation of Cations with Crown Ethers and Related Ligands. *J. Chem. Soc., Perkin Trans. 2* **1985,** (7), 935-946.

98. Inoue, Y.; Hakushi, T.; Liu.Y.; Tong, L.-H.; Shen, B.-J.; Jin, D.-S. Thermodynamics of molecular recognition by cyclodextrins. 1. Calorimetric titration of inclusion complexation of naphthalenesulfonates with α–, β–, and γ-cyclodextrins: enthalpy-entropy compensation. *J. Am. Chem. Soc.* **1993,** *115*, 475-481.

99. Ondo, D.; Tkadlecova, M.; Dohnal, V.; Rak, J.; Kvicala, J.; Lehmann, J. K.; Heintz, A.; Ignatiev, N. Interaction of Ionic Liquids Ions with Natural Cyclodextrins. *J. Phys. Chem. B* **2011,** *115* (34), 10285-10297.

100. Castronuovo, G.; Niccoli, M. Solvent effects on the complexation of 1-alkanols by parent and modified cyclodextrins. Calorimetric studies at 298 K. *J. Therm. Anal. Calorim.* **2011,** *103* (2), 641-646.

101. Wintgens, V.; Biczok, L.; Miskolczy, Z. Thermodynamics of host-guest complexation between p-sulfonatocalixarenes and 1-alkyl-3-methylimidazolium type ionic liquids. *Thermochim. Acta* **2011,** *523* (1-2), 227-231.

102. Ross, P. D.; Rekharsky, M. V. Thermodynamics of hydrogen bond and hydrophobic interactions in cyclodextrin complexes. *Biophys. J.* **1996,** *71*, 2144-2154.

103. Olvera, A.; Perez-Casas, S.; Costas, M. Heat capacity contributions to the formation of inclusion complexes. *J. Phys. Chem. B* **2007,** *111* (39), 11497-11505.

104. Cameron, D. L.; Jakus, J.; Pauleta, S. R.; Pettigrew, G. W.; Cooper, A. Pressure Perturbation Calorimetry and the Thermodynamics of Noncovalent Interactions in Water: Comparison of Protein-Protein, Protein-Ligand, and Cyclodextrin-Adamantane Complexes. *J. Phys. Chem. B* **2010,** *114* (49), 16228-16235.

105. Hallen, D.; Schon, A.; Shehatta, I.; Wadsi, I. Microcalorimetric titration of alpha-cyclodextrin with some straight-chain alkan-1-ols at 288.15 K, 298.15 K and 308.15 K. *J. Chem. Soc. Faraday Trans.* **1992,** *88*, 2859-2863.

106. Kano, K.; Ishida, Y.; Kitagawa, K.; Yasuda, M.; Watanabe, M. Heat-capacity changes in host-guest complexation by coulomb interactions in aqueous solution. *Chem.--Asian J.* **2007,** *2* (10), 1305-1313.

107. Makhatadze, G. I.; Privalov, P. L. Heat-Capacity of Alcohols in Aqueous-Solutions in the Temperature-Range from 5-Degrees-C to 125-Degrees-C. *J. Solution Chem.* **1989,** *18* (10), 927-936.

108. Makhatadze, G. I.; Privalov, P. L. Energetics of Interactions of Aromatic-Hydrocarbons with Water. *Biophys. Chem.* **1994,** *50* (3), 285-291.

109. Naghibi, H.; Dec, S. F.; Gill, S. J. Heats of Solution of Ethane and Propane in Water from 0-Degrees-C to 50-Degrees-C. *J. Phys. Chem.* **1987,** *91* (1), 245-248.

110. Privalov, P. L. Stability of Proteins Small Globular Proteins. In *Advances in Protein Chemistry*, Volume 33 ed.; Anfinsen, C. B., Ed.; Academic Press: 1979; pp 167-241.

111. Baldwin, R. L. Temperature-Dependence of the Hydrophobic Interaction in Protein Folding. *Proc. Natl. Acad. Sci. U. S. A.* **1986,** *83* (21), 8069-8072.

112. Graziano, G. Entropy convergence in the hydration thermodynamics of n-alcohols. *J. Phys. Chem. B* **2005,** *109* (24), 12160-12166.

113. Murphy, K. P.; Privalov, P. L.; Gill, S. J. Common Features of Protein Unfolding and Dissolution of Hydrophobic Compounds. *Science* **1990,** *247* (4942), 559-561.

114. Lee, B. Isoenthalpic and Isoentropic Temperatures and the Thermodynamics of Protein Denaturation. *Proc. Natl. Acad. Sci. U. S. A.* **1991,** *88* (12), 5154-5158.

115. Murphy, K. P. Hydration and Convergence Temperatures - on the Use and Interpretation of Correlation Plots. *Biophys. Chem.* **1994,** *51* (2-3), 311-326.

116. Cooper, A. Microcalorimetry of heat capacity and volumetric changes in biomolecular interactions-the link to solvation? *J. Therm. Anal. Calorim.* **2011,** *104* (1), 69-73.

117. Somprasirt, P. A study of salt effect on the stability of complexation between cyclodextrin and bile salts based on the Hofmeister series. University of Copenhagen, Faculty of health and medical sciences, 2012.

118. Pegram, L. M.; Record, M. T. Thermodynamic origin of Hofmeister ion effects. *J. Phys. Chem. B* **2008,** *112* (31), 9428-9436.

119. Rand, R. P. Probing the role of water in protein conformation and function. *Philos. Trans. R. Soc., B* **2004,** *359* (1448), 1277-1284.

120. Harries, D.; Rau, D. C.; Parsegian, V. A. Solutes probe hydration in specific association of cyclodextrin and adamantane. *J. Am. Chem. Soc.* **2005,** *127* (7), 2184-2190.

121. Wuthrich, K.; Billeter, M.; Guntert, P.; Luginbuhl, P.; Riek, R.; Wider, G. NMR studies of the hydration of biological macromolecules. *Faraday Discuss.* **1996,** *103*, 245-253.

122. Qvist, J.; Halle, B. Thermal signature of hydrophobic hydration dynamics. *J. Am. Chem. Soc.* **2008,** *130* (31), 10345-10353.

Appendix: List of papers

I. Schönbeck, C.; Westh, P.; Madsen, J. C.; Larsen, K. L.; Städe, L. W.; Holm, R. Hydroxypropyl substituted β-cyclodextrins: influence of degree of substitution on the thermodynamics of complexation with tauro- and glyco-conjugated bile salts. *Langmuir* **2010,** *26* (23), 17949-17957.

II. Schönbeck, C.; Westh, P.; Madsen, J. C.; Larsen, K. L.; Stade, L. W.; Holm, R. Methylated β-Cyclodextrins: Influence of Degree and Pattern of Substitution on the Thermodynamics of Complexation with Tauro- and Glyco-Conjugated Bile Salts. *Langmuir* **2011,** *27* (10), 5832-5841.

III. Holm, R.; Schonbeck, C.; Askjaer, S.; Jensen, H.; Westh, P.; Ostergaard, J. Complexation of tauro- and glyco-conjugated bile salts with α-cyclodextrin and hydroxypropyl-α-cyclodextrin studied by affinity capillary electrophoresis and molecular modelling. *J. Sep. Sci.* **2011,** *34* (22), 3221-3230.

IV. Schönbeck, C.; Holm, R.; Westh, P. Higher Order Inclusion Complexes and Secondary Interactions Studied by Global Analysis of Calorimetric Titrations. *Anal. Chem.* **2012,** *84* (5), 2305-2312.

V. Holm, R.; Schönbeck, C.; Askjær, S.; Westh, P. Thermodynamics of the interaction of γ-cyclodextrin and tauro- and glyco-conjugated bile salts. *J. Incl. Phenom. Macrocycl. Chem.* **2012,** DOI 10.1007/s10847-012-0165-1

VI. Holm, R.; Østergaard, J.; Schönbeck, C.; Jensen, H.; Shi, W.; Günthers, P.; Westh, P. Determination of stability constants of tauro- and glyco-conjugated bile salts with the negatively charged sulfobutylether-β-cyclodextrin: comparison of affinity capillary electrophoresis and isothermal titration calorimetry and thermodynamic analysis of the interaction. *J. Incl. Phenom. Macrocycl. Chem.* **2013,** DOI 10.1007/s10847-013-0287-0

VII. Schönbeck, C.; Holm, R.; Westh, P.; Günthers, P. Extending the hydrophobic cavity of β-cyclodextrin results in more negative heat capacity changes but reduced binding affinities. *J. Incl. Phenom. Macrocycl. Chem.* **2013,** DOI 10.1007/s10847-013-0305-2